Modeling of Piston Ring Assembly and Connecting Rod Bearing Lubrication and Tribological Performance

ScuDo

Scuola di Dottorato ~ Doctoral School

WHAT YOU ARE, TAKES YOU FAR

Doctoral Dissertation

Doctoral Program in Mechanical Engineering (31^{th}cycle)

Predictive Modeling of Piston Ring Assembly and Connecting Rod Bearing Lubrication and Tribological Performance

By

Abbas Razavykia

******

Supervisor(s):

Prof. Cristiana Delprete

Doctoral Examination Committee:

Prof. H. Rahnejat, Referee, Loughborough University

Prof. F. Furgiuele, Referee, Università della Calabria

Politecnico di Torino

2019

Declaration

I hereby declare that, the contents and organization of this dissertation constitute my own original work and does not compromise in any way the rights of third parties, including those relating to the security of personal data.

Abbas Razavykia
2019

* This dissertation is presented in partial fulfillment of the requirements for **Ph.D. degree** in the Graduate School of Politecnico di Torino (ScuDo).

I would like to dedicate this thesis to my lovely mother and those who have taught me that affection is the only way of redemption

Acknowledgements

First and foremost, I would like to express my sincerest thanks to my supervisor Prof. Cristiana Delprete, for her invaluable support, advice and encouragement throughout this study. It has been a great pleasure and honor to work under the supervision of such a distinguished scholar.

I would like to thank Prof. Carlo Rosso, Prof. Elvio Bonisoli and Dr. Paolo Baldissera for their support and kindness for each single moments during my PhD.

I would also like to thank all my teachers and professors who accompanied and motivated me in my whole life.

Abstract

Due to strict environmental legislation and the fact that internal combustion engines (ICEs) are recognized as majority of energy sources in transportation, car manufacturers are motivated to improve ICEs efficiency. Mechanical power loss of lubricated and bearing surfaces serves as an attractive domain to study and research as way to take step to increase ICEs productivity regarding to fuel and oil consumption. Friction reduction at lubricated and bearing surface is one of the most cost-effective tool to reduce gas emission and improve ICEs efficiency. The majority of the mechanical power loss in an engine can be attributed to the main tribological components of an engine, piston-cylinder system (PCS), connecting rod big-end and crankshaft main bearings.

The objective of this dissertation is to develop a complete mathematical and numerical model, firstly to evaluate the piston-cylinder system lubrication mechanisms in terms of design parameters and lubricant rheology. PCS enjoys different lubrication regimes during engine strokes including hydrodynamic, mixed and boundary lubrication. To simplify modeling, most of early studies usually considered full film hydrodynamic lubrication using lubrication theory governed by Reynolds equation. This study makes effort to evaluate piston ring pack lubrication taking into account different operating circumstance and corresponding lubricant film shape at rings and cylinder junction. Oil is treated as viscous and iso-viscous fluid to consider the role of lubricant viscosity dependence on temperature. To simplify the problem rings and liner are treated as iso-thermal bodies.

Secondary motion of piston is analyzed considering hydrodynamic lubrication at bearing surfaces interface. The effect of piston ring pack tribology on piston dynamics has been considered to gain insight into skirt lubrication mechanism. Numerical scheme is introduced to calculate power loss contributed by viscous shear stress.

An analytical model is introduced to evaluate connecting rod big-end and crankshaft main bearings. Besides, Mobility method as well-known approach to evaluate dynamically loaded journal bearings lubrication has been applied to validate analytical model.

The current study tends to evaluate the effects of different boundary condition and oil film shape at ring and liner interface. Full Sommerfeld, oil separation, and Reynolds cavitation and reformation as boundary conditions are applied and their influences have been examined. Design of experiment and ANOVA are used to study the effect of ring profile geometry on oil film thickness and power loss at bearing surfaces interface. In contrary to maturity of conducted investigations, the effect of piston ring pack lubrication on piston secondary motion and tribological performance. General formulation have been developed to evaluate hydrodynamic journal bearing. The analytical model is applied to study connecting rod big-end tribology.

Contents

List of Figures

List of Tables

Nomenclature

Chapter 2

α	constant for given oil so called pressure viscosity coefficient $(\frac{\mathrm{m}^2}{\mathrm{N}})$
$\alpha^\star$	modified pressure viscosity coefficient $(\frac{\mathrm{m}^2}{\mathrm{N}})$
α_0	atmospheric pressure (Pa)
β	viscosity–temperature coefficient
β_0	atmospheric temperature $(^\circ\mathrm{C})$
$\Delta\theta$	temperature increment step (Pa·s)
η	dynamic viscosity (Pa·s)
η_0	viscosity at reference point (Pa·s)
ν	kinematic viscosity (cSt)
ρ	lubricant density $(\frac{\mathrm{kg}}{\mathrm{m}^3})$
σ_{ij}	stress tensor (Pa)
τ	shear stress (Pa)
a	Vogel constant for given oil (Pa·s)
b	Vogel constant for given oil $(^\circ\mathrm{C})$
c	Vogel constant for given oil $(^\circ\mathrm{C})$

du velocity difference between top and bottom of layer $(\frac{\mathrm{m}}{\mathrm{s}})$

f_x external mass force density $(\frac{\mathrm{N}}{\mathrm{m}^3})$

G shear modulus (Pa)

p pressure (Pa)

S_0 constant

T temperature (°C)

T_0 temperature (°C)

U_1, U_2 boundary velocities in x direction $(\frac{\mathrm{m}}{\mathrm{s}})$

u_x, u_y, u_z fluid entraining speed in x, y and z direction $(\frac{\mathrm{m}^3}{\mathrm{t}})$

V_1, V_2 boundary velocities in y direction $(\frac{\mathrm{m}}{\mathrm{s}})$

W_1, W_2 boundary velocities in z direction $(\frac{\mathrm{m}}{\mathrm{s}})$

Z constant

Chapter 3

η dynamic viscosity (Pa·s)

μ friction coefficient

ω rotating speed (rad/s)

$\partial h/\partial\theta$ oil squeeze action $(\frac{\mathrm{m}}{\mathrm{rad}})$

σ combined surface roughness (μ m)

θ crank angle (deg)

θ_1 Vogel constant for given oil (°C)

a half of the ring width (m)

B ring carvature parameter $(\frac{1}{\mathrm{m}})$

b ring axial width (m)

c ring crown hieght (m)

$C_{1,down}$ integration constant in downward stroke (Pa·m^2)

$C_{1,up}$ integration constant in upward stroke (Pa·m^2)

$C_{2,down}$ integration constant in downward stroke (Pa)

$C_{2,up}$ integration constant in upward stroke (Pa)

C_d discharge coefficient through the orifice

D cylinder bore (m)

F_f friction force (N)

F_{hyd} hydrodynamic force acting on ring face (N)

$F_{ring,gas}$ force acting on the back side of the ring due to ring elasticity and gas pressure (N)

h nominal oil film thickness at ring and liner interface (m)

h_{min} minimum oil film thickness (m)

k Vogel constant for given oil (Pa·s)

K_c orifice discharge coefficient

l connecting rod length (m)

m gas mass (kg)

o ring crown offset (m)

p_1 combustion chamber pressure (Pa)

p_2 inter-ring gas pressure between frist and second ring (Pa)

p_3 inter-ring gas pressure between second and oil control ring (Pa)

p_4 crankcase pressure (Pa)

p_{down} pressure acting on lower edge of ring (Pa)

P_f power loss (W)

p_{gas} gas pressure (Pa)

p_o atmospheric pressure (Pa)

p_{sat} saturation pressure (Pa)

p_{up} pressure acting on upper edge of ring (Pa)

Q volume flow rate per unit width $(\frac{\mathrm{m}^3}{\mathrm{s}})$

r crank radius (m)

R_j gas constant(J/kgK)

S_p average piston speed $(\frac{\mathrm{m}}{\mathrm{s}})$

T temperature $(^\circ\mathrm{C})$

t time (s)

T_{BDC} bottom dead center temperature $(^\circ\mathrm{C})$

T_{TDC} top dead center temperature $(^\circ\mathrm{C})$

U piston velocity (m/s)

V volume (m^3)

x_1, x_2, x_3, x_4, x_e oil film shape parameters (m)

z_{owp} wrist-pin offset (m)

Chapter 4

α circumferential coordinate (Pa·s)

$\bar{F}$ dimensionless force

$\bar{M}$ dimensionless moment

$\bar{p}$ dimensionless pressure

$\ddot{e}_b$	acceleration at piston skirt bottom $(\frac{\mathrm{m}}{\mathrm{s}^2})$
$\ddot{e}_t$	acceleration at piston skirt top $(\frac{\mathrm{m}}{\mathrm{s}^2})$
$\ddot{x}$	piston axial acceleration $(\frac{\mathrm{m}}{\mathrm{s}^2})$
Δt	time step (s)
δ	dimensionless offset parameter
$\dot{E}_b$	dimensionless velocity at piston skirt bottom
$\dot{E}_t$	dimensionless velocity at piston skirt top
η	oil dynamic viscosity (Pa·s)
Λ	elongation ratio
ω	engine angular velocity $(\frac{\mathrm{rad}}{\mathrm{s}})$
θ	crank angle (deg)
c	skirt/liner clearance (m)
D	cylinder bore (m)
d_1	vertical distance of piston skirt top from wrist pin axis (m)
d_2	vertical distance of piston skirt top from piston center of gravity (m)
E_b	dimensionless eccentricity at skirt bottom
e_b	eccentricity at piston skirt bottom (m)
E_t	dimensionless eccentricity at skirt top
e_t	eccentricity at piston skirt top (m)
F_{ap}	piston inertial force in x direction (N)
F_{awp}	wrist pin inertial force in x direction (N)
F_{cr}	connecting rod force (N)

F_{fr} piston ring pack friction force (N)

F_{fs} friction force acting on piston skirt (N)

F_g gas force acting on piston (N)

F_h hydrodynamic force on piston skirt (N)

F_{zp} piston inertial force in z direction (N)

F_{zwp} wrist pin inertial force in z direction (N)

h nominal oil film thickness (m)

h_{min} minimum oil film thickness (m)

j_p piston rotational inertia about its center of gravity (kgm^2)

K coefficient

l connecting rod length (m)

l_{ps} piston skirt length (m)

M_{fr} piston ring pack friction moment about wrist-pin axis (Nm)

M_{fs} piston skirt friction moment about wrist-pin axis (Nm)

M_h hydrodynamic moment about wrist-pin axis (Nm)

M_{ip} piston inertial torque (Nm)

m_p piston mass (kg)

m_{wp} wrist-pin mass (kg)

o ring profile offset (m)

p hydrodynamic pressure (Pa)

p_{gas} gas pressure behind the ring (Pa)

R piston radius (m)

r crank radius (m)

U piston reciprocating velocity $(\frac{\text{m}}{\text{s}})$

z_{Gp} distance of piston center of gravity from piston symmetry axis (m)

z_{owp} wrist pin offset (m)

Chapter 5

α circumferential coordinate

β connecting rod angle (rad)

$\Delta\theta$ crank angle increment (deg)

$\Delta x, R\Delta\alpha$ spatial grid spacing in axial and circumferential coordinates (m)

δ dimensionless offset parameter

ε eccentricity ratio

η lubricant viscosity (Pa·s)

Λ elongation ratio

ω engine speed $(\frac{\text{rad}}{\text{s}})$

ω_b connecting rod big-end rotational speed $(\frac{\text{rad}}{\text{s}})$

ω_j journal rotational speed $(\frac{\text{rad}}{\text{s}})$

ϕ angle between normal load and line of the centers (rad)

τ shear stress (Pa)

θ crank angle (deg)

a_{pis} piston axial acceleration $(\frac{\text{m}}{\text{s}^2})$

c clearance (m)

e eccentricity (m)

F total load acting on journal (N)

F_{cr} connecting rod force (N)

F_{gas} gas force acting on piston (N)

F_h hydrodynamic force at bearing surfaces interface (N)

F_{rec} reciprocating inertial force due to piston mass (N)

F_{rot} rotational inertial force due to connecting rod big-end (N)

F_r radial hydrodynamic force component at bearing surfaces interface (N)

F_t tangential hydrodynamic force component at bearing surfaces interface (N)

h nominal oil film thickness (m)

J_1^{00} Booker journal bearing integral

L_x journal axial width (m)

m_{cr} connecting rod mass (kg)

m_{pin} wrist-pin mass (kg)

m_{pis} piston mass (kg)

p hydrodynamic pressure (Pa)

p_f power loss (W)

p_{gas} gas pressure (Pa)

r crank radius (m)

R_j journal radius (m)

t time (s)

U piston velocity $(\frac{\mathrm{m}}{\mathrm{s}})$

W normal load acting on journal (N)

x coordinate parallel to journal axis

Chapter 1

Introduction

1.1 Overview

Mechanical power loss at lubricated surfaces interface those execute sliding or rotating motions is one the remarkable issues that can be reduced to take steps to improve internal combustion engines (ICEs) efficiency. Tribological interactions between the piston ring assembly and liner are one of the major contributor to mechanical friction losses of ICEs. Hydrodynamic lubrication is predominant in mid-phase of engine strokes where bearing surfaces are separated by sufficient lubricant film and power loss is a consequence of viscous stress within the lubricant film. But in the vicinity of critical regions, top dead and bottom dead centers, lubrication mechanism is affected by squeeze action and boundary lubrication. In order to gain an estimation of ICEs performance at early steps of design analytical simulation can be a reliable tool that can become along designers and researchers. Besides, analytical investigation can prepare a guideline to direct engineers to realize where the improvement can be applied to have better performance in terms of fuel and emissions reduction. Improving fuel economy and promoting environment protection can be achieved by reducing engine mechanical loss, such as piston-cylinder system (PCS) friction. PCS includes piston ring pack, piston skirt but in this study connecting rod big end and main journal bearings lubrication have been also evaluated.

1.2 Problem statement

It is widely recognized that PCS followed by connecting rod big-end and main bearings are the major contributors to power losses and that there is a pressing need to gain insight into lubrication mechanisms. Therefore it is vital to understand the lubrication mechanism of these components. Experimental investigation as one approach can be adopted to conduct the test trials but requires time and it is costly. Analytical and numerical analyses of engine lubricated components lubrication and tribology would be considered as reliable tools. The modeling of PCS and journal bearings lubrication characteristics has prime importance because the development of analytical tools to assess the contribution of each influential parameters in friction losses would direct designers to improve ICE efficiency. The development of reliable engine friction model, that could be applied in transient engine simulations, would allow for predictions of actual engine output. Thus the present study is aimed to develop analytical models and numerical solutions to evaluate the piston ring assembly, connecting rod big-end and main bearings lubrication mechanisms.

1.3 Objectives of the research project

The main aim of this research project was to develop a mathematical model to examine reciprocating and rotating engine components lubrication including piston ring assembly, connecting rod big-end bearing and crankshaft main bearings over a range of loads (motored and fired condition), engine angular speeds and lubricant temperatures.

Specific aspects of the present research to address the above objectives are:

• To analyze the inter ring gas pressure (blow-by) to feed piston ring pack model as boundary pressures acting on each ring to evaluate piston ring pack lubrication;

• To construct and implement a piston ring pack lubrication model that accounts for three different scenarios. Fully flooded condition in which ring face is entirely engulfed by oil applying Full Sommerfeld boundary conditions. Second one, taking into account oil separation: ring face is partially covered by lubricant and some part of trailing is exposed to gas, without film rupture. For the last scenario, starvation and

cavitation has been considered. The effect of oil viscosity variation with temperature has been also incorporated in piston ring pack model;

• To conduct a statistical evaluation of ring geometry and elastic properties using classical design of experiment (DoE) and perform ANOVA analysis;

• To develop a model to examine piston secondary motion and lubrication taking into account the effect of piston ring pack friction;

• To develop a model to evaluate connecting rod big-end lubrication to avoid complexity and huge effort associated with Mobility method.

1.4 Organization of the dissertation

Structure of the thesis is organized in seven chapters that are briefly introduce as following:

CHAPTER 1 gives an overview of the PhD dissertation.

CHAPTER 2 looks into the lubrication mechanisms and describes four different types of possible lubrication regimes at bearing surface interface. Hydrodynamic (HL), elasto-hydrodynamic (EHL), mixed and boundary lubrication mechanisms are the possible lubrication and their properties are addressed in this chapter. Reynolds equation is derived and discussed in details. Numerical solution of Reynolds equation has been presented.

CHAPTER 3 describes the evaluation procedure of piston ring pack lubrication giving a true picture of piston ring pack tribological performance considering hydrodynamic lubrication at ring and liner interface. Inter ring gas analysis (blow-by) has been done to feed ring pack model as boundary conditions. Three distinct possible lubricant behavior are considered at rings and liner junction: fully flooded, oil separation condition as well as oil starvation and cavitation. Boundary lubrication has been considered at critical areas in which the load sustain with asperities contact top dead center (TDC) and bottom dead center (BDC). Design of experiment (DoE) is applied to statistically examine the effect of influential parameters that affect the ring lubrication.

CHAPTER 4 addresses piston skirt secondary motion due to unbalanced forces and moments acting in plane perpendicular to wrist-pin axis. The effect of wrist-pin

location, piston liner clearance, engine speed and oil viscosity have been studied. Piston skirt lubrication has been evaluated taking into account the effect of piston ring pack lubrication.

CHAPTER 5 evaluates connecting rod big-end and engine journal bearings. Two different approach has been used to define instantaneous journal and bush eccentricity. Reynolds equation and finite difference scheme have been used to define the hydrodynamic pressure at journal and bearing interface and calculate friction and power loss.

CHAPTER 6 briefly describes the experimental procedure to obtain data and compares them against the power loss contributed by piston ring assembly and connecting rod big-end, estimated by developed model.

CHAPTER 7 as final part of this study presents the conclusions arising from the current research along with suggestions for further development of possible topic that can be considered.

Chapter 2

Background

2.1 Lubrication mechanisms

Loaded reciprocating and rotating bodies can experience four distinct lubrication regimes in which each mechanism can be recognized with special characteristics that affect the total system performance such as load capacity, thermal and mechanical deformation of bearing surface and tribological behavior. In hydrodynamic lubrication (HL), or full film lubrication, the lubricant film is sufficiently thick to sustain loads and to separate the rotating and sliding bodies. Elasto-hydrodynamic lubrication (EHL) is a type of hydrodynamic lubrication associated with significant elastic deformation of coupled surfaces; it extensively alters the shape of the film thickness profile. Mixed lubrication is the transition region between EHL and boundary regimes in which the load is sustained by both lubricant film and asperity contacts. Mixed lubrication (ML) occurs in the presence of high load, low speed, or low viscosity due to high temperature. When the bearing surfaces come into contact under mixed lubrication, surface properties such as combined surface roughness and pressure flow factors become important considerations in the design of load carrying and sliding surfaces. Boundary lubrication (BL) deals with conditions where lubricant film is thin and the load is mainly or completely supported by asperity contacts [1, 2]. The dependence of friction coefficient and transition between lubrication regimes on fluid viscosity, η, the entrainment speed of the fluid, U and normal load in the tribological contact, p have been illustrated by Stribeck curve (Fig. 2.1). Figure 2.1 qualitatively

illustrates the different reciprocating and rotating engine components that typically enjoy distinct or combined lubrication mechanisms.

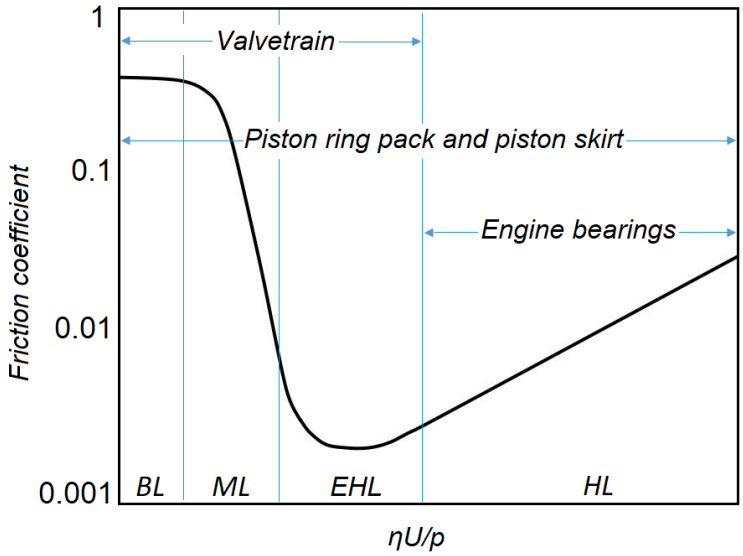

Fig. 2.1 Stribeck curve for engine components.

2.2 Lubricant properties

2.2.1 Lubricant viscosity

Imagine a one-dimensional flow of a fluid thin layer in which du is velocity difference between top and bottom of this thin film (Fig. 2.2). As the speed varies across film with respect to its thickness, du/dz is velocity gradient across the fluid which is called shear strain rate or simply strain rate, therefore:

$$\frac{du}{dx} = \frac{d}{dz}\left(\frac{dx}{dt}\right) = \frac{d}{dt}\left(\frac{dx}{dz}\right) = \frac{d\gamma}{dt} \tag{2.1}$$

therefore, $\frac{d\gamma}{dt}$ fraction is the strain rate which is related to the velocity gradient of the fluid flow.

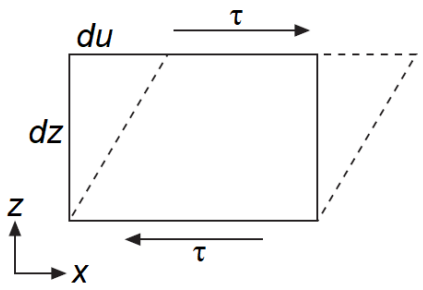

Fig. 2.2 Coordinate system and dynamic viscosity.

Considering shear modulus as:

$$G = \frac{\tau}{dx/dz} = \frac{\tau}{d\gamma} \tag{2.2}$$

For fluids, shear strain is replaced by shear strain rate, du/dz and G replaced by the dynamic viscosity (Pa·s), η is obtained as follow for a Newtonian fluid [3]:

$$\eta = \frac{\tau}{du/dz} \tag{2.3}$$

Kinematic viscosity (cSt) or (mm^2/s) is a frequently used unit of viscosity defined as:

$$\nu = \frac{\eta}{\rho} \tag{2.4}$$

where ρ is the lubricant density ($kg.m^{-3}$) .

2.2.2 Viscosity dependence on temperature

In contrary to gases, the fluid viscosity drastically reduces with temperature increment. There are some models to consider the viscosity variation with temperature those are briefly described as following.

The first and simplest one is called Reynolds viscosity equation:

$$\eta = \eta_0 \exp(-\beta \Delta\theta) \tag{2.5}$$

where η_0 is the viscosity at reference point (θ_0), β viscosity–temperature coefficient and $\Delta\theta$ the temperature increment (°C): it is worth to mention that Eq. (2.5) is valid over a very low temperature range.

Later in 1921, Vogel [3] introduced more accurate model that further analyzed by Cameron the take into account the viscosity dependence on temperature:

$$\eta(T) = a\exp\left(\frac{b}{T+c}\right) \tag{2.6}$$

where a (Pa·s), b (°C) and c (°C) are the constant for given oil that must be determined by manufacturer and T (°C) is the temperature.

2.2.3 Viscosity dependence on pressure

The effect pressure on fluids viscosity is most significant when there are concentrated contacts in which a large normal force is imposed on small area. In 1893 Barus [4] described how the lubricant viscosity varies with pressure at given temperature:

$$\eta = \eta_0\exp\left(\alpha p\right) \tag{2.7}$$

where η_0 is the oil viscosity at $p = 0$, α a constant for given oil so called pressure viscosity coefficient with units of (m^2/N) and p the pressure. This estimation can be quite inaccurate as α varies both with pressure and temperature.

In 1966 Roelands [5] introduced a model that later in 1985 was improved by Houpert [6] that is frequently used in numerical solutions. The exasperation takes into account the effect of both temperature and pressure on viscosity and it is similar to Eq. (2.7) but with a modified α:

$$\eta = \eta_0\exp\left(\alpha^* p\right) \tag{2.8}$$

where

$$\alpha^* = \frac{1}{p}\left[\ln(\eta_0) + 9.67\right]\left(-1 + \left(\frac{T-138}{T_0-138}\right)^{-s_0}(1+5.1e-09p)^z\right) \tag{2.9}$$

where z and s_0 are constants defined using Eqs. (2.10) and (2.11), p the pressure (Pa), T and T_0 the temperatures (K).

$$z = \frac{\alpha_0}{5.1e-09\Big[\ln(\eta_0)+9.67\Big]} \tag{2.10}$$

$$s_0 = \frac{\beta_0(T_0-138)}{\ln(\eta_0)+9.67} \tag{2.11}$$

where β_0 and α_0 are atmospheric temperature and pressure, supplied by the oil company [3].

2.2.4 Lubricant density

Knowing the lubricant density dependency on pressure has prime importance especially under severe condition. The density variation with respect to pressure can be governed using following formula:

$$\rho = \rho_0\left(1+\frac{0.6e-09p}{1+1.7e-09p}\right) \tag{2.12}$$

where p is in (N/m^2) and ρ_0 for oils is typically 870 (kg/m^2) at 20 °C. It is worth to notice that density dependency on temperature is found to be negligible in most lubrication analysis problems.

Fluid density variation dependence on both pressure and temperature can be expressed as follow:

$$\rho = \rho_0\left(\frac{1}{(1+\beta\Delta t)(1-\frac{\Delta p}{E})}\right) \tag{2.13}$$

where β is volumetric temperature expansion coefficient (1/°C), Δt the temperature change (°C), Δp the pressure change (Pa) and E is the difference between bulk modulus and liquid elasticity (N/m^2).

2.2.5 Effect of shear rate on viscosity

A Newtonian fluid is a fluid that its flow behavior is described as simple linear relation between shear stress and shear rate. This relationship is now known as Newton's Law of Viscosity. On the other hand, viscous stress arising from Newtonian fluid flow, at each point, is linearly proportional to the local strain rate.

In contrary if a fluid is recognized as non-Newtonian, its viscosity is affected by the shear rate and is dependent on strain rate or deformation over the time. Non-Newtonian behavior of fluids can be caused by several factors, all of them related to structural reorganization of the fluid molecules due to flow. Along the treating the fluid as Newtonian, also laminar flow has been assumed to be exist.

2.3 Reynolds equation

In 1886, Osborne Reynolds successfully proved that hydrodynamic pressure generated due to viscous shear rate within the lubricant can physically separate two sliding surfaces. The brief derivation of Reynolds equation is presented as following.

Reynolds applied mass conservation low:

$$\frac{\partial \rho}{\partial t} + \frac{\partial}{\partial x}(\rho u_x) = 0 \tag{2.14}$$

where ρ and u_x are the fluid density and entraining speed in x direction, respectively.

Then he took next step using conservation of linear momentum as:

$$\rho\left(\frac{\partial u_x}{\partial t} + u_y\frac{\partial u_x}{\partial y}\right) = \rho f_x + \frac{\partial \sigma_{ij}}{\partial y} \tag{2.15}$$

where f_x is the external mass force density, and σ_{ij} the stress tensor. Eq. (2.15) creates three relationships along 3D space.

For common Newtonian fluids, the fluid rheological behavior can be written as:

$$\sigma_{ij} = \left(-p - \frac{2}{3}\eta\frac{\partial u_z}{\partial z}\right)\delta_{ij} + \eta\left(\frac{\partial u_x}{\partial y} + \frac{\partial u_y}{\partial x}\right) \tag{2.16}$$

where η is the absolute viscosity, p the hydrostatic pressure, and δ_{ij} the Kroenecker delta defined as:

$$\begin{cases} \delta_{ij} = 1, & \text{for} \quad i = j \\ \delta_{ij} = 0, & \text{for} \quad i \neq j \end{cases}$$

By substituting Eq. (2.16) into Eq. (2.15) and considering the constant fluid viscosity, the Navier-Stokes equation can be obtained as:

$$\rho\left(\frac{\partial u_x}{\partial t} + u_y\frac{\partial u_x}{\partial y}\right) = \rho f_x - \frac{\partial p}{\partial x} + \eta\left(\frac{\partial^2 u_x}{\partial z \partial z} + \frac{1}{3}\frac{\partial^2 u_z}{\partial z \partial x}\right) \tag{2.17}$$

Considering constant density or incompressible flow, Eq. (2.17) can be further simplified as:

$$\rho\left(\frac{\partial u_x}{\partial t} + u_y\frac{\partial u_x}{\partial y}\right) = \rho f_x - \frac{\partial p}{\partial x} + \eta\left(\frac{\partial^2 u_x}{\partial z^2}\right) \tag{2.18}$$

considering corresponding continuity equation as

$$\frac{\partial u_x}{\partial x} = 0 \tag{2.19}$$

Combining Eq. of motion (2.18), with the continuity Eq. (2.19) gives a complete mathematical expression of flow. Due to nonlinear convective acceleration terms, exact solutions need huge mathematical effort, considering laminar flow between bearing surfaces, closed-form solution is available. Reynolds equation addressed thin film lubrication characteristics at narrow channels interface.

Considering the following assumptions

• Body forces are neglected as the narrowness of the gap is presented at bearing surfaces interface which means small elemental volumes;

• Constant pressure across the film thickness as the film is thin;

• Lubricant is considered as Newtonian fluid that encourages the elimination of slip and boundaries;

• Flow is laminar which is encourage lower Reynolds number;

• As the oil film is thin, pressure can be assumed to be constant across the film and therefore fluid density variation with pressure can be assumed to be constant;

• Fluid inertia is neglected as the film thickness is thin and has negligible mass, therefore gravity forces can be neglected;

• As the lubricant is Newtonian, high shear rates are not present and fluid viscosity variation with respect to temperature can be neglected.

Navier-Stokes Eq. (2.18) can be written as following:

$$-\frac{\partial p}{\partial x}+\eta\left(\frac{\partial^2 u_x}{\partial z^2}\right)=0 \tag{2.20}$$

For most of bearing geometries, dimensional analysis indicates that terms of order h/W or h/B are second-order and less than 10^{-4} in which h is the film thickness, and W and B are the width and length of bearing area. Considering constant pressure across the film thickness, Eq. (2.20) applied to the coordinate system in Fig. 2.3 yields the simplified momentum equations as follow:

$$\frac{\partial^2 u}{\partial y^2}=\frac{1}{\eta}\frac{\partial p}{\partial x} \tag{2.21}$$

$$\frac{\partial^2 v}{\partial y^2}=0 \tag{2.22}$$

$$\frac{\partial^2 w}{\partial y^2}=\frac{1}{\eta}\frac{\partial p}{\partial z} \tag{2.23}$$

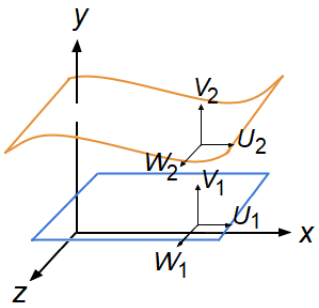

Fig. 2.3 Coordinate system and notations.

Integration of the above equations with no-slip boundary velocities gives three flow velocity components as:

$$u = \frac{1}{2\eta}\frac{\partial p}{\partial x}y(y-h) + U_1 + \frac{y}{h}(U_2 - U_1) \tag{2.24}$$

$$v = (V_2 - V_1)\frac{y}{h} + V_1 \tag{2.25}$$

$$w = \frac{1}{2\eta}\frac{\partial p}{\partial z}y(y-h) + W_1 + \frac{y}{h}(W_2 - W_1) \tag{2.26}$$

where U_1, U_2, V_1, V_2, W_1 and W_2 are the boundary velocities as shown by Fig. 2.3. Substituting Eqs. (2.24) to (2.26) in Eq. (2.19) and integrating across the lubricant film thickness and applying Leibnitz's rule, the generalized Reynolds equation treating the lubricant as an incompressible fluid can be obtained as:

$$\begin{aligned}\frac{\partial}{\partial x}\left(\frac{h^3}{\eta}\frac{\partial p}{\partial x}\right) + \frac{\partial}{\partial z}\left(\frac{h^3}{\eta}\frac{\partial p}{\partial z}\right) = 6(U_2 - U_1)\frac{\partial h}{\partial x} + 6(W_2 - W_1)\frac{\partial h}{\partial z} + \\ +6h\frac{\partial (U_1 + U_2)}{\partial x} + 6h\frac{\partial (W_1 + W_2)}{\partial z} + 12\frac{\partial h}{\partial t}\end{aligned} \tag{2.27}$$

The two terms on the left-side are Poiseuille terms that describe net flow rates due to pressure gradients. The first two terms on the right-side are physical "wedge" terms, the third and fourth terms are "stretch" terms. Those four terms consist of the Couette terms describing the net entraining flow rates due to surface velocities. The last term is the net flow rate due to a squeezing action as:

$$\frac{\partial h}{\partial t} = (V_2 - V_1) \tag{2.28}$$

2.4 Numerical solution of Reynolds equation

In simple problem there is analytical or exact solution for Reynolds equation, but in sophisticated circumstance, numerical solutions come along. Finite difference scheme (central finite difference) is one of the most promised method that can

be employed to solve Reynolds equation. This method is briefly described here. Considering two plates that the top one is sliding and the bottom plate is stationary, Reynolds equation can be written as follows:

$$\frac{\partial}{\partial x}\left(\frac{h^3}{\eta}\frac{\partial p}{\partial x}\right)+\frac{\partial}{\partial y}\left(\frac{h^3}{\eta}\frac{\partial p}{\partial y}\right)=6U\frac{\partial h}{\partial x}+6V\frac{\partial h}{\partial y}+12\frac{\partial h}{\partial t} \tag{2.29}$$

.

Finite difference approximation for Eq. (2.29) can be developed as follows for each term:

$$\frac{\partial}{\partial x}\left(\frac{h^3}{\eta}\frac{\partial p}{\partial x}\right)\approx\frac{h^3_{i+\frac{1}{2},j}\frac{p_{i+1,j}-p_{i,j}}{\Delta x}-h^3_{i-\frac{1}{2},j}\frac{p_{i,j}-p_{i-1,j}}{\Delta x}}{\eta\Delta x} \tag{2.30}$$

$$\frac{\partial}{\partial y}\left(\frac{h^3}{\eta}\frac{\partial p}{\partial y}\right)\approx\frac{h^3_{i,j+\frac{1}{2}}\frac{p_{i,j+1}-p_{i,j}}{\Delta y}-h^3_{i,j-\frac{1}{2}}\frac{p_{i,j}-p_{i,j-1}}{\Delta y}}{\eta\Delta y} \tag{2.31}$$

$$\frac{\partial h}{\partial x}\approx\frac{h_{i+\frac{1}{2},j}-h_{i-\frac{1}{2},j}}{\Delta x} \tag{2.32}$$

$$\frac{\partial h}{\partial y}\approx\frac{h_{i,j+\frac{1}{2}}-h_{i,j-\frac{1}{2}}}{\Delta y} \tag{2.33}$$

for spatial derivatives, and forward differences:

$$\frac{\partial h}{\partial t}\approx\frac{h^{t+\Delta t}_{i,j}-h^t_{i,j}}{\Delta t} \tag{2.34}$$

In explicit form, Reynolds equation with above the difference approximations of Eqs. (2.30) to (2.34) gives:

$$p_{i,j} = \Big(a_1 p_{i+1,j} + a_2 p_{i-1,j} + a_3 p_{i,j+1} + a_4 p_{i,j-1} - a_5\Big)/a_0 \tag{2.35}$$

where

$$\begin{aligned}
a_0 &= \left[\frac{(\frac{(h_{i,j+1}+h_{i,j})}{2})^3}{(\Delta x)^2} + \frac{(\frac{(h_{i,j}+h_{i,j-1})}{2})^3}{(\Delta x)^2} + \frac{(\frac{h_{i+1,j}+h_{i,j}}{2})^3}{(\Delta z)^2} + \frac{(\frac{h_{i,j}+h_{i-1,j}}{2})^3}{(\Delta z)^2}\right] \\
a_1 &= \left[\frac{(\frac{h_{i+1,j}+h_{i,j}}{2})^3}{(\Delta x)^2}\right] \\
a_2 &= \left[\frac{(\frac{h_{i,j}+h_{i-1,j}}{2})^3}{(\Delta x)^2}\right] \\
a_3 &= \left[\frac{(\frac{h_{i,j+1}+h_{i,j}}{2})^3}{(\Delta y)^2}\right] \\
a_4 &= \left[\frac{(\frac{h_{i,j}+h_{i,j-1}}{2})^3}{(\Delta y)^2}\right] \\
a_5 &= \left[6\eta U\frac{h_{i+1,j}+h_{i-1,j}}{2\Delta x} + 6\eta V\frac{h_{i,j+1}+h_{i,j-1}}{2\Delta y} + 12\eta\frac{h_{i,j}^{t+\Delta t}+h_{i,j}^{t}}{\Delta t}\right]
\end{aligned} \tag{2.36}$$

Figures 2.4 and 2.5 show the finite difference nodes distribution over the bearing surface and calculated hydrodynamic pressure at piston skirt and liner interface using finite difference scheme, respectively.

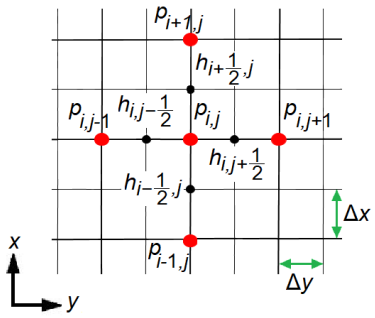

Fig. 2.4 Finite difference nodes over the bearing surface.

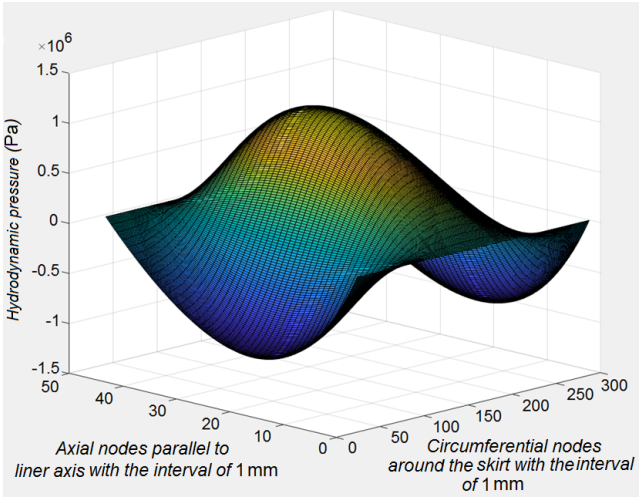

Fig. 2.5 Hydrodynamic pressure at piston skirt and cylinder wall junction at engine speed of 2000 rpm.

2.5 Summary

An overview of lubrication mechanisms and lubricant properties have been addressed. Generalized Reynolds equation was derived, and a numerical solution method was described.

Chapter 3

Piston Ring Pack Lubrication and Tribology

3.1 Introduction

Internal combustion engines are considered as one of the main power sources for transportation. Improvement of the internal combustion engine (ICE) efficiency has prime importance due to strict environmental legislation and energy costs. Any reduction in oil consumption, friction power losses and emissions results in improving engines' performance and durability. Mechanical power loss at the interface of lubricated surfaces becomes an attractive domain to study and research in the field of internal combustion engines engineering. Friction reduction at lubricated surfaces is one of the most cost-effective solution that can be adopted to reduce gas emission and improve ICEs efficiency. Therefore this strategy encourages the automotive industries and researchers to evaluate tribological performance and take steps to design productive and efficient ICEs. In all reciprocating engines from the first-generation immersion to high-performance ones, the main function of piston rings is to strengthen piston and cylinder sealing and prevent the leakage. There is no denying that piston-cylinder system is the major contributor to total mechanical power loss. Piston rings enjoy hydrodynamic, mixed and boundary lubrication during piston stroke. Hydrodynamic lubrication at ring and liner interface has been evaluated in this study considering different interaction of lubricant and ring face, such as fully flooded, partial engulfment and oil starvation and cavitation.

3.2 State of the Art

3.2.1 Hydrodynamic and elasto-hydrodynamic lubrication

Hydrodynamic theory considering speed and load variation has been applied to calculate instantaneous oil film thickness and hydrodynamic pressure. The generated hydrodynamic pressure is due to fluid incompressibility and squeeze action. Fully flooded boundary conditions were applied to model and two different approaches were adopted to examine the reliability of the developed model. At first step, piston was stationary and the cylinder reciprocated across the piston to evaluate the effect of speed, load protocol, and temperature applying movable anode tube. As second validation method oil film thick at ring/liner interface was measured using a circuit to define electric resistance between the liner and the ring end gap size variation [7–9].

Ting and Mayer in [10, 11] conducted an analytical evaluation to study the cylinder bore wear patterns. The model comprises blow-by, lubrication mechanisms, and piston side thrust force analysis. Generated hydrodynamic pressure at ring and liner interface is governed by lubrication theory relied on average Reynolds equation. Since the model is well developed in detail, has capability to be applied as reliable tool to other reciprocating engines.

Dowson et al. [12] considered elasto-hydrodynamic lubrication of piston ring, in which lubricant was treated as non-Newtonian fluid. It is assumed that the oil viscosity mostly varies along the liner with temperature, to make allowances to consider the effect of pressure on viscosity. It was found that minimum oil film thickness under elasto-hydrodynamic lubrication is thicker in comparison to hydrodynamic regime.

In contrary to the method introduce by Dowson [12], a system of non-linear algebraic equation that includes Reynolds and load equations has been used to evaluate ring tribological performance [13]. A finite-element scheme relying on the Newton-Raphson-Murty algorithm was used to evaluate ring tribological performance under hydrodynamic and elasto-hydrodynamic lubrication. The model is able to calculate instantaneous hydrodynamic pressure and minimum oil film thickness at each crank angle.

Jeng [14, 15] introduced a comprehensive numerical study of piston ring lubrication considering fully flooded and oil starvation. The effects and interaction between ring geometry, ring elastic characteristics, and operating conditions were considered to evaluate piston ring pack tribological performance. A system of two nonlinear differential equations including Reynolds equation and flow continuity was applied as governing equations. Influential ring geometry parameters considered in these studies were ring width, crown height and ring profile offset.

Richardson and Borman [16] carried out an analytical and experimental observation to gain insight into piston ring tribology. Lubricant was treated as a Newtonian fluid. A good deal was found between Reynolds boundary conditions and experimental data.

Wakuri et al. [17] considered an axisymmetrical piston ring lubrication model, taking into account oil starvation and lubricant viscosity variation with respect to temperature. Temperature gradient and oil viscosity variation along the liner have been incorporated by model. It was proved that oil starvation plays an important role and affects oil film thickness and viscous friction.

As the development of compact engines with high efficiency is in progress, ring wear has prime importance that affects engine tribology. Therefore, evaluation of lubrication mechanisms and how friction contributes the ring and liner wear, become an interesting area for researchers. Chung et al. [18] analytically evaluate piston ring wear and assumed linear relationship between ring wear and friction force acting on ring face. The main aim of this study was to evaluate the effect of power output and engine speed on ring wear rate.

Taylor et al. [19, 20] conduct a numerical and experimental investigation to study the effect of viscosity variation with respect to temperature and shear rate. Considering circumferential uniform oil film thickness, 1-D Reynolds equation neglecting squeeze action was applied as governing equation. Oil starvation without cavitation or oil rupture was considered using modified Reynolds separation boundary conditions. It is observed that the presence of cavitation in the film, is due to lubricant incapacitation to sustain large and continuous negative pressure.

Yang and Keith [21] performed a numerical observation considering elasto hydrodynamic lubrication similar to the one carried out by Dowson in 1983 [12], with the difference of taking into account cavitation. The model enables the determination of full film, cavitation, and pressure reformation regions using mass conservation.

Besides, the approach incorporates the effect of viscosity variation with temperature and elastic deformation of bearing surfaces.

In contrary to most of studies considering piston/cylinder axisymmetric, Ma et al. [22, 23] conducted an analytical investigation to examine the effects of bore out-of-roundness. The model relies on lubrication theory under hydrodynamic lubrication applying the finite difference method. Axial and circumferential variation of oil film thickness were incorporated into the nominal oil film thickness equation. It was concluded that more realistic assumptions such as oil starvation and cavitation, would improve the model accuracy.

Yang and Keith in [24, 25] presented a non-axisymmetric elasto-hydrodynamic model to take into account oil rupture and ring elastic properties. Ring was treated as deformable and rigid to comprise the ring elastic properties. Elliptic cylinder liner has been assumed and Reynolds equation was employed to evaluate oil flow rate over the liner and generated hydrodynamic pressure. The results showed that minimum film thickness is thin in non-axisymmetric model due to non-uniform hydrodynamic pressure.

Harigaya et al. [26] evaluate piston ring/liner interface lubrication applying thermo-hydrodynamic lubrication. As oil film temperature and viscous dissipation are affected by ring and liner temperature, lubricant viscosity variation was taken into consideration. Reynolds equation and energy equations have been used as governing equations to evaluate oil film temperature and generated heat by viscous dissipation.

In [27], a non-axisymmetric lubrication analysis considering starvation relying on flow continuity algorithm and mass conservation principle to evaluate piston-ring lubrication has been conducted. To examine approach reliability, lubricant flow continuity was observed under both steady-state and dynamic loading conditions and the results were compared with the Reynolds solution. Finite difference scheme and open cavitation without reformation boundary conditions were applied to model formulation considering unchanged oil viscosity and density.

Brown and Hamilton [28] developed a numerical scheme considering hydrodynamic lubrication to calculate minimum oil film thickness using fully flooded and starved boundary conditions. Besides, experimental trials has been conducted to measure minimum oil thickness. The comparison between calculated and measured values reveals that the difference is due to oil starvation.

Ma et al. in [22] performed a piston ring lubrication analysis using modified flow continuity model with consideration for non-uniform circumference and variable film thickness. To consider bore geometry and distortion, a bore geometry model and an approximate approach to evaluate ring conformability were incorporated into the flow continuity model. The results highlight that bore distortion significantly reduces the power loss and increases the oil consumption. The effect of relative ring location, engine speed, ring geometrical and elastic characteristics, rings interaction, and liner temperature on lubrication and tribological performance were examined [23, 29]. Ma et al. in [30] summarized the development and improvement of their model [22] and examined the effect of bore distortion, ring conformability and ring profile variation.

Han and Lee [31] performed a piston ring lubrication investigation applying open-end boundary conditions. Observation revealed that the effective ring width was reduced about 20-30% for the same strokes considering fully flooded condition but due to the squeeze effect, effective ring become equal to the entire ring width at top dead center (TDC) and bottom dead center (BDC). Flow continuity between oil inlet and outlet was satisfied by open-end assumption.

Esfahanian et al. [32] presented a numerical scheme to solve a system of two non-liner equations including Reynolds equation and force equilibrium under hydrodynamic lubrication. The detailed non-dimensional approach of Reynolds equation was developed and to being more realistic, cavitation within the oil film was incorporated.

A numerical scheme has been presented [33, 34] based on lubrication theory to study the tribological performance of piston ring-pack and piston skirt. The output of the piston ring model results in Stribeck diagram to examine the effect of oil viscosity and ring geometry variations and parameter dependencies and interactions. The piston skirt model analyses the effect of influential parameters and their interactions.

Sawicki and Yu [35] applied the model introduced by Jeng [14] to perform an analytical study of piston ring lubrication using mass conservation. In order to consider enclosed cavitation, Jakobsson-Floberg-Olsson boundary conditions [36, 37] were used to gain an accurate calculation of friction force, power loss, and flow rate. A system of five nonlinear equations have been derived to define the mass fraction of cavitated regions, film rapture and film reformation position.

Tian in [38, 39] adopted a numerical method to study the effect of piston ring dynamic behavior and its effect on ring/liner tribology. Dynamic behaviors of the ring was evaluated in terms of ring flutter and ring collapse. The impacts of influential parameters, such as ring twist, ring torsional stiffness, and ring-groove clearance on ring flutter were comprehensively discussed. Ring radial collapse was empirically treated for critical parameters to eliminate ring radial collapse effect. The effects of oil transport with emphasizing on oil availability in the vicinity of TDC on wear and oil consumption have been examined.

Gamble et al. [40] analyzed oil availability and flow between piston ring and liner. In contrary to most studies that only consider oil flow through the piston ring and liner interface, the approach takes into account additional oil flow paths and gas blow-by interactions. These considered additional oil flow path were circumferential flow on piston lands, oil accumulation, and axial oil flow through the ring gap.

Mufti et al. [41] presented a piston assembly friction model and designed a test-bench to evaluate the friction loss of the ring pack and piston skirt. Axial symmetry and uniform oil film thickness and cavitation and reformation boundary conditions were considered under hydrodynamic lubrication. A system of two equations, comprising force equilibrium and 2-D Reynolds equations has been solved to calculate piston skirt friction loss.

Livanos and Kyrtatos in [42] presented an instantaneous engine power loss model, including ring-pack, piston skirt, main bearings, connecting rod bearings, and valve train based on lubrication theory considering quasi-steady-state. This model is able to predict complete engine friction either in crank angle or in engine cycle resolution by computing Friction Mean Effective Pressure (FMEP).

Later in 2007, Livanos and Kyrtatos [43] developed a model to evaluate engine friction components relying on lubrication theory to consider detailed geometry and piston dynamics. In conflict to previous investigations that proved the most friction losses is contributed by the piston ring-pack, their findings provide evidence that the piston skirt made the largest contribution to total power loss.

Mishra et al. in [44] conducted a piston ring lubrication analysis under elasto-hydrodynamic regime using detailed calculations for ring elastic properties and gas pressure behind the ring.

In contrast to many models that are developed based on lubrication theory and solving Reynolds equation, Felter in [45] developed a free surface model based on Navier-Stokes equation. Two dimensional Navier-Stokes equations were used to govern fluid flow with dynamic viscosity. The drawback of this model is that simulation does not consider cavitation and is valid only in its absence.

Oil starvation occures under circumstances such as absence or other inaccessibility of adequate amount of lubricant or when piston speed is too high. Kumar et al. [46] studied the effect of oil starvation on friction coefficient and minimum oil film thickness under elasto-hydrodynamic regime neglecting the impact of squeeze action at different operating condition. The model is adjusted to incorporates oil density and viscosity variations with respect to pressure.

The accurate evaluation of oil film thickness with adequate lubrication properties results in an optimum reduction in oil viscosity without disturbing lubrication action. An investigation based on lubrication theory [47] has been conducted to investigate the dependency of oil film thickness on lubrication properties such as oil viscosity and temperature. In order to accurately estimate minimum oil film thickness and proportion boundary friction losses, the inclusion of the squeeze effect was considered in the model.

3.2.2 Mixed and boundary lubrication

The main disadvantages associated with the stochastic theories those are used to evaluate the effect of surface roughness on mixed lubrication, encourages the new approaches to be introduced. The main advantage of these new methods is that, with known statistical distribution of asperities any type of surface can be analyzed [48, 49].

Dowson et al. [50] introduced a model to estimate the oil film thickness, friction force, flow continuity for a single ring and a set of piston rings considering mixed lubrication with a constant friction coefficient. Latter in 1980, the model was modified by Ruddy et al. [51] adding ring twist and considering the effects of ring groove distortion and wear on piston ring tribology.

Rohde [52] conducted an observation to study the effect of surface roughness on piston ring lubrication motivated by Patir and Cheng's research [53]. The model relied on lubrication theory to examine a piston ring-pack tribological performance

considering different operating conditions. It was highlighted that surface texture has a remarkable effect on piston ring lubrication.

Miltsios et al. [54] applied finite element method to solve the governing Reynolds equation to evaluate piston ring lubrication. Fully flooded boundary conditions and two dimensional Reynolds equation were applied as governing equations. Mixed lubrication was considered where the film thickness reduced to a certain value with respect to composite surface roughness. The alteration of the ring profile due to ring tilting in groove considered to stay toward more realistic condition.

Keribar et al. [55] conducted a comprehensive and combine treatment of the HL and boundary lubrication models to examine the piston ring-pack tribology. The model is a multi-purpose analysis which has capability to determine the effect of ring axial, radial and twist dynamics, inter-ring gas blow-by, surface roughness and lubrication mechanism on minimum oil film thickness. The Greenwood-Tripp model [56] was employed to study the effect of surface roughness and asperity contact with Gaussian distribution of asperity heights considering fix asperity radius of curvature.

Sui and Ariga [57] examined the effect of ring surface topology on piston ring tribology considering mixed lubrication. To validate the reliability of the model, a moving liner test-rig was used and different types of surface roughness orientation (transversal, isotropic and longitudinal) were analyzed. The results provide evidence that surface topology is an influential parameter and oil film thickness and friction are sensitive to surface roughness.

A non-axially-symmetric piston-ring lubrication model [58] with an arbitrary free ring shape when it fits into the cylinder was developed and considered as a Linear Complementary Problem (LCP). The LCP solution was incorporated with lubrication theory to determine the oil film thickness and distributed contact load over the ring face area. The model examined the effect of liner static distortion, gas pressure variation, and lubricant starvation under mixed lubrication. Greenwood-Tripp's model [56] was used to calculate the average contact pressure considering a Gaussian distribution of asperities.

Regarding to the fact that after a running-in period, the cylinder wall is received plateau surface texture, the honed surface can be modeled by means of appropriate amplitude, direction, and spatial frequency. Michail and Barber [59] presented a model to evaluate lubrication mechanism and the effect of honing parameters on oil film thickness and engine tribology performance [60]. Later, the effect of surface

roughness was examined using Patir-Cheng model [53] to define flow factors. It was assumed that the ring has a smooth surface and only the roughness of the liner was incorporated with lubrication theory, therefore the combined roughness was equal to the roughness of the liner. The dependency of oil film thickness on surface parameters and operating conditions was addressed.

Knopf et al. [61] conducted an analytical observation to study the effect of liner surface texture on the lubrication of ring-liner conjunction. With alteration in honing angle, it is possible to find a good compromise between oil transport and hydrodynamic pressure build-up. The investigation proved that surfaces with asymmetrical amplitude density distribution and transversely oriented topography improve lubrication mechanism.

Gulwadi [62] numerically studied the interactions between different lubrication regimes (hydrodynamic, mixed, and boundary), oil availability, and ring dynamics applying a mass-conserving algorithm to take into account cavitation. The model encourages the calculation of oil accumulation at the leading and trailing edges of the piston ring to estimate oil consumption.

Priest et al. [63] developed a model to evaluate piston ring dynamics, lubrication, and wear in an interactive fashion. The model firstly evaluate the lubrication of new and worn rings at constant speed and load, to introduce wear factor to consider ring profile alteration. Wear factor is defined in terms of material properties, surface topography, lubricant and operating condition. The model considering wear factor, was used to examine the lubrication and wear of the top compression ring in the same engine.

Later in 2000, Priest et al. [64] evaluate the model sensitivity to different boundary conditions those encourage the consideration of cavitation in the lubricant film. The applied boundary conditions were full Sommerfeld, Reynolds cavitation, flow separation, and modified Reynolds separation. Axisymmetric analysis was conducted on a single compression piston ring with a convex profile. It was proved that different cavitation descriptions in piston lubrication models affect hydrodynamic pressure profile, lubricant film boundaries, oil film thickness, oil flow and friction.

Gulwadi [65] made effort to study piston ring-pack tribological performance and interactions between oil consumption, blow-by, and power loss considering mixed lubrication. Force equilibrium and Reynolds equations were governed problem. Power losses were expressed in terms of hydrodynamic and boundary lubrication.

Oil consumption is contributed to by oil evaporation taking into account the effect of oil film thickness, inter-ring gas pressure, temperature and liner thermal properties.

A mixed lubrication model was introduced to understand contact mechanisms and lubrication to improve design and efficiency [66]. The model divides the contact area into two distinct regions, the hydrodynamic region and the asperity contact region. In the hydrodynamic region, oil pressure is governed by Reynolds equation. For mixed lubrication where oil film thickness is null, a simple mathematical description of the dry contact problem has been applied. The influence of geometry, surface roughness, and surface deformation were implicitly taken in the nominal oil thickness expression.

Akalin and Newaz [67, 68] used average Reynolds equation incorporating the Greenwood-Tripp asperity contact model [56] to analyze piston ring lubrication. The model encourages to take into account the considerations of the boundary conditions with respect to crank angle or piston displacement and cavitation occurrence probability. In some crank angles, especially in dead centers where the squeeze action dominates and prevents cavitation occurrence, fully flooded boundary condition were applied to ignore cavitation within oil film thickness. For other crank angles, Reynolds boundary conditions were used to consider cavitation, but this approach just takes into account the oil film rupture and not the oil film reformation.

Xu et al. [69] conducted a numerical study considering two approaches to evaluate lubrication mechanism at piston ring and liner interface. In the first method, the effect of surface roughness under mixed lubrication has been investigated using stochastic rough contact. In the second one, an effort was made to evaluate lubricant film rupture and cavitation taking into account surface topographies of ring and liner. Comparing the findings with experimental approved that the top compression ring can work under hydrodynamic, mixed and boundary lubrication throughout the engine cycle with respect to surface irregularities.

Bolander et al. [70] considered mixed lubrication model applying Elrod cavitation boundary conditions. A stochastic/deterministic model has been used to examine asperities contact and their effects on lubrication mechanism. The model modified the conventional stochastic model to apply Gaussian distribution. The impact of speed, load, and surface topography have been evaluated analytically and experimentally.

Chong et al. in [71] applied Erold algorithm to determine correlations between starvation and cavitation. Uniform radial loading was taken into account and piston and ring dynamics were neglected. The Elrod algorithm was incorporated by Reynolds equation assuming laminar flow of lubricent. The approach considers lubricant viscosity and density variation, and three different algorithms (transient Reynolds, steady-state modified Elrod and transient modified Elrod) have been examined.

A solution to isothermal mixed lubrication of compression ring and liner using Patir-Cheng average flow model [53] has been presented [72]. The effect of ring face profile and wear on ring tribology was evaluated. The approach takes into account oil starvation and non-axisymmetric piston and bore.

Morris et al. [73] presented an analytical thermal model and numerical solutions for an average flow model. It was concluded that friction losses are contributed to by viscous shear under low temperture condition, but boundary friction losses dominate at high temperature operating conditions. The model is based on lubrication theory considering variation of lubricant viscosity with temperature.

Guo et al. [74] conducted numerical and experimental investigation of piston ring tribology under mixed lubrication. The model accounts elastic and elasto-plastic deformation of the ring and cylinder wall. Lubrication theory was incorporated with the Greenwood-Tripp model [56], and applied as governing equation. This model eccourges the consideration of both fully flooded and starved-lubrication conditions.

Ahmed et al. [75] evaluated the effect of piston ring dynamics on piston ring tribology under mixed lubrication. Dynamic analysis software Excite Designer by AVL was applied to analyse piston ring dynamic influence. The model considers variations in lubricant viscosity with respect to temperature using Vogel's equation and oil consumption. The approach accounts the impacts of engine speed, viscosity grades, surface roughness, and piston ring dynamics on the tribological performance of piston ring-pack.

Gu et al. [76] suggested that friction reduction can be obtained using ono-flat textured top compression ring as they conducted an investigation to study the effects of surface properties under mixed lubrication considering the lubricant supply. The study has been performed on full and partial textured non-flat ring under steady state and engine-like conditions.

Fluid-structure interaction analysis has been performed to solve Navier–Stokes equation considering hydrodynamic lubrication. Lubricant was treated as monograde and multigrade oils to study the effects of oil viscosity on the generated hydrodynamic pressure at ring and liner interface. Power law lubricants, which act in non-Newtonian shear has been used during the solution of Navier–Stokes equation [77].

Zavos and Nikolakopoulos [78] introduced a thermo-mixed hydrodynamic model incorporating a CFD model to evaluate top compression ring lubrication. The effects of main geometrical parameters of piston assembly system has been examined which are obtained by a 3D coordinate measuring machine. Navier–Stokes equations and energy equation have been solved via developing a 2D axisymmetric CFD/ FLOTRAN model imposing realistic boundary conditions to simulate in-plane dynamic motion.

Bewsher et al. [79] evaluated the application of cylinder de-activation (CDA) on emission control. To consider the effects of CDA a two dimensional numerical model has been used to evaluate hydrodynamic lubrication at piston and liner interface.

Yang et al. [80] conducted a comprehensive study to evaluate the effects of oil storage of the cross-hatched texture to develop flow continuity lubrication model for the piston ring pack. A two-dimensional two-scale mass-conserving homogenized mixed lubrication model has been developed to take into account the impact of the cross-hatched texture and plateau roughness. Oil availability to each ring was determined by means of oil transport analysis and trapped oil in texture was treated as an extra oil supply to the contact interface.

Gu et al. [81] numerically examined the interaction of coating and texturing on the tribological performance of piston rings. A thermal mixed lubrication model has been presented to study the effects of the coating's thermal and mechanical properties under the cold and warm engine operating conditions.

A direct method has been presented to measure piston ring pack and noise in an air-cooled single cylinder gasoline engine. PRA friction has been measured by means of strain gauge mounted on external surface of the liner and noise was captured using a microphone bonded on thrust side [82].

Zavos and Nikolakopoulos conducted a CFD model considering ring deformations measured via experimental investigation employing a strain gauge through the

cylinder bore. The observation evaluates the tribological performance of thin top compression ring under mixed and hydrodynamic regimes. It was highlighted that reliable prediction of ring friction especially at TDC requires adequate consideration of surface roughness [83].

The modified Elrod algorithm for Jakobsson–Floberg–Olsson (JFO) cavitation boundary conditions has been used to solve the Reynolds equation and made comparison between two-dimensional computational fluid dynamics model and one-dimensional Reynolds model. The effects of surface texture has been examined to evaluate piston compression ring tribology [84].

In order to examine the effect of oil availability and extent of starvation a two-dimensional hydrodynamic model has been developed to evaluate film thickness, friction and total power loss. It was highlighted that oil starvation happens due to two main sources. First, due to a physical lack of inlet meniscus and second, due to reverse flow at the inlet wedge significantly affecting the prevailing conditions from the generally assumed idealized boundary conditions [85].

Bewsher et al. [86] evaluated the effects and interaction of the deposition of combustion by-product and any resulting tribo-film in different positions along the liner on boundary friction at ring and liner interface. Investigation was relied on local pressure coefficient of boundary shear strength of asperities considering localized effects of surface texture, coating and surface deposition.

3.3 Piston Ring Pack

3.3.1 Inter-ring pressure

The computation of the inter-ring pressure variation (blow-by) is needed to evaluate the tribological performance of the piston rings during the piston reciprocating motion under the effect of engine gas pressure. The calculated inter-ring pressure variation represents the boundary condition and the pressure acting on the ring backside.

Piston rings provide a labyrinth passage way for the gases to escape the piston. Assuming that the ring gaps are the only openings for the gas to leak out, the ring

pack may be represented by a gas passage system consisting of a series of chambers connected by square-edged orifices, as shown in Fig. 3.1.

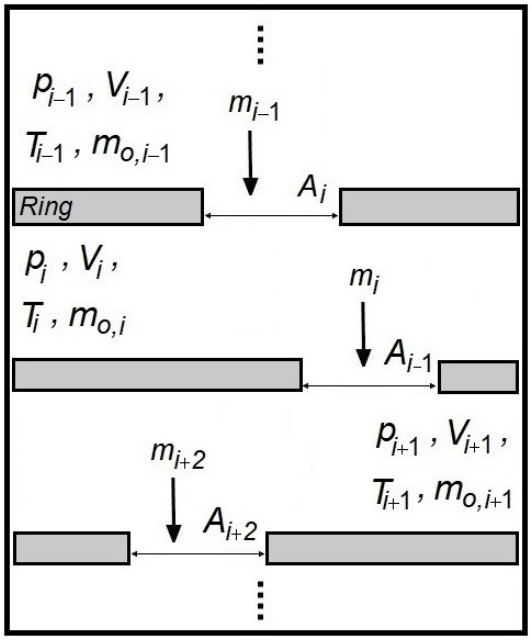

Fig. 3.1 Ring pack schematic representation: p gas pressures, T gas temperatures, m gas masses, V chamber volumes, A cavity areas.

The inter-ring gas pressure estimation is then based on the Orifice and Volume Method [10, 11, 87], where two equations are required: one for the flow rate through the orifices and the other one describing the pressure variation within the inter-ring volumes. The ideal gas law (also named general gas equation), is the state equation of a hypothetical ideal gas which is a good approximation of the behaviour of many gases under several conditions:

$$pV = mR_gT \tag{3.1}$$

where p is the gas pressure (Pa), T the gas temperature (K), m the gas mass (kg), V the chamber volume (m^3), and R_g the gas constant (J/(kgK)).

The following dimensionless variables were used to write dimensionless governing equations:

$$\bar{p} = \frac{p_i}{p_o} \qquad \bar{m}_i = \frac{m_i}{m_o} \qquad \bar{T}_i = \frac{T_i}{T_1} \qquad \bar{A}_i = \frac{A_i}{A_1} \qquad \bar{V}_i = \frac{V_i}{V_1}$$

where $m_o = p_o V_2 / (R_g T_1)$ (kg), p_o is the atmospheric pressure, and A_i the ith total effective passage area (or ith cavity area).

Applying the ideal gas law (3.1) to the ith ring it follows:

$$p_i V_i = (m_{o,i} + m_{i-1} - m_i) R_g T_i \tag{3.2}$$

and deriving it results:

$$\frac{dm_{i-1}}{dt} = A_i K_c \sqrt{\frac{2\gamma}{(\gamma-1) R_g T_{i-1}}}\, p_{i-1} \left(\frac{p_i}{p_{i-1}}\right)^{\frac{1}{\gamma}} \sqrt{1 - \left(\frac{p_i}{p_{i-1}}\right)^{\frac{\gamma-1}{\gamma}}} \tag{3.3}$$

where γ is the isentropic adiabatic index (or heat capacity ratio, or specific heat ratio), and $K_c = 1/{C_d}^2$ the orifice discharge coefficient (with C_d the discharge coefficient through the orifice).

Applying the dimensionless variables and remembering that $\theta = \omega t$ (i.e. $t = \theta/\omega$), Eq. (3.3) can be rewritten as:

$$\frac{d\bar{m}_{i-1}}{d\theta} = K \bar{A}_i \frac{\bar{p}_{i-1}}{\sqrt{\bar{T}_{i-1}}} \left(\frac{\bar{p}_i}{\bar{p}_{i-1}}\right)^{\frac{1}{\gamma}} \sqrt{1 - \left(\frac{\bar{p}_i}{\bar{p}_{i-1}}\right)^{\frac{\gamma-1}{\gamma}}} \tag{3.4}$$

where $K = K_c \dfrac{A_1}{\omega V_2} \sqrt{\dfrac{2\gamma R_g T_1}{\gamma - 1}}$ (1/rad).

With the same approach it can be obtained:

$$\frac{d\bar{m}_i}{d\theta} = K \bar{A}_{i+1} \frac{\bar{p}_i}{\sqrt{\bar{T}_i}} \left(\frac{\bar{p}_{i+1}}{\bar{p}_i}\right)^{\frac{1}{\gamma}} \sqrt{1 - \left(\frac{\bar{p}_{i+1}}{\bar{p}_i}\right)^{\frac{\gamma-1}{\gamma}}} \tag{3.5}$$

Substituting the dimensionless variables in Eq. (3.2) and differentiating with respect to θ it results:

$$\frac{d\bar{p}_i}{d\theta} = \frac{\bar{T}_i}{\bar{V}_i} \left(\frac{d\bar{m}_{i-1}}{d\theta} - \frac{d\bar{m}_i}{d\theta}\right) \tag{3.6}$$

Considering Eqs. (3.4), (3.5) and (3.6) in case of a ring-pack with two compression rings and one oil control ring, a system of two first order differential equations can be written as:

$$\begin{cases} \dfrac{d\bar{p}_2}{d\theta} = \dfrac{\bar{T}_2}{\bar{V}_2}\left(\dfrac{d\bar{m}_1}{d\theta} - \dfrac{d\bar{m}_2}{d\theta}\right) \\ \dfrac{d\bar{p}_3}{d\theta} = \dfrac{\bar{T}_3}{\bar{V}_3}\left(\dfrac{d\bar{m}_2}{d\theta} - \dfrac{d\bar{m}_3}{d\theta}\right) \end{cases} \tag{3.7}$$

where $\dfrac{d\bar{m}_1}{d\theta}$, $\dfrac{d\bar{m}_2}{d\theta}$ and $\dfrac{d\bar{m}_3}{d\theta}$ can be computed using the following formulations:

$$\begin{cases} \dfrac{d\bar{m}_{i-1}}{d\theta} = K\bar{A}_i \dfrac{\bar{p}_{i-1}}{\sqrt{\bar{T}_{i-1}}} \left(\dfrac{\bar{p}_i}{\bar{p}_{i-1}}\right)^{\frac{1}{\gamma}} \sqrt{1 - \left(\dfrac{\bar{p}_i}{\bar{p}_{i-1}}\right)^{\frac{\gamma-1}{\gamma}}} & \text{for} \quad \dfrac{\bar{p}_i}{\bar{p}_{i-1}} > 0.546 \\ \dfrac{d\bar{m}_{i-1}}{d\theta} = K\bar{A}_i \dfrac{\bar{p}_{i-1}}{\sqrt{\bar{T}_{i-1}}} 0.227 & \text{for} \quad \dfrac{\bar{p}_i}{\bar{p}_{i-1}} < 0.546 \end{cases} \tag{3.8}$$

$$\begin{cases} \dfrac{d\bar{m}_i}{d\theta} = K\bar{A}_{i+1} \dfrac{\bar{p}_i}{\sqrt{\bar{T}_i}} \left(\dfrac{\bar{p}_{i+1}}{\bar{p}_i}\right)^{\frac{1}{\gamma}} \sqrt{1 - \left(\dfrac{\bar{p}_{i+1}}{\bar{p}_i}\right)^{\frac{\gamma-1}{\gamma}}} & \text{for} \quad \dfrac{\bar{p}_{i+1}}{\bar{p}_i} > 0.546 \\ \dfrac{d\bar{m}_i}{d\theta} = K\bar{A}_{i+1} \dfrac{\bar{p}_i}{\sqrt{\bar{T}_i}} 0.227 & \text{for} \quad \dfrac{\bar{p}_{i+1}}{\bar{p}_i} < 0.546 \end{cases} \tag{3.9}$$

The solution of the equation system (3.7) gives the inter-ring pressures, as function of the crank angle θ, for the whole engine cycle.

3.4 Ring pack analytical model

Alternative boundary conditions that have been applied in this study to solve Reynolds equation and to evaluate the piston ring pack lubrication are full Sommerfeld, separation, and Reynolds cavitation and reformation. Full Sommerfeld boundary condition, that is the simplest solution of Reynold equation considering no oil film rupture and gas pressure acting on upper and lower edges of the ring, are the

only boundary conditions and associated hydrodynamic pressure is shown by Fig. 3.2 (a). This boundary condition has been used to Reynolds equation solution in case of oil control ring as the adequate amount of oil is available for both rails and environment pressure is more moderate in comparison to first and second compression rings.

Separation boundary condition is used for the second compression ring, which the leading edge is completely engulfed by the lubricant and trialling edge is partially covered by the oil and some area of this edge is exposed to gas as illustrated by Fig. 3.2 (b). It is due to that as the second ring moves and sweeps the oil, lubricant accumulated in front of ring leading edge and covered the edge. In contrary trialling edge partially engulfed and expose to gas due to converging and diverging profile of the ring and pressure reduction suddenly.

Reynolds cavitation and reformation boundary conditions are used for the first compression ring due to large gas pressure acting on both ring edge especially on the trialling edge and shortage of appropriate oil amount to be supplied to the ring liner interface to control oil consumption, as displayed by Fig. 3.2 (c). In this circumstance, gas bubbles dissolved within oil film and the pressure in the gas cavities is considered as saturation pressure and often assumed to be atmospheric. The pressure gradient at reformation point is determined considering oil flow continuity across the cavity. Figure 3.3 is a schematic of piston ring pack lubrication considering above mentioned alternative solution to Reynolds equation.

To evaluate the tribological performance of the piston ring, following assumptions were made to simplify the problem:

• oil is assumed to be incompressible;

• there is no circumferential variations in oil film thickness (circumferential symmetry), but film thickness varies in ring motion direction that encourages the using of one dimensional Reynolds equation;

• oil flow is laminar;

• there is no slippage at the boundaries;

• ring does not tilt or rotate during operations or it may rotate at very low frequently.

In the present model the piston ring is considered stationary and the liner is sliding in opposite direction to determine the coordinate system on the ring face.For the rings with length exceeding their axial width (face width) by a factor of 30 [88], and in addition, considering an axisymmetric condition between piston and liner, the one-dimensional Reynolds equation can be applied to examine the lubrication mechanism at piston ring/liner junction:

$$\frac{\partial}{\partial x}\left(h^3\frac{\partial p}{\partial x}\right) = -6\eta U\frac{\partial h}{\partial x} + 12\eta\frac{\partial h}{\partial t} \tag{3.10}$$

It is proved that any shape of the ring face after running-in time undergoes wear and receive parabolic profile [14, 89], as shown in Fig. 3.4. Oil film thickness at each point on the ring face and time step (crank angle) is compromised of two terms, h_{min} time varying minimum film thickness and ring profile that can be expressed as:

$$h(x,\theta) = h_{min} + \frac{c}{\left(\frac{b}{2}+o\right)^2}(x-o)^2 = h_{min} + B(x-o)^2 \tag{3.11}$$

First integration of Eq. (3.10) with respect to x results in:

$$\frac{dp}{dx} = -6\eta U\frac{1}{h^2(x,\theta)} + 12\eta\omega\frac{dh}{d\theta}\frac{x}{h^3(x,\theta)} + C_1\frac{1}{h^3(x,\theta)} \tag{3.12}$$

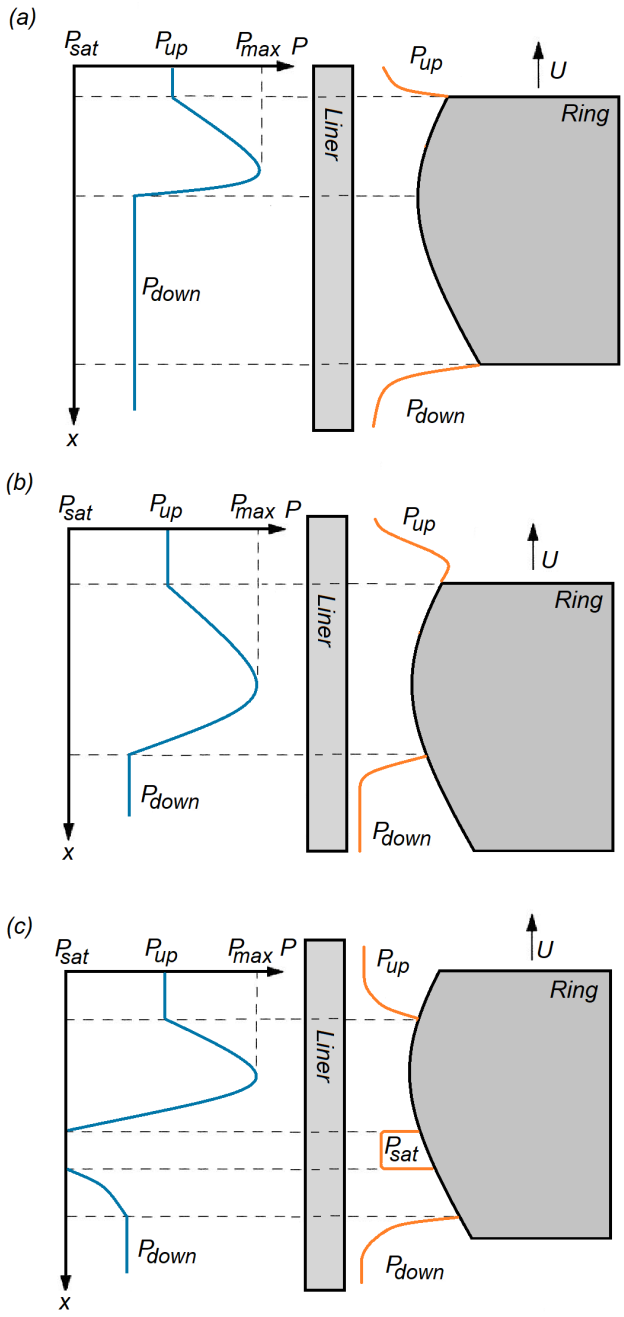

Fig. 3.2 Applicable lubrication scenarios and boundary conditions for piston ring; (a) full Sommerfeld, (b) Separation and (c) Reynolds cavitation and reformation boundary conditions.

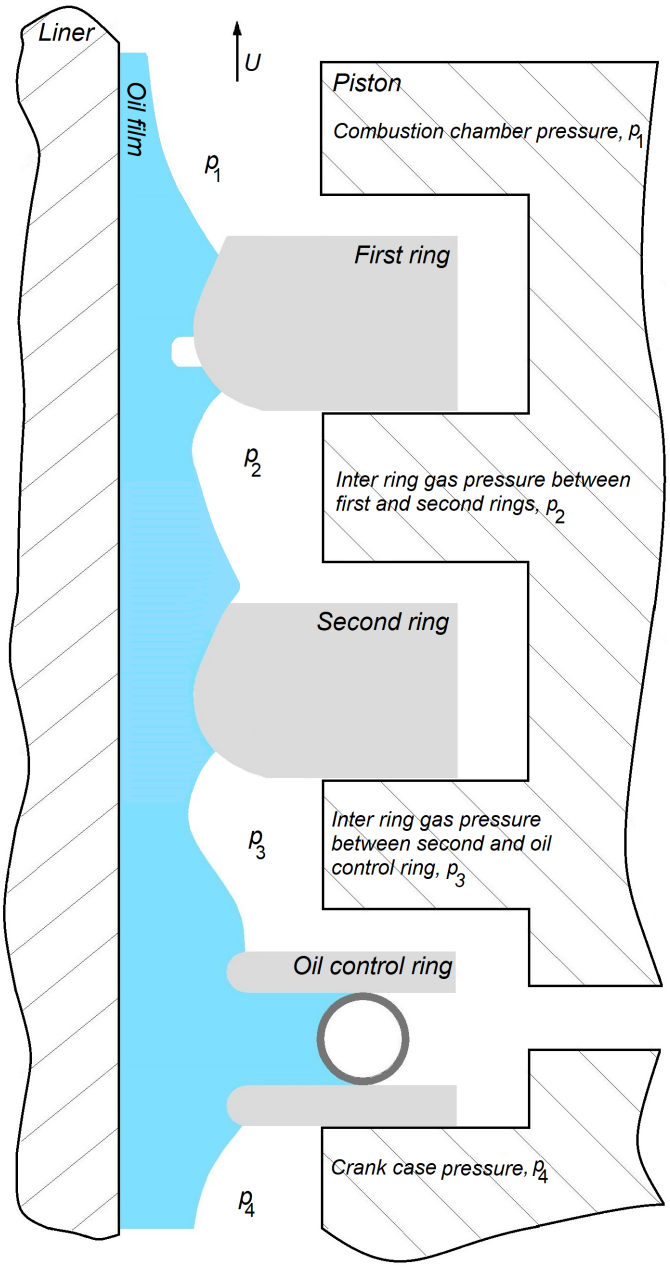

Fig. 3.3 Piston ring pack lubrication scheme.

Second integration of Eq. (3.12) with respect to x gives the hydrodynamic pressure profile as:

$$p(x) = -6\eta U I_0(x) + 12\eta\omega\frac{dh}{d\theta}I_1(x) + C_1 I_2(x) + C_2 \tag{3.13}$$

where:

$$I_0(x) = \int_x \frac{1}{h^2(x,\theta)}\,dx = \frac{1}{2h_{min}\sqrt{Bh_{min}}}\tan^{-1}\left((x-o)\sqrt{\frac{B}{h_{min}}}\right) +$$

$$+\frac{(x-o)}{2h_{min}\left(h_{min}+B(x-o)^2\right)}$$

$$I_1(x) = \int_x \frac{x}{h^3(x,\theta)}\,dx = \frac{3o}{8h_{min}^2\sqrt{Bh_{min}}}\tan^{-1}\left((x-o)\sqrt{\frac{B}{h_{min}}}\right) +$$

$$+\frac{3o(x-o)}{8h_{min}^2\left(h_{min}+B(x-o)^2\right)} + \frac{o(x-o)}{4h_{min}\left(h_{min}+B(x-o)^2\right)^2} + \tag{3.14}$$

$$-\frac{1}{4B\left(h_{min}+B(x-o)^2\right)^2}$$

$$I_2(x) = \int_x \frac{1}{h^3(x,\theta)}\,dx = \frac{3}{8h_{min}^2\sqrt{Bh_{min}}}\tan^{-1}\left((x-o)\sqrt{\frac{B}{h_{min}}}\right) +$$

$$+\frac{(x-o)\left(5h_{min}+3B(x-o)^2\right)}{8h_{min}^2\left(h_{min}+B(x-o)^2\right)^2}$$

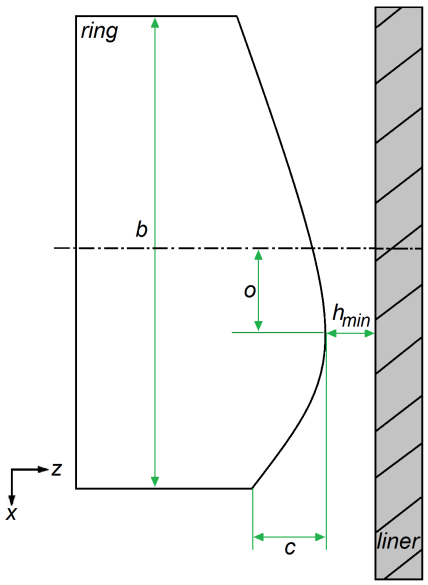

Fig. 3.4 Ring profile schematic.

Hydrodynamic force acting on ring face is obtained via integration of Eq. (4.5) with respect to x

$$F_{hyd} = \int_x p dx = -6\eta U J_0(x) + 12\eta\omega \frac{\partial h}{\partial \theta} J_1(x) + C_1 J_2(x) + C_2 x \tag{3.15}$$

where:

$$\begin{aligned}
J_0(x) &= \int_x I_0(x)dx = \frac{(x-o)}{2h_{min}\sqrt{Bh_{min}}} \tan^{-1}\left((x-o)\sqrt{\frac{B}{h_{min}}}\right) \\
J_1(x) &= \int_x I_1(x)dx = \frac{(3Bo(x-o)-h_{min})}{8Bh_{min}^2\sqrt{Bh_{min}}} \tan^{-1}\left((x-o)\sqrt{\frac{B}{h_{min}}}\right) + \\
&- \frac{x}{8Bh_{min}(h_{min}+B(x-o)^2)} \\
J_2(x) &= \int_x I_2(x)dx = \frac{3(x-o)}{8h_{min}^2\sqrt{Bh_{min}}} \tan^{-1}\left((x-o)\sqrt{\frac{B}{h_{min}}}\right) + \\
&- \frac{1}{8Bh_{min}(h_{min}+B(x-o)^2)}
\end{aligned} \tag{3.16}$$

Viscosity variation with respect to temperature is well described by Vogel equation, Eq. (3.17), and temperature profile along the piston liner has been defined applying Woschni correlation, Eq. (3.18):

$$\eta(T) = k \exp\left[\frac{\theta_1}{\theta_2 + T}\right] \tag{3.17}$$

$$T(x) = T_{TDC} - (T_{TDC} - T_{BDC})\sqrt{\frac{x}{S_P}} \tag{3.18}$$

3.4.1 First compression ring lubrication and tribology

In order to define the integration constants in Eq. (4.5), C_1 and C_2, and assuming minimum oil film thickness occurs under ring face offset, Reynolds cavitation and reformation boundary conditions in downward stroke as illustrated by Fig. 3.5 (a),

can be written as:

$$\begin{aligned} &p = p_{down}, && x = x_1 \\ &p = 0,\ \frac{dp}{dx} = 0, && x = x_2 \\ &p = 0,\ \frac{dp}{dx} = 6\eta U\left(\frac{h(x_3,\theta)-h(x_2,\theta)}{h^3(x_3,\theta)}\right) && x = x_3 \\ &p = p_{up}, && x = x_4, x = o \text{ (ring offset)} \end{aligned} \tag{3.19}$$

and in upward stroke as shown by Fig. 3.5 (b), boundary conditions are as:

$$\begin{aligned} &p = p_{up}, && x = x_1 \\ &p = 0,\ \frac{dp}{dx} = 0, && x = x_2 \\ &p = 0,\ \frac{dp}{dx} = 6\eta U\left(\frac{h(x_3,\theta)-h(x_2,\theta)}{h^3(x_3,\theta)}\right) && x = x_3 \\ &p = p_{down}, && x = x_4, x = o \text{ (ring offset)} \end{aligned} \tag{3.20}$$

where the pressure gradient at the reformation point is obtained considering oil flow continuity across the cavitation.

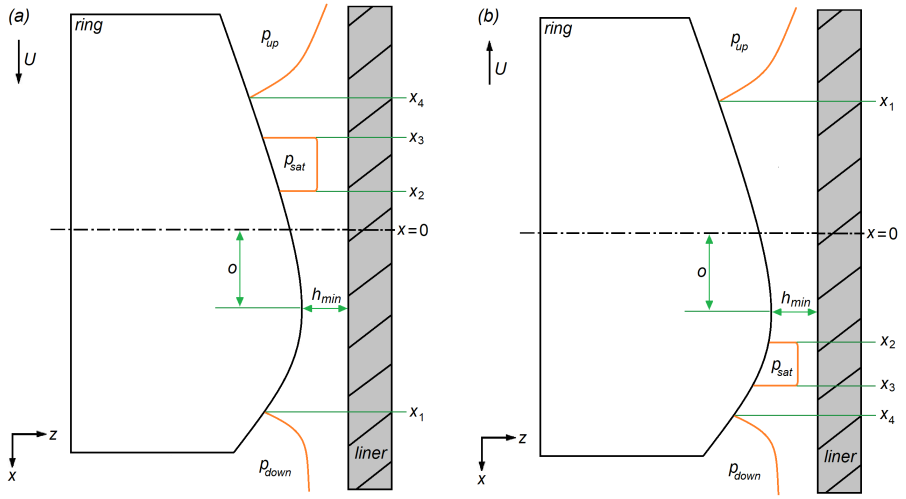

Fig. 3.5 Hydrodynamic film shape and pressure at the first compression ring and liner interface.

From Eq. (4.5) and substituting boundary conditions (Eqs. 3.19 and 3.20) in downward and upward strokes yields to:

$$C_{1,down} = \frac{p_{down} + 6\eta U I_0(x_1) - 12\eta\omega\frac{dh}{d\theta}I_1(x_1) - C_{2,down}}{I_2(x_2)} \tag{3.21}$$

$$C_{2,down} = p_{up} + 12\eta\omega\frac{dh}{d\theta}\left(\frac{1}{4Bh_{min}^2}\right) \tag{3.22}$$

By specifying that the load $F_{ring,gas}$ contributed by ring tension force and gas pressure acting on the ring must be balanced by the generated hydrodynamic pressure F_{hyd} in the lubricant film (Eqs. (3.23) and (3.24)). In Eq. (3.24), p_{gas} is the pressure acting on the rear of the ring which is the maximum of boundary pressures acting on the ring upper and lower edges which is simply $p_{gas} = p_{up}$ if $p_{up} > p_{down}$ and $p_{gas} = p_{down}$ if $p_{down} > p_{up}$ (Fig. 3.6).

$$F_{hyd}(\theta) - F_{ring,gas}(\theta) = 0 \tag{3.23}$$

$$F_{ring,gas}(\theta) = b\,(p_{ring} + p_{gas}) = b\left(\frac{2T}{bD} + p_{gas}\right) \tag{3.24}$$

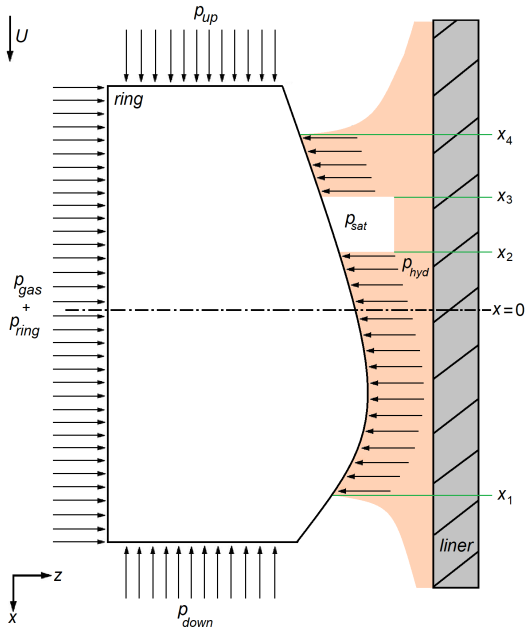

Fig. 3.6 Hydrodynamic film shape and pressure at the first compression ring and liner interface.

In order to define the instantaneous minimum oil film thickness h_{min} and the oil separation and reformation points (x_1, x_2, x_3 and x_4) on the ring face, a system of

equation must be solved. The relevant equations in downward are:

$$\int_{x_1}^{x_2} p(x)dx + \int_{x_3}^{x_4} p(x)dx + p_{down}(b-x_1) + p_{up}(b-x_4) = b\left(\frac{2T}{bD} + p_{gas}\right) \quad (3.25)$$

$$p(x_1) = p_{down} \quad (3.26)$$

$$p(x_2) = \frac{dp}{dx}(x_2) = 0 \quad (3.27)$$

$$p(x_3) = 0,\ \frac{dp}{dx}(x_3) = 6\eta U\left(\frac{h(x_3,\theta) - h(x_2,\theta)}{h^3(x_3,\theta)}\right) \quad (3.28)$$

$$p(x_4) = p_{up} \quad (3.29)$$

and relevant equations in upward stroke are:

$$\int_{x_1}^{x_2} p(x)dx + \int_{x_3}^{x_4} p(x)dx + p_{up}(b-x_1) + p_{down}(b-x_4) = b\left(\frac{2T}{bD} + p_{gas}\right) \quad (3.30)$$

$$p(x_1) = p_{up} \quad (3.31)$$

$$p(x_2) = \frac{dp}{dx}(x_2) = 0 \quad (3.32)$$

$$p(x_3) = 0,\ \frac{dp}{dx}(x_3) = 6\eta U\left(\frac{h(x_3,\theta) - h(x_2,\theta)}{h^3(x_3,\theta)}\right) \quad (3.33)$$

$$p(x_4) = p_{down} \quad (3.34)$$

After defining the minimum oil film thickness, h_{min}, and the points of ring face covered by the lubricant (x_1, x_2, x_3 and x_4), instantaneous friction force due to viscose shear stress at film thickness ant contributed power loss can be calculated via Eqs. (3.35) and (3.35) respectively. These equations are recommended as the friction force and power loss due to squeeze action are taken into account automatically [90].

$$F_f(\theta) = \int_A \left(\frac{\eta U}{h(x,\theta)} + \frac{h(x,\theta)}{2}\frac{dp}{dx}\right) dA \quad (3.35)$$

$$P_f(\theta) = \int_A \left(\frac{\eta}{h(x,\theta)}\right) U^2 dA + \int_A \left(\frac{h^3(x,\theta)}{12\eta}\right) |\nabla p|^2\, dA \quad (3.36)$$

In case of boundary lubrication, lubricant film is thin and the load is mainly or completely supported by asperity contacts. Considering oil film parameter, λ, which

is the ratio of minimum oil film thickness, h_{min}, to combined surface roughness, σ, the transition from hydrodynamic lubrication to mixed and boundary lubrication has been determined. At each crank angle or time instance in which λ>3, fully hydrodynamic lubrication has been dominated and in contrary, at each crank angle in which λ<1, boundary lubrication is dominated (Fig. 3.15). In case of boundary lubrication, friction force can be calculated using:

$$F_f(\theta) = \mu(\pi D F_{ring,gas}(\theta))sign(-U) \tag{3.37}$$

3.4.2 Second compression ring lubrication and tribology

If oil film ahead of the ring does not flow beneath the ring face as the piston moves along the cylinder, oil will begin to accumulate in front of the leading edge of the ring. This phenomenon takes place mostly under moderate boundary pressure [40]. Therefore, it is assumed that lubricant accumulates in front of the leading edge of second compression ring as the ring slides and motivates the laminar motion of oil layers on each other under moderate boundary pressures as shown by Fig. 3.3.

Assuming that minimum oil film thickness locates under crown offset, separation boundary condition has been applied to define the integration constants in Eq. (4.5) using following expression (Eqs. (3.38) and (3.39) in downward and upward strokes, respectively) as is illustrated by Fig. 3.7:

$$\begin{aligned} p &= p_{down}, & x &= a \\ p &= p_{up}, & x &= x_e, x = o \end{aligned} \tag{3.38}$$

$$\begin{aligned} p &= p_{up}, & x &= -a \\ p &= p_{down}, & x &= x_e, x = o \end{aligned} \tag{3.39}$$

Pressures acting on the second compression ring is displayed by Fig. 3.8. Gas pressure acting on the back side of the ring, p_{gas}, is determined by magnitude of pressures acting on upper and lower edges of the ring, and p_{gas} equals to the larger one.

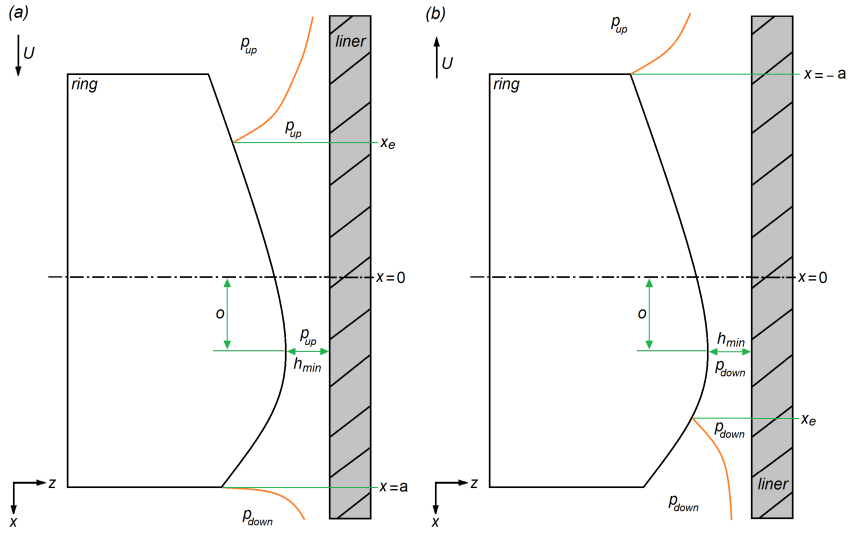

Fig. 3.7 Oil film shape and boundary pressures considering full separation boundary conditions: (a) in downward and (b) in upward strokes.

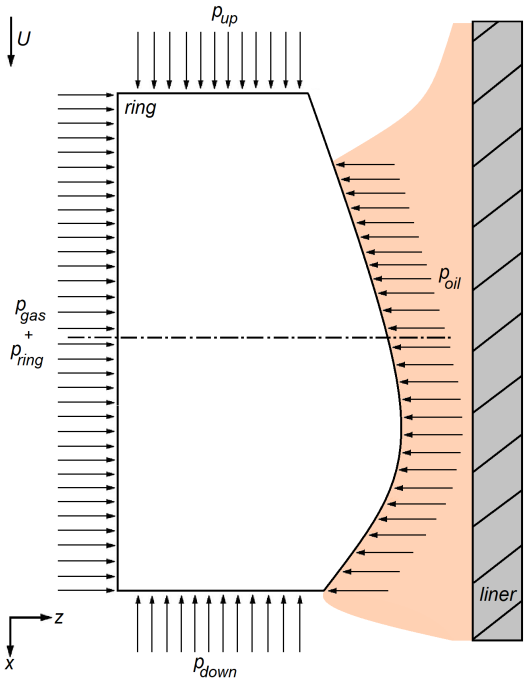

Fig. 3.8 Pressures acting on the ring includes, gas pressure, ring tension and hydrodynamic pressure for the second compression ring.

Therefore integration constants in downward and upward strokes using separation boundary condition can be calculated as:

$$C_{1,down} = \frac{p_{down} + 6\eta U I_0(a) - 12\eta\omega\frac{dh}{d\theta} I_1(a) - C_{2,down}}{I_2(a)} \tag{3.40}$$

$$C_{2,down} = p_{up} + 12\eta\omega\frac{dh}{d\theta}\left(\frac{1}{4Bh_{min}^2}\right) \tag{3.41}$$

$$C_{1,up} = \frac{p_{up} + 6\eta U I_0(-a) - 12\eta\omega\frac{dh}{d\theta} I_1(-a) - C_{2,up}}{I_2(-a)} \tag{3.42}$$

$$C_{2,up} = p_{down} + 12\eta\omega\frac{dh}{d\theta}\left(\frac{1}{4Bh_{min}^2}\right) \tag{3.43}$$

Considering load balance criterion and pressure equilibrium at lubricant separation point, there are three unknowns, h_{min}, x_e and $\frac{dh}{d\theta}$ those must be defined via following equations and numerical approach in downward:

$$p(x_e) = p_{up} \tag{3.44}$$

$$\int_{x_e}^{a} p(x)dx + p_{up}(a - x_e) = b\left(\frac{2T}{bD} + p_{gas}\right) \tag{3.45}$$

and in upward stroke:

$$p(x_e) = p_{down} \tag{3.46}$$

$$\int_{-a}^{x_e} p(x)dx + p_{down}(a - x_e) = b\left(\frac{2T}{bD} + p_{gas}\right) \tag{3.47}$$

The effect of first compression ring lubrication on the second compression ring can be considered with the amount of the oil left on the liner behind the trailing edge of the first ring. Therefore, according to Reynolds equation, the expression for the volume rate per unit circumferential length can be calculated using Eq. (3.48). Hence, according to oil availability to second ring, calculated minimum oil film thickness h_{min} at second ring/liner interface cannot be thicker than oil left on the cylinder wall behind the first ring.

$$Q = -\frac{h^3(x,\theta)}{12\eta}\frac{dp}{dx} + \frac{Uh(x,\theta)}{2} \tag{3.48}$$

3.4.3 Oil control ring lubrication and tribology

It is common to use two-piece oil control rings in diesel engines and some gasoline applications. Therefore oil control ring is assumed to have two rails and one coil spring which is responsible for holding the rails at the required relative axial distance (Fig. 3.3). In this study each rail is treated as one distinct compression ring. Due to presence of adequate amount of lubricant and moderate boundary pressure acting on oil control ring rails, full Sommerfeld boundary condition has been applied to each rail as shown by Fig. 3.2.

According to full Sommerfeld boundary condition, there is oil film rupture and the pressure acting on the ring rail upper edge is the inter-ring gas pressure between the second compression ring and the first oil control rail and the crankcase pressure acting on the lower edge of the ring rail. Assuming that minimum oil film thickness occurs under ring crown offset (Fig. 3.9), o, full Sommerfeld boundary conditions can be written in downward and upward strokes, respectively as:

$$\begin{aligned} p &= p_{down}, \qquad x = a \\ p &= p_{up}, \qquad x = o \end{aligned} \tag{3.49}$$

$$\begin{aligned} p &= p_{up}, \qquad x = a \\ p &= p_{down}, \qquad x = o \end{aligned} \tag{3.50}$$

From Eq. (4.5) and substituting boundary conditions (Eqs (3.49) and (3.50)) yields integration constants, C_1 and C_2, in downward (Eqs. (3.51) and (3.52)) and upward stroke (Eqs. (3.53) and (3.54)):

$$C_{1,down} = \frac{p_{down} + 6\eta U I_0(a) - 12\eta\omega\frac{dh}{d\theta} I_1(a) - C_{2,down}}{I_2(a)} \tag{3.51}$$

$$C_{2,down} = p_{up} + 12\eta\omega\frac{dh}{d\theta}\left(\frac{1}{4Bh_{min}^2}\right) \tag{3.52}$$

$$C_{1,up} = \frac{p_{up} + 6\eta U I_0(-a) - 12\eta\omega\frac{dh}{d\theta} I_1(-a) - C_{2,up}}{I_2(-a)} \tag{3.53}$$

$$C_{2,up} = p_{down} + 12\eta\omega\frac{dh}{d\theta}\left(\frac{1}{4Bh_{min}^2}\right) \tag{3.54}$$

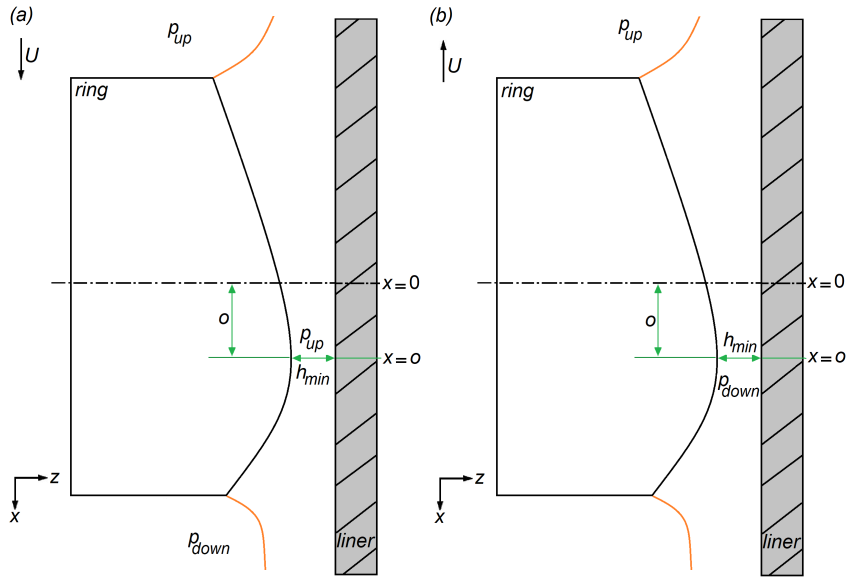

Fig. 3.9 Oil film shape and boundary pressures considering full Sommerfeld boundary condition: (a) in downward and (b) in upward strokes.

Minimum instantaneous oil film thickness can be gained through the force balance acting on the ring in which hydrodynamic force, F_{hyd} acting on the ring face is in equilibrium with the ring tension force, T and the gas pressure, p_{gas} acting on the back side of the ring (Eqs. (3.23) and (3.24)) as shown by Fig. 3.10. Force balance equilibrium using full Sommerfeld boundary condition can be written in downward, Eq. (3.55) and upward, Eq. (3.56) strokes as follows:

$$\int_o^a p(x)dx + (a+o)p_{up} = b\left(\frac{2T}{bD} + p_{gas}\right) \tag{3.55}$$

$$\int_{-a}^o p(x)dx + (a-o)p_{down} = b\left(\frac{2T}{bD} + p_{gas}\right) \tag{3.56}$$

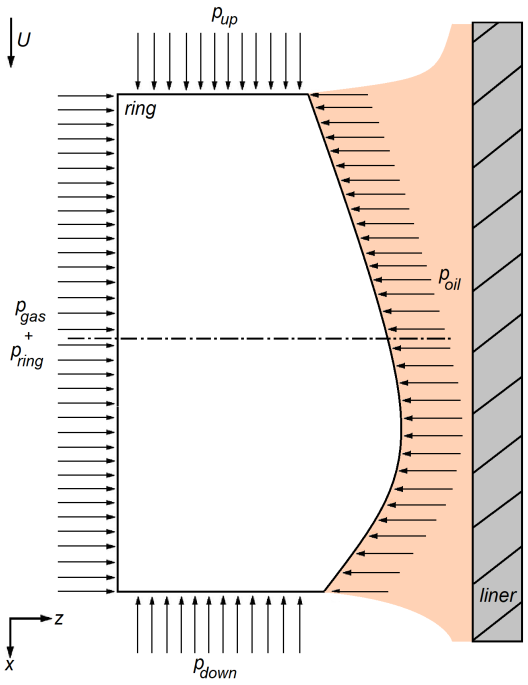

Fig. 3.10 Pressure acting on the ring includes, gas pressure, ring tension and hydrodynamic pressure for oil control ring's rail.

Friction force due to viscous shear stress within the film and mechanical power loss can be calculated using Eqs. (3.35) and (5.29) respectively. In case of boundary lubrication, Eq (3.37) can be applied to estimate friction force.

3.4.4 Solution strategy

In this section the solution methodology for the oil control ring, that is the most simplest problem in comparison to the two compression rings with respect to lubrication mechanisms, has been described and solution can be developed and used for first and second rings. The solution of Eqs. (3.55) and (3.56) can be found applying iterative method and numerical approach as shown by Fig. 3.11.

In upward and downward strokes, both $\partial h/\partial\theta$ and h_{min} are unknowns but the radial oil film thickness variation with respect to the crank angle, $\partial h/\partial\theta$, can be calculated if an estimation of h_{min} is available at some crank angles, in which the axial oil film thickness is expected to change slightly. Starting at the mid-phase position of the expansion phase where $\partial h/\partial\theta$ can be neglected, the h_{min} estimation

can be obtained by solving Eq. (3.55) using numerical methods. At the subsequent crank angle θ_i this h_{min} estimated at the previous angle, θ_{i-1} (corresponding to the expansion mid-phase), can be used to calculate the value of $\partial h/\partial\theta$ at the current angle, θ_i. Finally, this estimation of $\partial h/\partial\theta$ can be used to calculate the h_{min} value at the current angle θ_i. Using this iterative solution and the Newton-Raphson method to enjoy its fast convergence, encourages the calculation of h_{min} for the complete engine cycle.

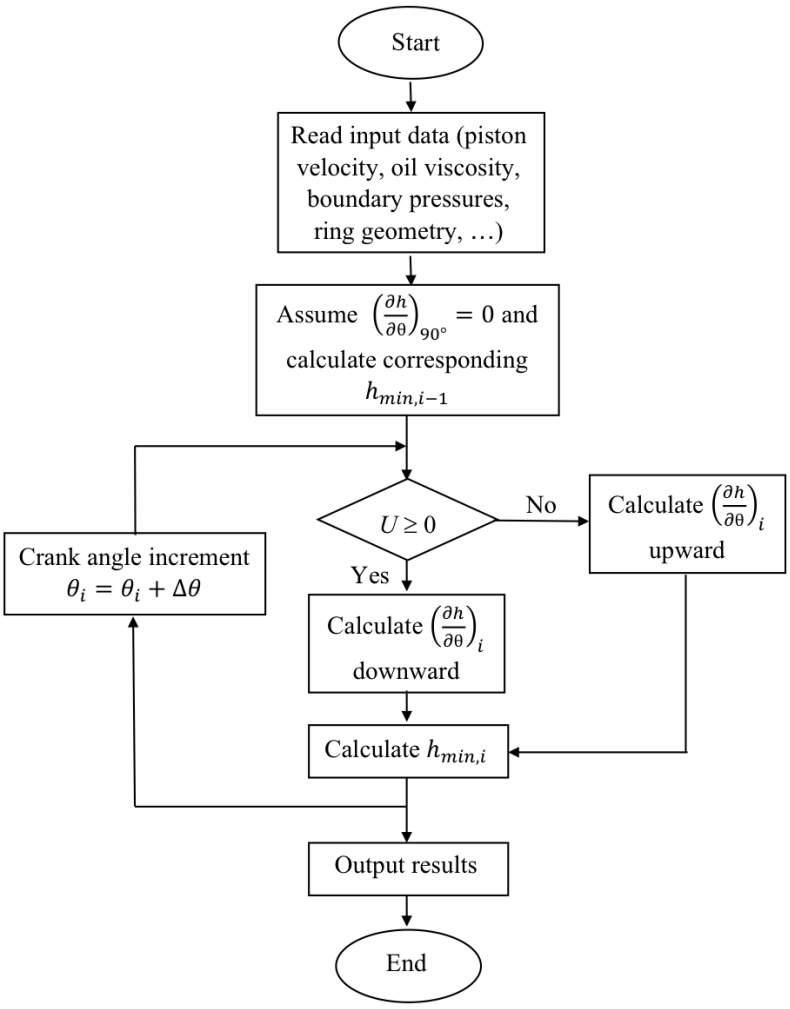

Fig. 3.11 Solution flow chart.

3.5 Statistical Analysis of Ring Geometry on Ring Tribology

To examine the effect of ring geometry and its elastic properties, Design of Experiment (DoE) has been employed considering fully flooded conditions to avoid the effect of starvation and oil rupture to treat them as noise and uncontrollable factors. Based on the literature review done by the author and manufacturers' recommendation, the most influential parameters (Table 3.1 and Fig. 3.12) those affecting piston ring lubrication are: ring width, crown height, ring end gap and ring tension force [1, 91]. A 2-level factorial design has been used, therefore, a single replicate of a 2^4 design is considered neglecting internal estimation of error, and combining their mean squares, to estimate the error. Regarding to 2-level factorial design, the observation includes 4 numeric factors at 2 levels which resulting in 16 combinations plus 1 center point, for a total of 17 evaluation trials. Design-Expert software version 11 free trial has been used to conduct ANOVA analysis.

Table 3.1 Influential parameters and design specification

Factor	Name	Type	No. of Levels	Low	Mean	High
A	Ring width (mm)	Numeric	2	1 mm	1.4 mm	1.8 mm
B	Crown height (mm)	Numeric	2	0.001 mm	0.0055 mm	0.01 mm
C	Ring tension (N)	Numeric	2	5 N	15 N	25 N
D	Ring end gap (mm)	Numeric	2	0.2 mm	0.8 mm	1.4 mm
E	Ring offset (μm)	Categoric	2	Absence	–	Presence

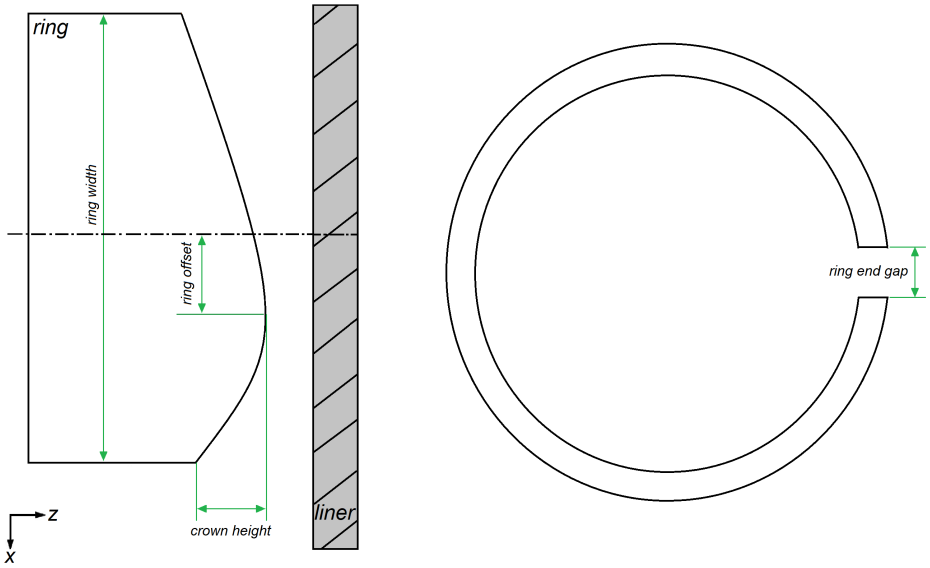

Fig. 3.12 Influential ring geometries parameters.

3.6 Results and Discussion

The relevant data have been used in this study to evaluate piston ring pack comprising engine data and piston ring pack including two compression rings and one oil control ring are tabulated by Tables 3.2 and 3.3 respectively.

Table 3.2 Relevant engine data.

D	Cylinder bore (mm)	83.80
l	Connecting rod length (mm)	153
r	Crank radius (mm)	49.5
Z_{owp}	Wrist-pin offset (mm)	0.5
η	Lubricant dynamic viscosity (Pa.s)	11.734E-03
σ	Ring Combined surface roughness (μm)	0.37

Table 3.3 Piston ring pack data.

First compression ring	
C	12 (μm)
b	1.5 (mm)
o	0.0 (mm)
T	10 (N)
Second compression ring	
C	7.7 (μm)
b	1.5 (mm)
o	0.3 (mm)
T	7 (N)
Oil control ring	
C	3.0 (μm)
b	2 (mm)
o	0.0 (mm)
T	15 (N)

3.6.1 Piston ring pack lubrication and tribological performance

Figure 3.13 displays inter ring gas analysis (blow-by) for a ring pack including two compression rings and one oil control ring at engine speed of 2000 rpm.

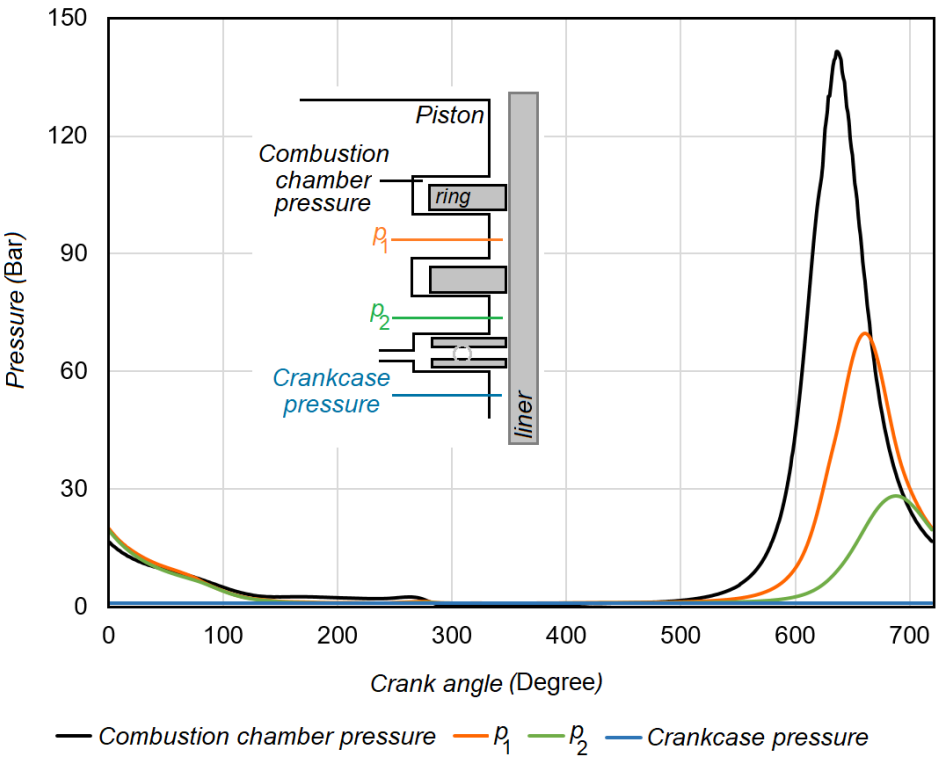

Fig. 3.13 blow-by analysis at 2000 rpm.

Figures 3.14 and 3.15 show the effect of engine rotating speed on minimum oil film thickness at first compression ring and liner junction under motored and fired conditions respectively, considering as Newtonian (neglecting oil viscosity dependence on temperature) lubricant at different engine speeds. Regarding to the assumption that lubricant has laminar flow, as the engine speed goes up, the shear rate within the oil layer increases and fluid load carrying capacity improves and consequently thicker minimum oil film thickness is expected. Therefore, the higher engine speed promotes hydrodynamic lubrication of ring/liner junction and gives higher film thickness and tends to reduce the contribution of asperities contacts to power loss especially in critical regions, TDC and BDC [14].

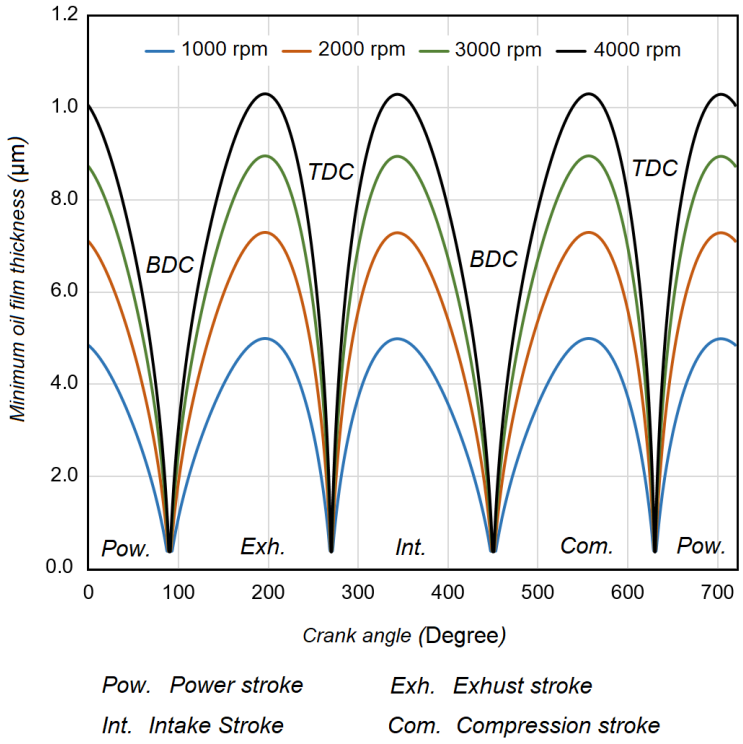

Fig. 3.14 Minimum oil film thickness at first ring and liner interface at different speed under motored condition.

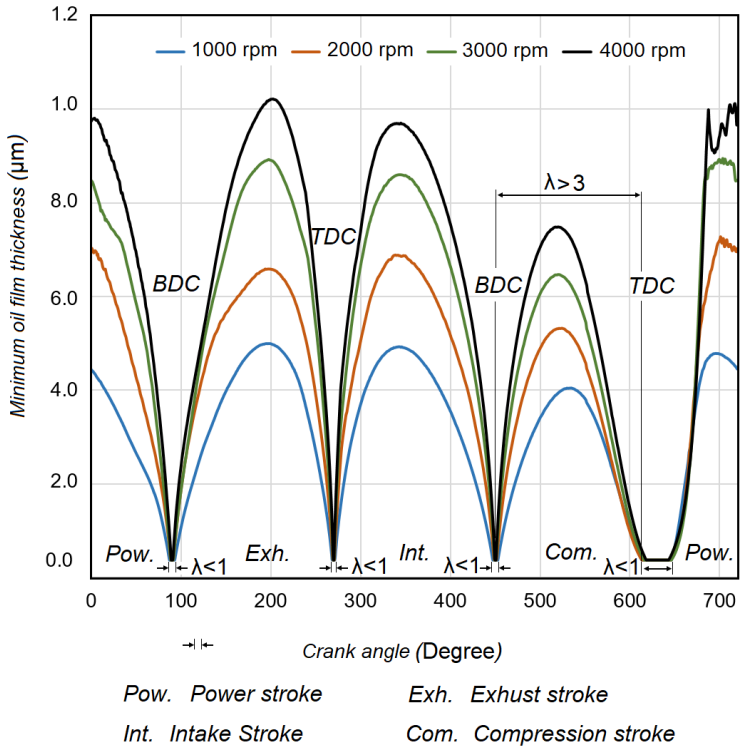

Fig. 3.15 Minimum oil film thickness at first ring and liner interface at different speed under fired condition.

Calculated minimum oil film thickness for a piston ring pack including two compression rings and one oil control ring with two rails, treating lubricant as Newtonian (neglecting oil viscosity dependence on temperature) and non-Newtonian (tacking to account oil viscosity variation with temperature) is shown by Figs. 3.16 and 3.17 at 2000 rpm of engine speed under motored and fired condition, respectively. Lower minimum oil film thickness is obtained as the temperature dependence of lubricant viscosity has been taken into consideration and oil is treated as non-Newtonian fluid. As the liner temperature increases results in increment of oil temperature at the ring/liner interface and reduction of oil viscosity and its resistance against the shear stress and consequently reduces lubricant load carrying capacity and smaller oil film thickness.

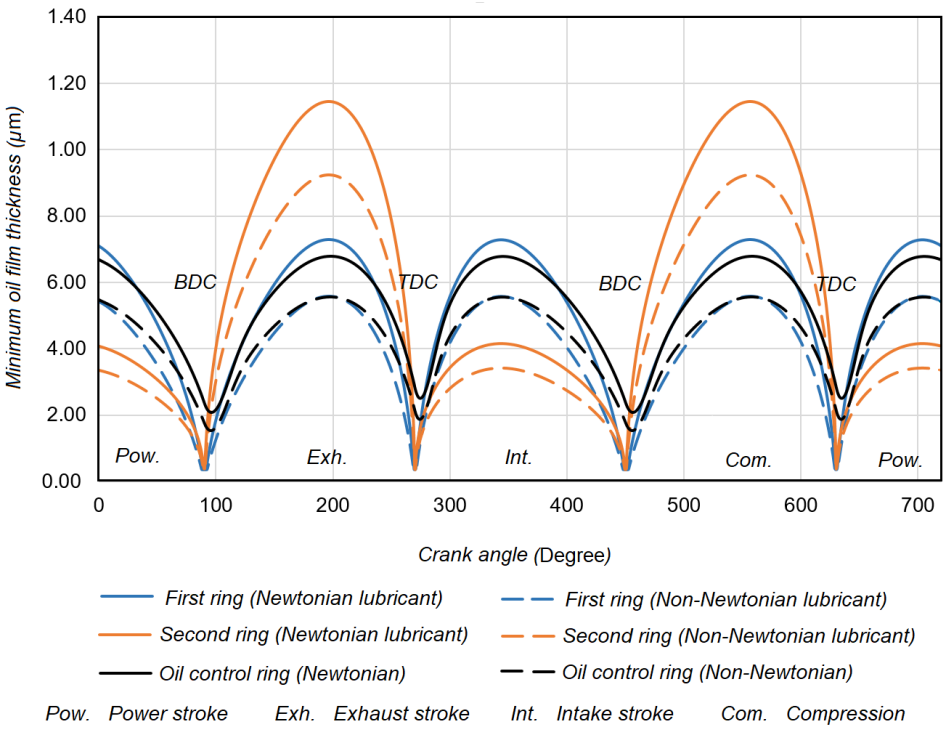

Fig. 3.16 Minimum oil film thickness for the ring pack applying Newtonian and non-Newtonian fluid under motored condition at 2000 rpm.

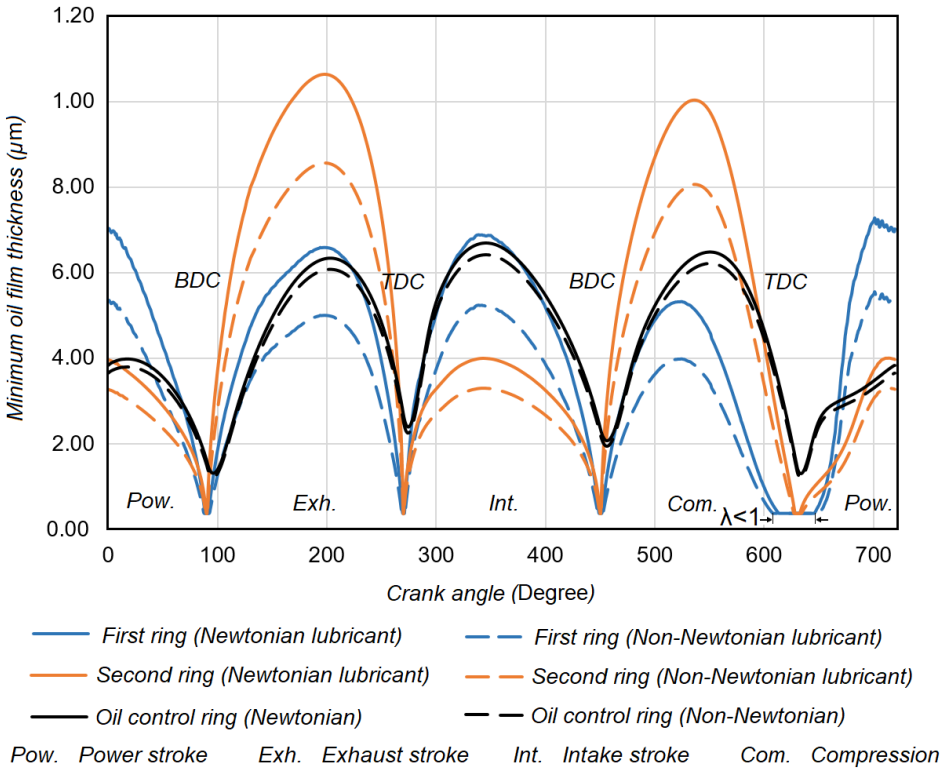

Fig. 3.17 Minimum oil film thickness for the ring pack applying Newtonian and non-Newtonian lubricant under fired condition at 2000 rpm.

Friction force and power loss at first ring and liner junction contributed by shear stress, oil squeeze action and boundary lubrication at critical regions (TDC and BDC) at different engine speed under motored condition is presented by Figs. 3.18 and 3.19. Considering lubricant dependence on temperature, due to oil viscosity reduction, film layers resistance to slide on each other reduces and consequently friction and power loss decrease. Meanwhile, lubricant viscosity reduction with temperature increment, is associated with oil load carrying capacity interruption and as result at critical areas higher amount of asperities contact is inevitable as displayed by Fig. 3.20. As engine speed increases, hydrodynamic regime prevails and reduces likelihood of boundary lubrication at critical regions, TDC and BDC. Therefore power loss mostly is due to the shear stress and oil squeeze action rather than asperities contact as shown by Fig. 3.19. Figure 3.21 compares mean friction force and power loss contributed by first ring under motored and fired conditions.

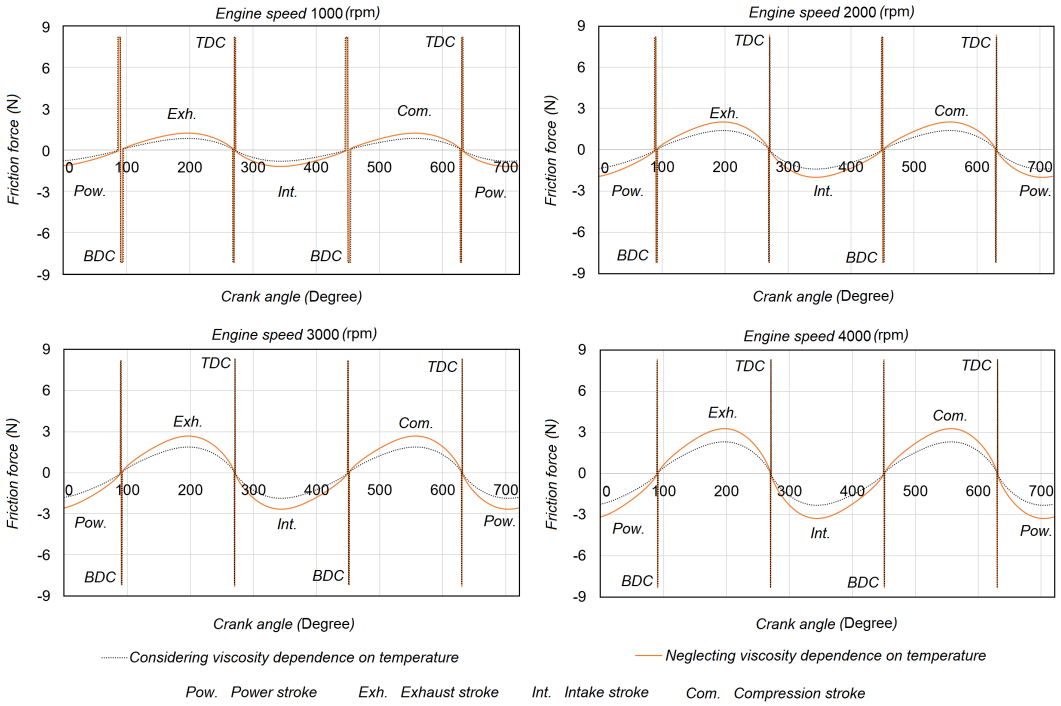

Fig. 3.18 Friction loss at 1st ring and liner interface under motored condition.

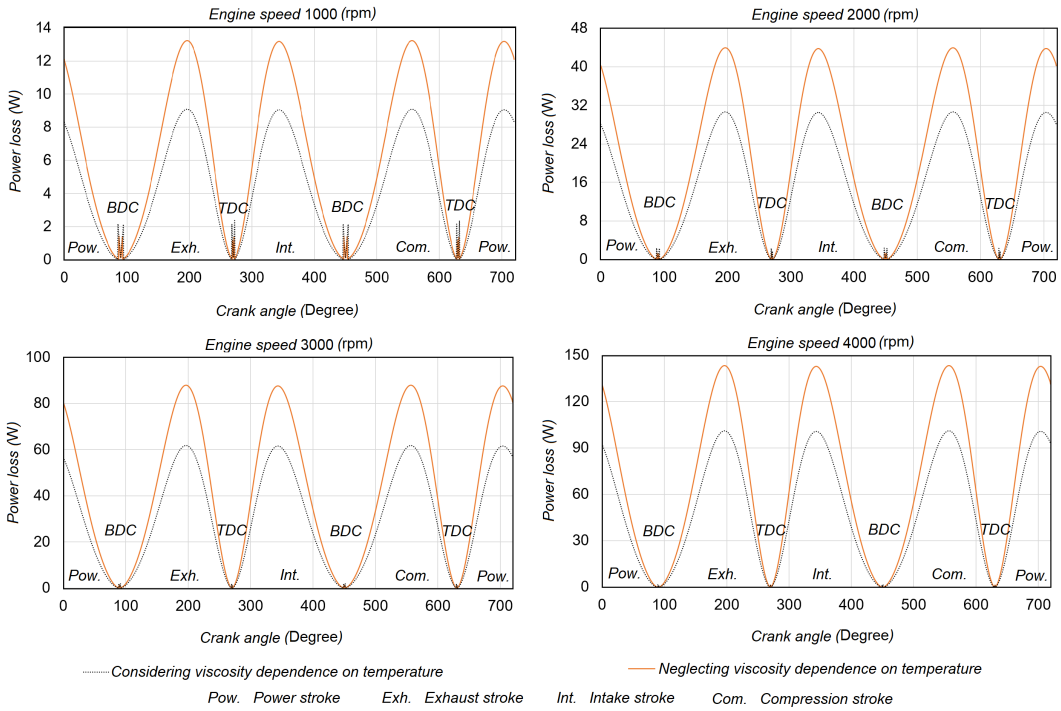

Fig. 3.19 Power loss at 1st ring and liner interface under motored condition.

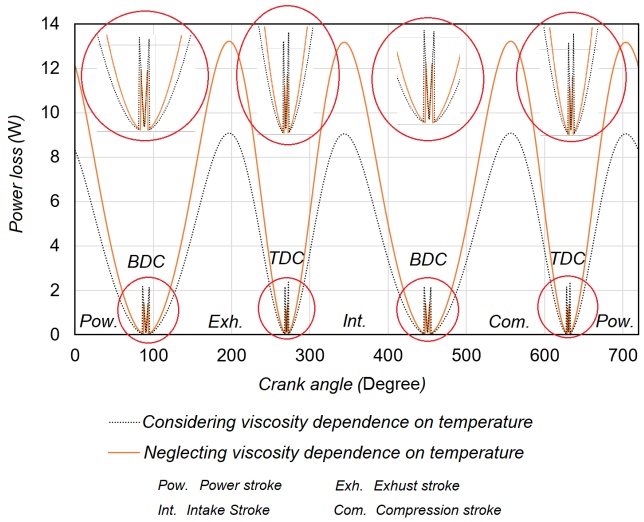

Fig. 3.20 Power loss at 1st ring and liner interface under motored condition.

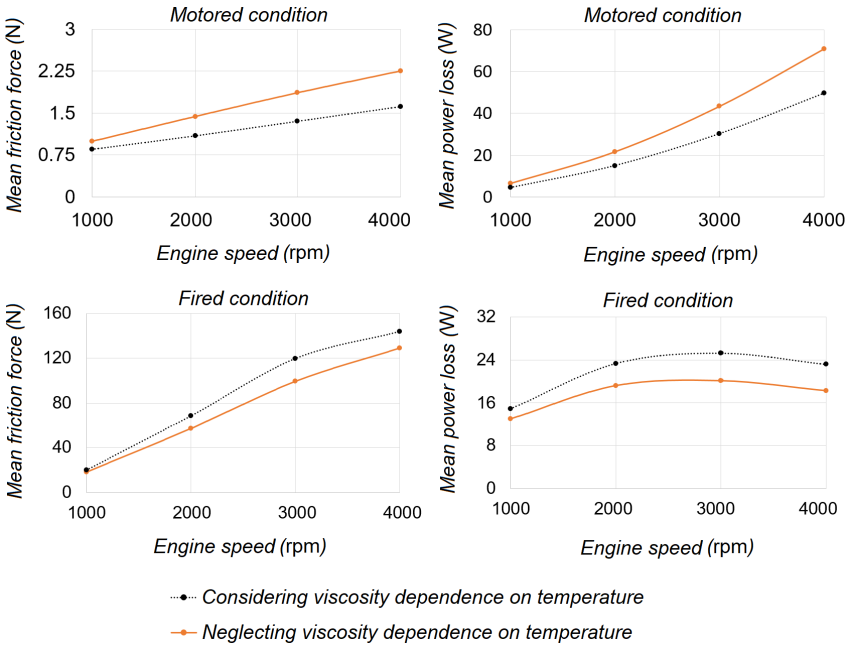

Fig. 3.21 Mean friction force and mean power loss at 1st ring and liner interface under motored and fired conditions.

Instantaneous calculated friction force at second compression ring and liner junction considering oil separation boundary conditions (Fig. 3.7) at different engine angular speed under motored and fired operating conditions are shown by Figs. 3.22 and 3.23 respectively. Figure 3.24 illustrates that, since the lower edge acts as

leading edge in downward stroke, the occurrence probability of boundary lubrication is reduced under both circumstances, considering or neglecting viscosity dependence on temperature. One reason behind this is that as the ring offset is located toward the lower edge, it provides larger wedge angle and higher hydrodynamic pressure and load carrying capacity which prevent boundary lubrication. Mean friction force and power loss at 2nd ring and liner at different engine rotating speed have been demonstrated by Fig. 3.25.

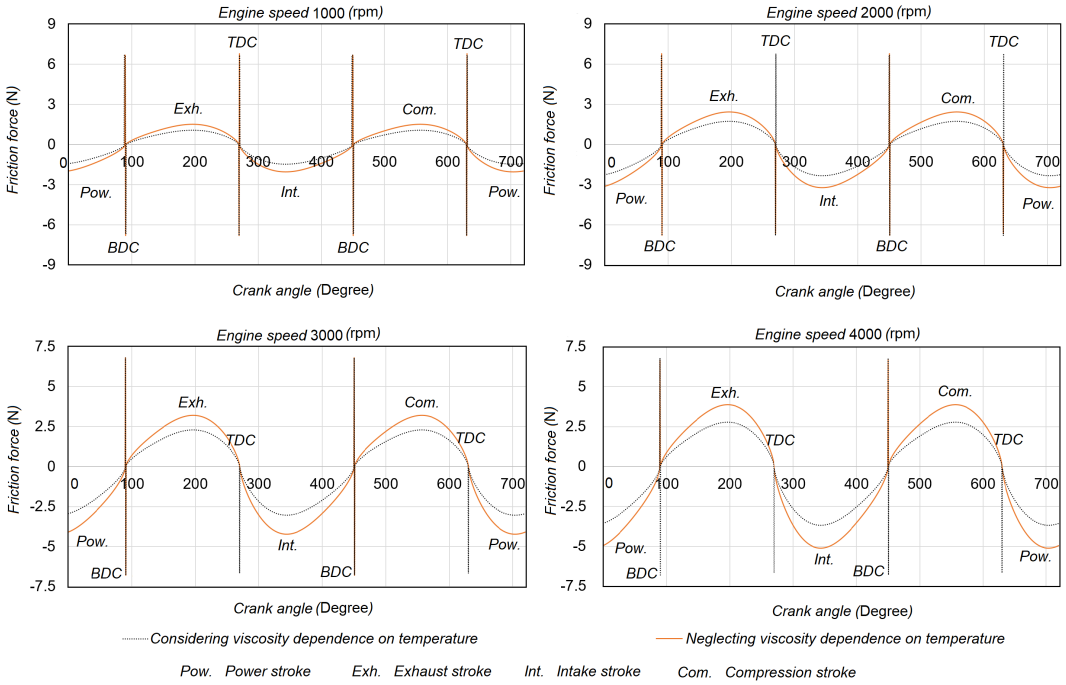

Fig. 3.22 Friction loss at 2nd ring and liner interface under motored condition.

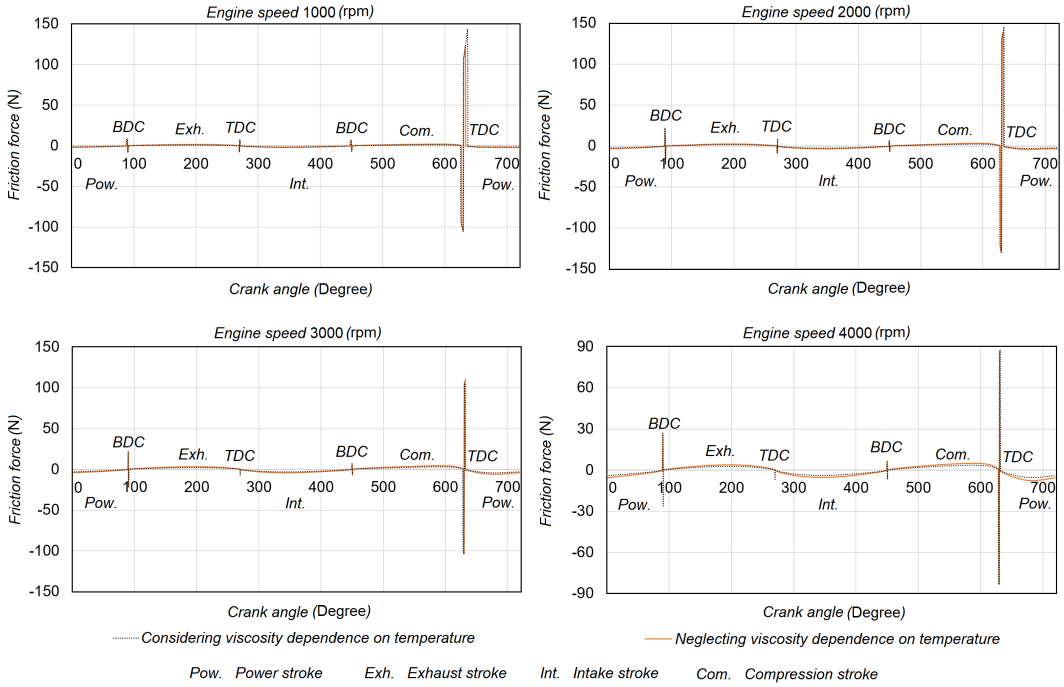

Fig. 3.23 Friction loss at 2nd ring and liner interface under fired condition.

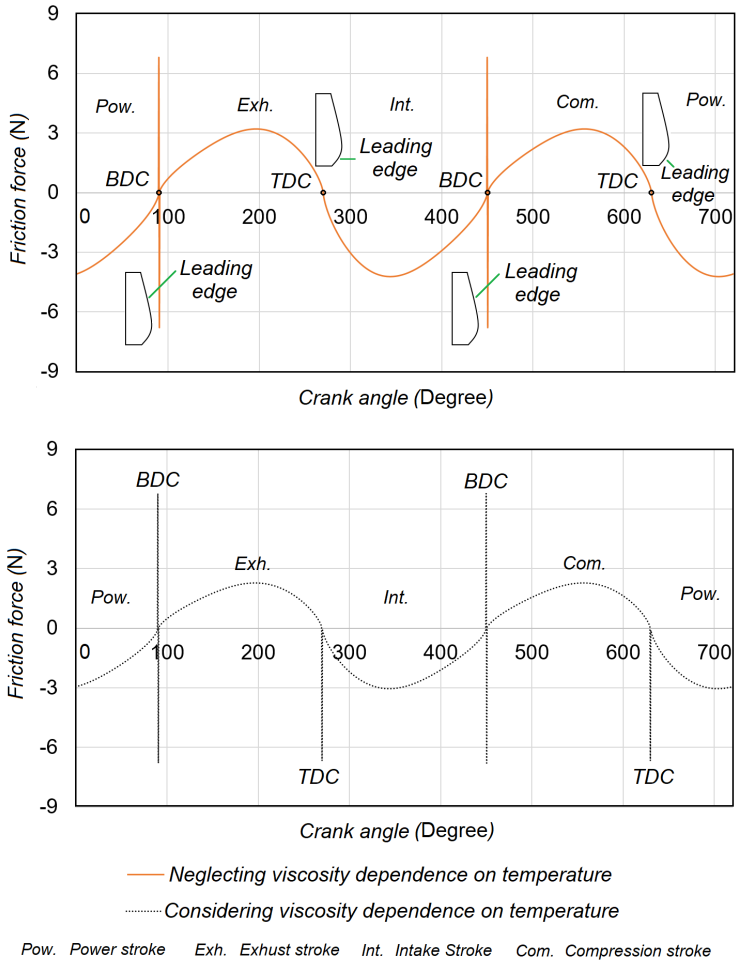

Fig. 3.24 Effect of ring geometry and leading edge on lubrication regime.

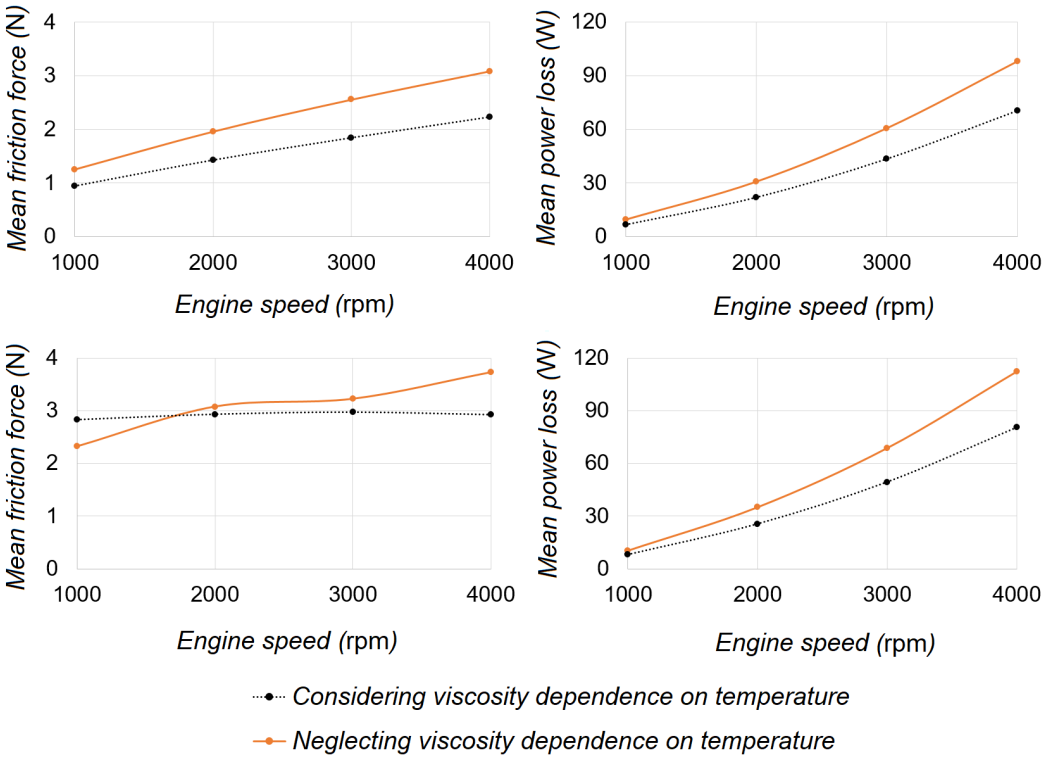

Fig. 3.25 power loss at 2nd ring and liner interface under fired condition.

Power loss at second ring and liner interface at different engine angular speed under motored and fired conditions have been demonstrated by Figs. 3.26 and 3.27 respectively. Power loss increases with engine speed increment due to higher imposed shear rate within the oil film thickness. Lower power loss is obtained considering oil viscosity variation with respect to temperature as lubricant resistance against shear stress reduces under both motored and fired operating conditions.

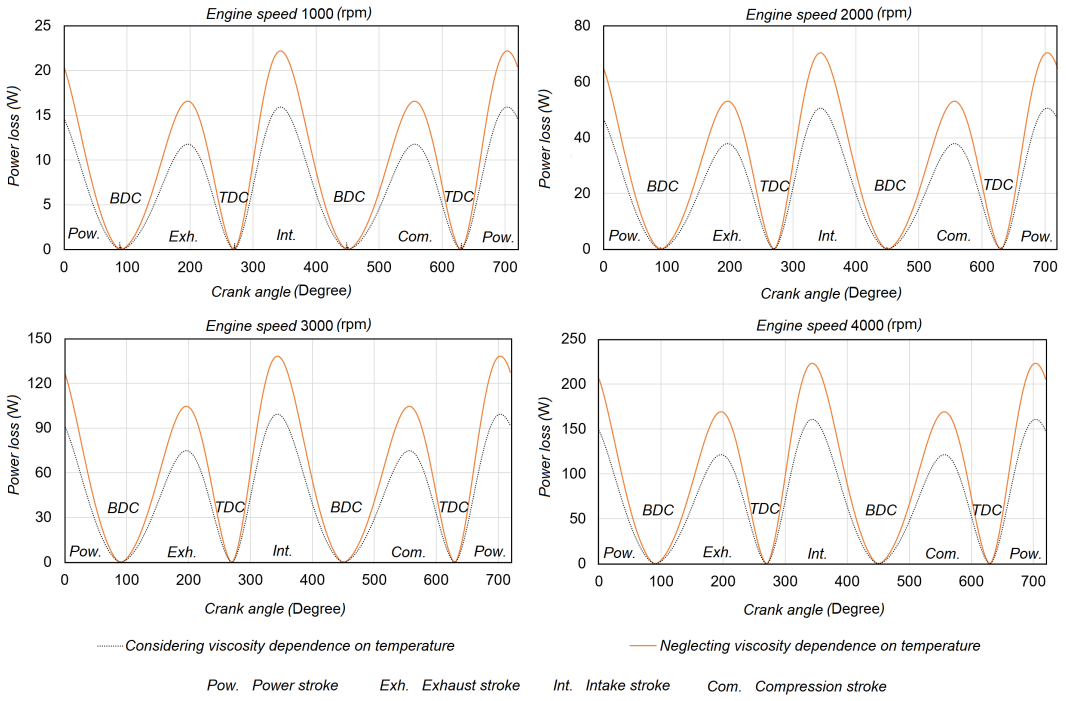

Fig. 3.26 Power loss at 2nd ring and liner interface under motored condition.

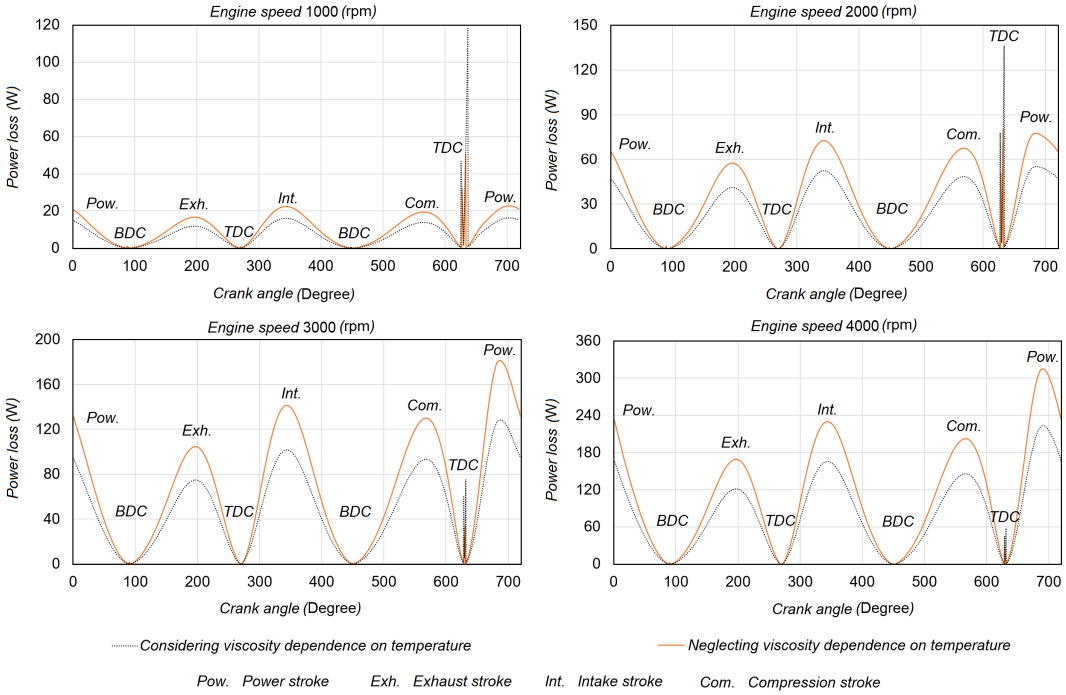

Fig. 3.27 Power loss at 2nd ring and liner interface under fired condition.

Figures 3.28 and 3.29 display the instantaneous friction force at oil control ring and cylinder wall under motored and fired condition. Power loss contributed by oil control ring under motored and fired are illustrated by Figs. 3.30 and 3.31.

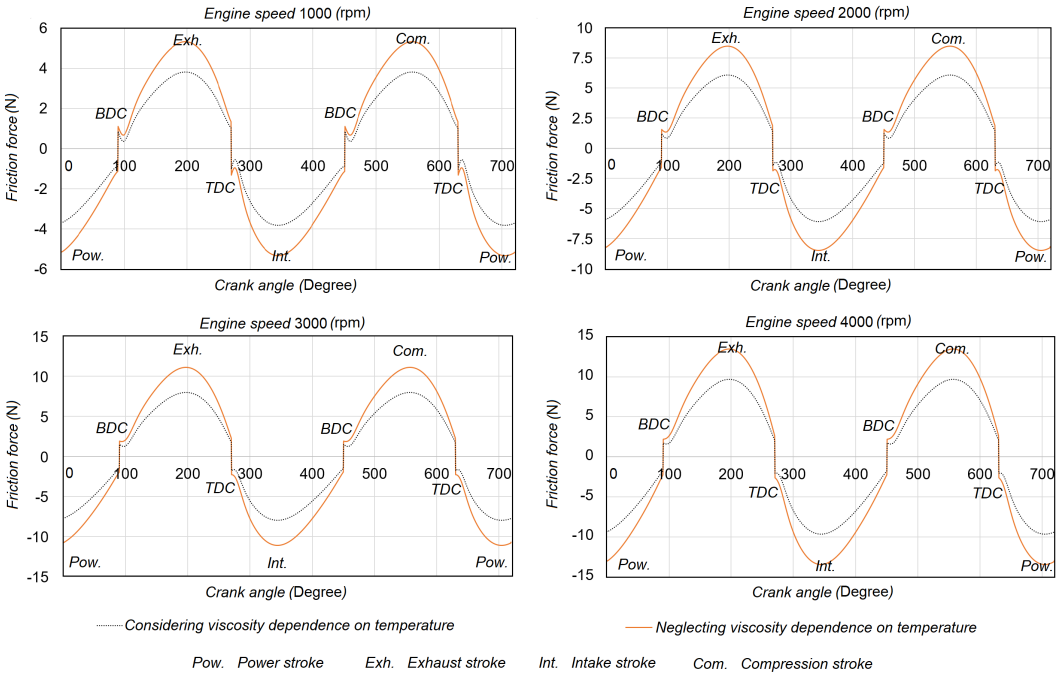

Fig. 3.28 Friction loss at oil control ring and liner interface under motored condition.

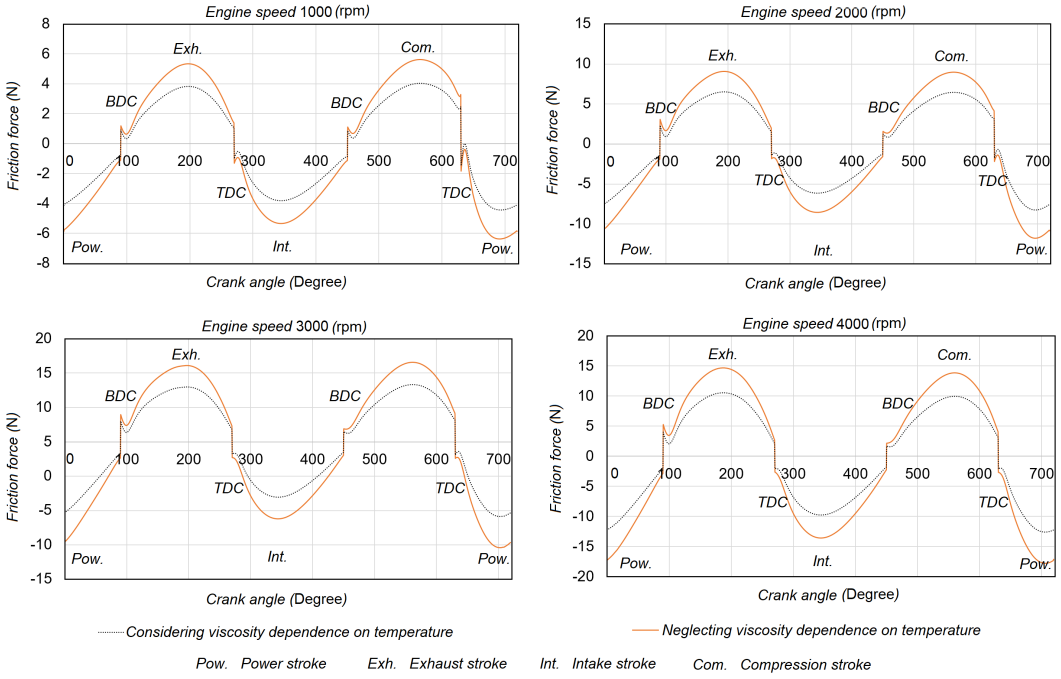

Fig. 3.29 Friction loss at oil control ring and liner interface under fired condition.

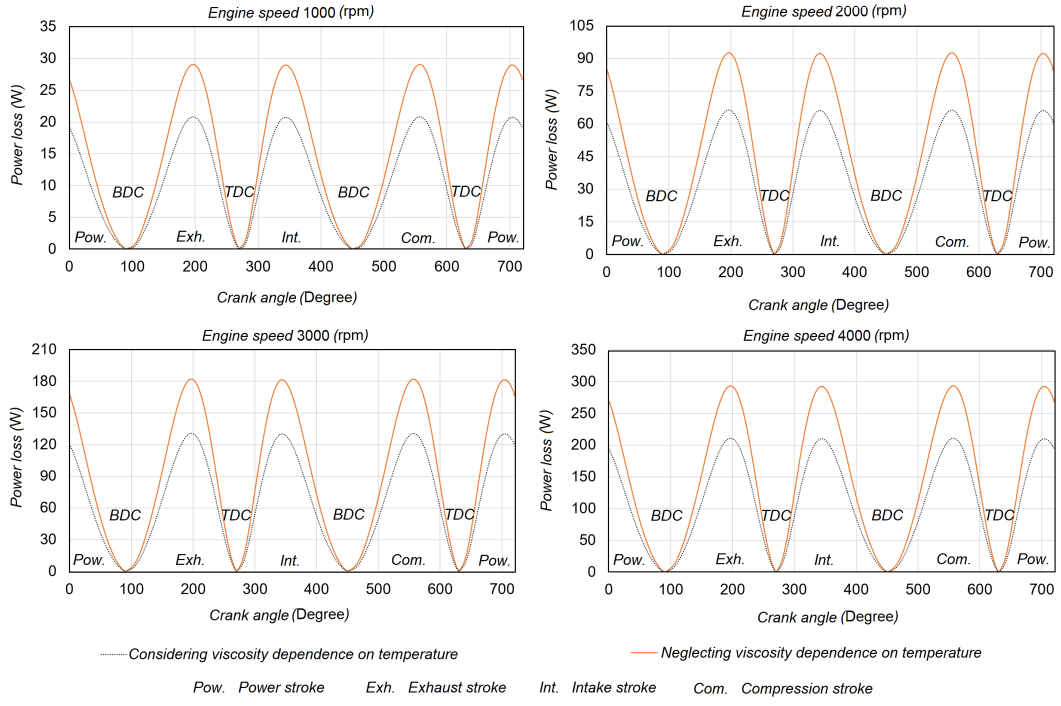

Fig. 3.30 Power loss at oil control ring and liner interface under motored condition.

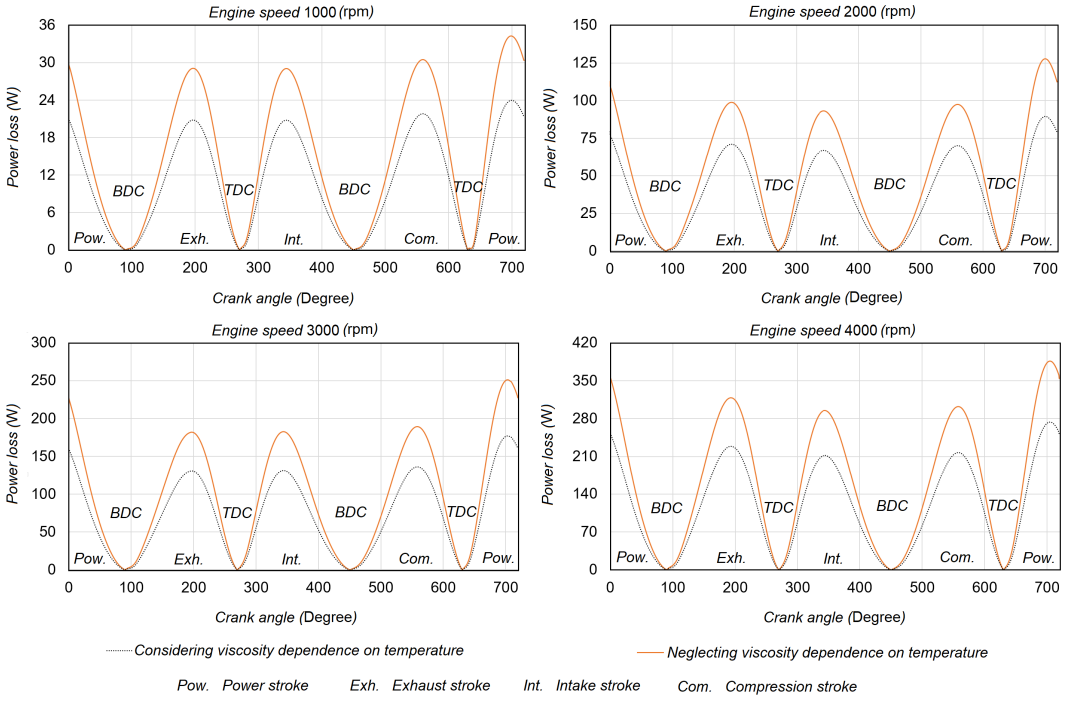

Fig. 3.31 Power loss at oil control ring and liner interface under fired condition.

Friction force and power loss contributed by viscous shear rate and oil squeeze action increase as the engine angular speed rises, at the same time reduction in lubricant viscosity with temperature increment results in lower friction force and power loss as shown by Fig. 3.32.

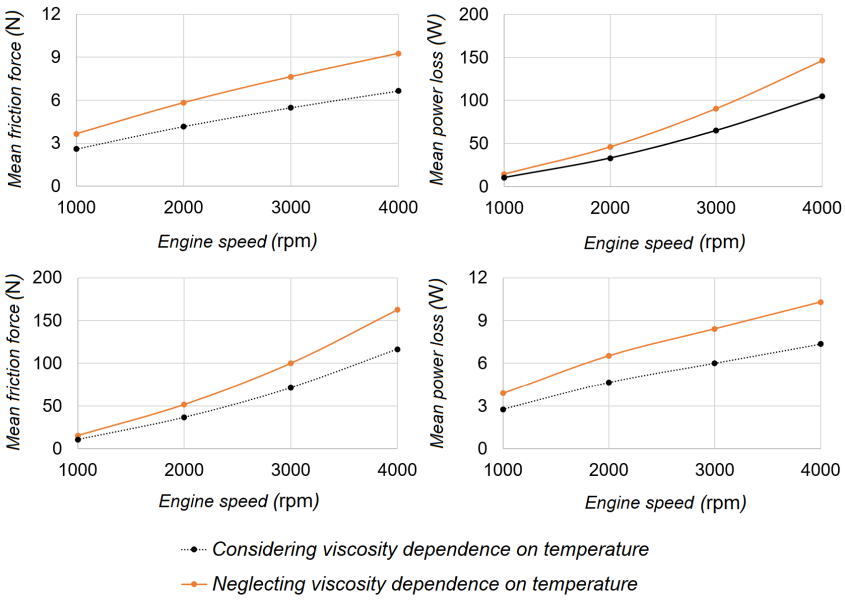

Fig. 3.32 Mean friction force and mean power loss at oil control ring and liner interface under motored and fired conditions.

3.6.2 ANOVA analysis to evaluate parameters affecting oil film thickness

Based on ANOVA table (Table 3.4), ring width (A), ring tension (C) and crown height (B), as well as interaction or joint effects of all single factors (BC, AC, AB and BE) are found to be significant as P-value is less than 0.05 at 95% confidence. Pareto chart proved that the ring width (A) and ring tension (C) are most influential parameter followed by the crown height (B) and interaction of single parameters as shown by Fig. 3.33.

Table 3.4 ANOVA table for average minimum oil film thickness

Source	Sum of Squares	df	Mean Square	F-value	p-Value	
Model	106.97	7	15.28	300.90	<0.0001	Sign.
A-Ring width	53.74	1	53.74	1058.20	<0.0001	Sign.
B-Crown height	2.63	1	2.63	51.74	<0.0001	Sign.
C-Ring tension	42.76	1	42.76	841.92	<0.0001	Sign.
AB	2.04	1	2.04	40.07	<0.0001	Sign.
AC	2.27	1	2.27	44.77	<0.0001	Sign.
BC	2.39	1	2.39	47.11	<0.0001	Sign.
BE	1.14	1	1.14	22.52	<0.0001	
Residual	1.32	26	0.0508			
Cor Total	108.29	33				
Std. Dev.		0.2254		R^2		0.9878
Mean		4.51		Adjusted R^2		0.9845
c.v.%		5.00		predicted R^2		0.9785
				Adeq Precision		57.9345

The R-Squared shows how accurate model predicts the response values or is the measurement of the amount of variation around the mean, lower deviation from 1 is more desirable which in this case a value of 0.9878 is favorite. The Predicted R^2 of 0.9845 is in reasonable agreement with the Adjusted R^2 of 0.9785 as the difference is less than 0.2. Signal to noise ratio is illustrated by Adequate Precision which compares the range of the predicted value at the design points to the average prediction error, and the desirable ratio is greater than 4 that in this analysis is 57.9345.

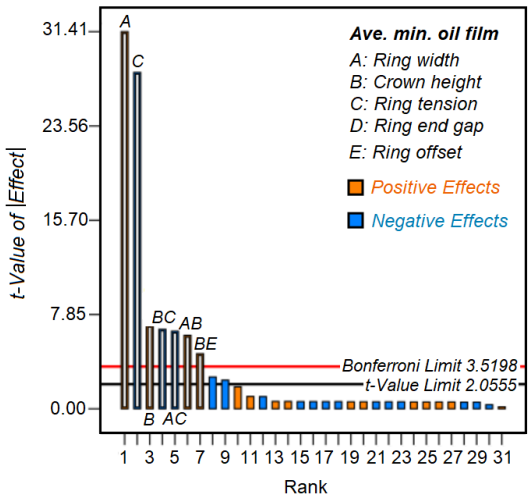

Fig. 3.33 Influential parameters affecting oil film thickness at ring/liner interface.

From Fig. 3.34, it can be observed that residuals follow a normal distribution as a straight line can fitted through the normal plot of residuals. Figure 3.35 is a normal plot of the residuals versus the evaluation run order looks for lurking variables that may have influenced the response during the analysis. Random scatter must be obvious; blocking and randomization provide insurance against trends ruining the analysis.

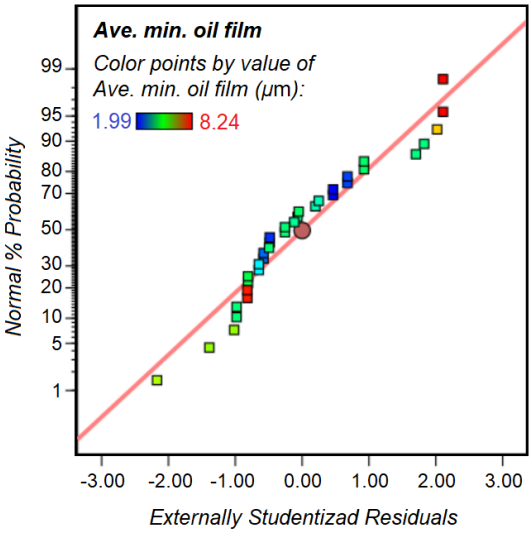

Fig. 3.34 Normal plot of Residuals for average minimum oil film thickness.

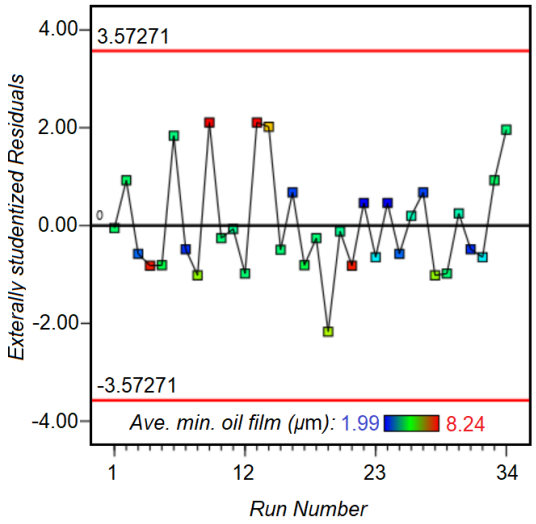

Fig. 3.35 Normal plot of Residuals for average minimum oil film thickness.

Figure 3.36 illustrates the effect of single-variables on average minimum oil film thickness. Ring width plays positive and most important role on increment of minimum oil film thickness followed by ring tension force which has negative contribution as the line slope is negative. On the order hand, the higher ring width the higher minimum oil film thickness obtained, and in opposite, increment of ring tension force results in lower thiner oil film thickness.

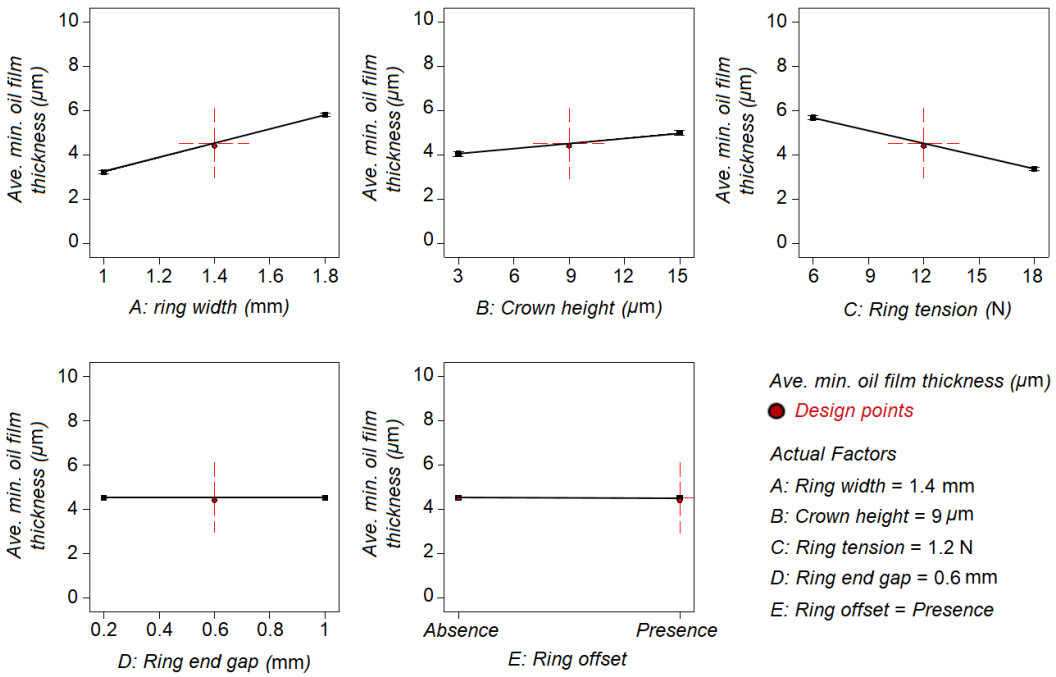

Fig. 3.36 The effect of each single variable on average minimum oil film thickness.

Ring width plays positive role regarding to Fig. 3.36, the larger ring width the thicker oil film thickness due to the reduction in ring elastic pressure over the ring face and consequently reduces the imposed load. Higher crown height results in thicker oil film thickness as strengthens the wedge action and consequently enlarges the hydrodynamic pressure and hydrodynamic lifting force that predominates normal load (contributed by ring tension force and gas pressure acting on backside of the ring) that acts against the hydrodynamic force. Increment of ring tension has negative contribution to the oil film thickness, the higher ring elastic pressure the thiner oil film thickness.

3.6.3 ANOVA analysis to evaluate parameters affecting power loss

Again based on ANOVA data in Table 3.5, all single parameters except ring end gap are significant variables followed by the interaction of ring tension and ring face offset (CE) as Pareto chart implies the same (Fig. 3.37).

Table 3.5 ANOVA table for average power loss

Source	Sum of Squares	df	Mean Square	F-value	p-Value	
Model	35.99	5	7.20	410.03	<0.0001	Sign.
A-Ring width	2.91	1	2.91	165.88	<0.0001	Sign.
B-Crown height	27.91	1	27.91	1590.02	<0.0001	Sign.
C-Ring tension	3.55	1	3.55	202.43	<0.0001	Sign.
E-Ring offset	1.40	1	1.40	79.56	<0.0001	Sign.
CE	0.2151	1	0.2151	12.25	0.0016	Sign.
Residual	0.4915	28	0.0176			
Cor Total	36.48	33				
Std. Dev.		0.1325		R^2		0.9865
Mean		5.76		Adjusted R^2		0.9841
c.v.%		2.30		predicted R^2		0.9813
				Adeq Precision		63.6568

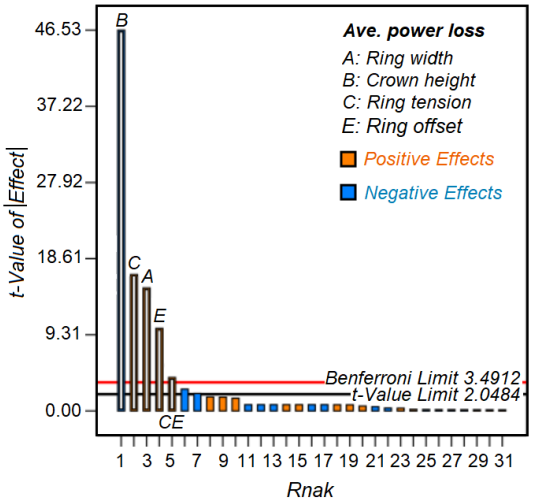

Fig. 3.37 Influential parameters affecting power loss at ring/liner interface.

The R-Squared with the value of 0.9865 is desirable as it is close to 1. The Predicted R² of 0.9813 is in reasonable agreement with the Adjusted R² of 0.9841 as the difference between them is less than 0.2. The Adequate Precision of 63.6568 is desirable ratio as it is greater than 4. Residuals normally are distributed regarding to Fig. 3.38 as they follow a straight line. Random scatter of residuals is obvious with respect to residuals versus the experimental as it checks the lurking variables that may affect the response as shown by Fig. 3.39.

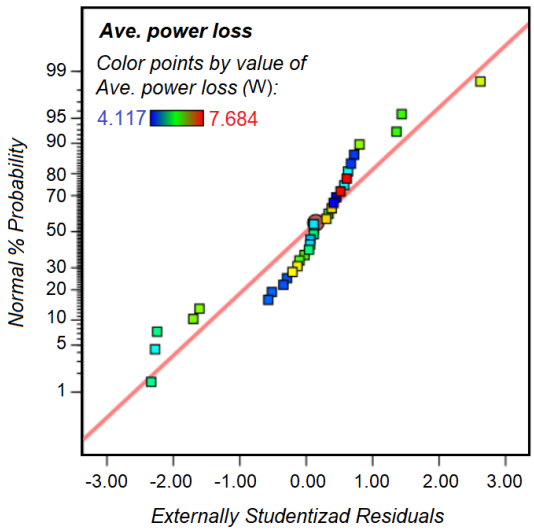

Fig. 3.38 Normal plot of Residuals for average power loss.

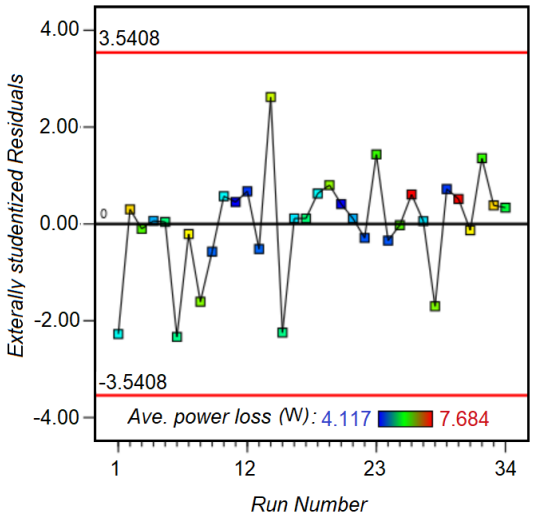

Fig. 3.39 Normal plot of Residuals for average power loss.

Figure 3.40 shows the effect of each single-variables on the average power loss. As ring width and ring tension force increase, average power loss increases, and the lower crown height the lower power loss.

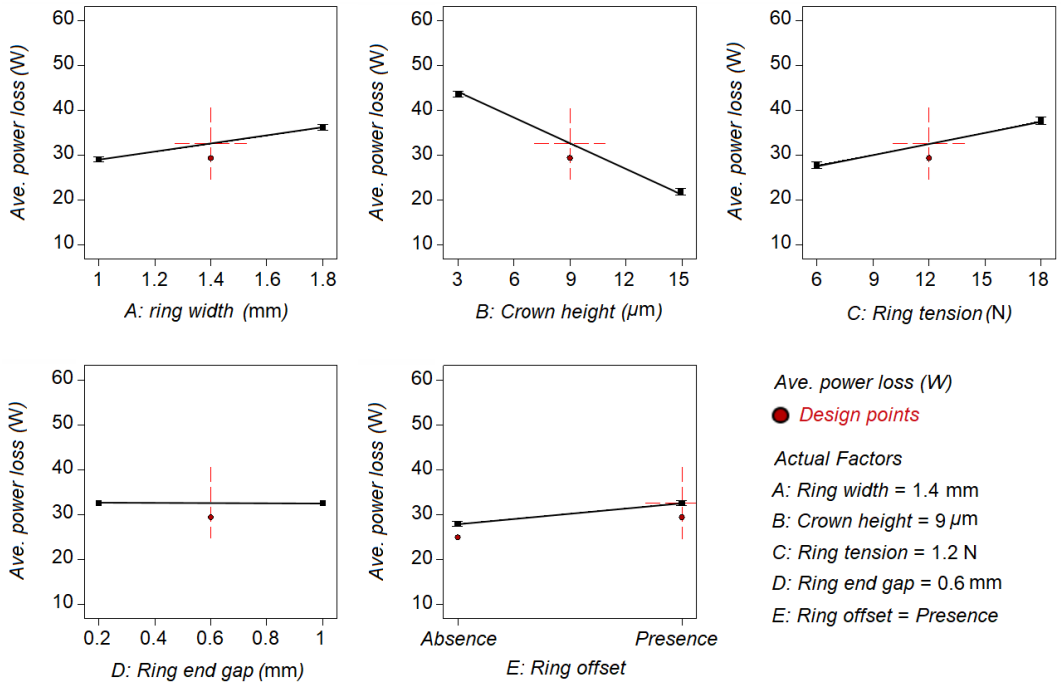

Fig. 3.40 The effect of each single variable on average power loss.

It is found that higher crown height results in reduction of power loss and enlargement of the minimum oil film thickness. Highly curved ring face encourages thick oil film thickness by wedge action, especially at mid-phase when wedge action is predominant. Besides, parabolic ring profile with high crown height provide larger inlet wedge angle and promotes higher hydrodynamic pressure gradient, and reduces the likelihood of mixed lubrication and then the power loss [92]. Higher crown height is associated with larger clearance between the ring and the liner, at critical regions, TDC and BTC reduces the amount of asperity contact when squeeze action prevails. Higher ring tension force results in reduction of oil film thickness and increment in power loss and likelihood of boundary lubrication. As it is expected, the nominal oil film thickness for higher ring elastic pressure is remarkably less than the nominal oil film thickness for the ring with lower elastic pressure.

3.7 Summary

An analytical model to evaluate piston ring pack consisting of two compression rings and one oil control ring has been presented. The model was relied on lubrication

theory and solving Reynolds and force equilibrium equations considering hydrodynamic lubrication at ring and liner interface. Three different scenarios have been considered to evaluate ring lubrication with respect to working conditions. For the first ring due to severe operating condition and the load imposed by combustion chamber, oil starvation and rupture (cavitation) was considered using Reynolds cavitation and reformation boundary conditions. For the second ring, oil speration has been taken into account in which the leading edge of the ring was engulfed by the oil and trailing edge was partially covered by the lubricant. In case of oil control ring, as it is working in moderate condition regarding the gas pressure acting on it, fully flooded condition was considered that there was no oil rupture and ring fully covered by the oil. Inter ring gas pressure analysis was conducted to feed the ring pack model as boundary pressures acting on upper and lower edges of each ring. Design of experiment (DoE) was employed to statistically analyses of ring geometry on oil film thickness and power loss; ANOVA analysis was carried out to examine the significance of each parameter.

Chapter 4

Piston Skirt Lubrication and Tribology

4.1 Introduction

Piston skirt is known as lowest part of the piston with the task of keeping piston from rocking excessively in the cylinder. Generally, piston skirt is machined with small grooves to improve oil retention and transporting lubricant to piston/liner interface to guarantee proper lubrication. Even though piston is centered by the ring pack, unbalanced forces and moments acting on the piston in a plane perpendicular to the wrist pin axis containing the thrust and anti-thrust sides cause small translation and rotation of the piston within defined clearance. These motions are known as piston secondary motion and can be defined by means of eccentricities at the top and bottom of the skirt. Piston secondary motion is associated with important effects on PRA tribological performance such as gas leakage (blow-by), piston slap impact force and radiated noise as well as viscous friction due to transported oil to piston and cylinder junction.

4.2 State of the art

4.2.1 Hydrodynamic lubrication (HL)

As the piston dynamics and triboloy models in this chapter are developed based on the hydrodynamic lubrication of piston/liner interface, the works those devoted to study the piston secondary motion and lubrication considering hydrodynamic regime are summarized in this section.

Knoll and Peeken [93] examine piston skirt lubrication and dynamics considering hydrodynamic lubrication. Piston dynamic investigation was conducted in terms of oscillatory, lateral and rotational motions. Piston primary motion was evaluated via a series of equations regarding design parameters, while its secondary motion was determined by piston dynamic equations, and forces and moments acting over the piston. Finite element scheme was employed to solve the Reynolds equation as governing equation to calculate generated hydrodynamic pressure at the skirt/liner junction.

Li et al. [94] applied lubrication theory and dynamic equations to evaluate piston misalignment in defined piston and liner clearance. Piston dynamics was determined as function of crank angle. The effect of wrist-pin offset location, piston/liner clearance, and lubricant properties have been examined. It was found that piston dynamics and tribological performance are dramatically influenced by the wrist-pin position. Besides, piston translational and rotational motions are remarkably affected by piston/liner clearance and oil viscosity.

Rezeka and Henein [95] introduced a set of empirical models to calculate the instantaneous skirt friction components. Hydrodynamic lubrication of piston skirt was assumed due to consideration of the point that gas load is sustained by the ring pack. The empirical model is relied on Newton's laws to calculate friction force, and its torque.

Ohta et al. [96] conduct a theoretical investigation to study the effect of piston secondary motion on side force and piston slap. Reversal resonant modes for the piston and liner and in addition a coupled system of equations were applied to govern the piston dynamics.

Mourelatos [97] performed theoretical evaluation of trajectory of a ring-less crosshead piston in an internal combustion engine (ICE). The flexible polytope

unconstrained minimization method has been employed to determine the correlation between piston elastic deformation and generated hydrodynamic pressure at bearing surfaces interface. It was found that if the piston profile was designed accurately, piston does not touch the cylinder wall; in the case of a double wedge piston skirt profile, piston slap is an inevitable occurrence.

Ciulli [98] examined the effect of wrist-pin offset position through theoretical and experimental investigation. Frictional loss in ICE was measure considering the contribution of piston skirt, valvetrain and journal bearing.

Haddad and Tjan [99] studied the effects of wrist-pin offset location, piston center of gravity (CG), crankshaft offset, and hydrodynamic pressure on piston slap. Engine efficiency reduces by reduction of piston kinetic energy contributed by piston slap. It was realized that piston pin and crankshaft offsets have significant effect on piston secondary motion and kinetic energy variation.

Radcliffe and Dowson [100] presented a simplified model to evaluate tribological performance piston ring pack in modern automotive. A simple piston skirt friction model has been developed to provide an approximation of piston skirt friction to be considered in the ring friction predictions.

Lubrication theory has been applied to examine the effect of hydrodynamic pressure on piston skirt considering oil viscosity as a function of axial piston position [101]. Piston and liner interface was considered as not engulfed by the lubricant circumferentially. The investigation has capability to evaluate the effect of combustion pressure excitation on piston secondary motion and slap.

Luca et al. [102] evaluated fluid film squeeze action to determine piston slap forces under hydrodynamic lubrication. Considering cavitation, the lubricant film was treated as a damper and bubbles were treated as springs. The result provides evidence that neglecting cavitation can yield an error of up to one order of magnitude, while the Reynolds equation may overestimate the impact force magnitude.

A model has been introduced to evaluate piston ring assembly tribology relying on lubrication theory [34]. A transient two dimensional (2D) Reynolds equation and piston dynamic equations were applied as governing equations. A finite difference method and a numerical solution were used to derive empirical equation taking into account the correlation between piston skirt geometry, operating condition, and oil viscosity to calculate the friction loss at the piston/liner junction.

Nakashima et al. [103] carried out a numerical investigation to evaluate piston skirt/liner junction lubrication to clarify the piston dynamics and impact force as a tool to reduce piston slap noise. To compensate the effect of piston inertial force, it was noticed that adequate attention must be put on the location of CG, which was estimated by a numerical approach. The findings provide evidence that the pin offset and CG are important controller parameters to reduce emitted noise.

A general model has been introduced to account the contribution of main components to the total frictional loss and for the effect of design parameters, and operating condition [104]. The model relied on consideration of lubrication mechanism, design parameters and the physics that govern the friction.

Haubner [105] simulated piston secondary motion to be applied as a boundary condition to assess the dynamic behavior of piston rings. The model takes into account bearing bodies, the surface texture and the thermal and thermodynamic behavior of the piston and liner. The surface texture was incorporated using statistical methods.

Two different methods has been used to study the effect of film thickness on piston slap and its frequency; the approaches were relied on lubrication theory [106]. First, treating piston and liner as rigid bodies, then by using an experimental approach to study lubricant squeeze action. Three test benches were designed to consider different impact configurations (angles) and geometries of bearing surfaces. In the second method, it was found that oil damping could be determined by the evaluation of lubricant squeeze action solving Reynolds equation.

Hoffman et al. [107] conducted a statistical analysis using design of experiment (DoE) to evaluate piston secondary motion. Piston skirt length, profile and skirt ovality along the wrist-pin offset were examined as independent input variables and piston slap and frictional losses as dependent variables. The input data to contact DoE were calculated using multibody dynamic simulation model treating piston as flexible body.

Jang and Cho [108] investigate the impact of skirt profile and wrist-pin on piston dynamic. Two different types of skirt profiles, flat and barrel, were evaluated. The flat profile has lubrication films on the narrower gap of the sliding direction and on wider gap on the other side but it cannot be supported by hydrodynamic pressure on both sides; conversely, the barrel profile is hydrodynamically supported at both sides.

The governing equations used in the model are coupled dynamic equations and the Reynolds equation.

Ligier and Ragot [109] carried out numerical simulation to evaluate wear on the wrist-pin bushes and friction loss at earlier design steps considering mixed lubrication in the wrist-pin and piston interface. To define the contact phases, piston dynamics was evaluated under hydrodynamic lubrication.

Livanos and Kyrtatos [42, 43] applied finite element scheme to solve the dynamic equations and the 2D Reynolds equation as governing equations. Hydrodynamic lubrication has been considered at skirt and liner interface.

Three-dimensional (3D) simulation of piston dynamics taking into account the thermal deformation of the piston and liner, bearing bodies stiffness (piston and liner) and lubrication regime is reported [110]. The model has capability to provide accurate estimation of liner vibration, piston slap noise, and evaluate the piston design in the early stage of engine development.

Wang et al. [111] performed a detailed analysis to study the piston slap and piston secondary motion considering oil damping and viscous friction. All possible contact states were considered and corresponding dynamic differential equations have been solved applying the Runge-Kutta method. Besides, piston dynamics and slap force were evaluated via the simulation code. It was found that piston slap is due to the gas pressure in the expansion stroke and to the inertial force in other strokes.

Kellaci et al. [112] classified the factors affecting piston skirt/liner tribology as design parameters (skirt profile, surface texture, and clearance), oil rheology and operating conditions. An analytical model was introduced to evaluate the effect of oil viscosity and its variation with respect to liner temperature during engine strokes on piston/skirt lubrication.

The effects of piston ring lubrication mechanism and skirt waviness on piston secondary motion have been studied using lubrication theory [113]. It was found that the consideration of piston ring tribology plays an important role on piston dynamics and lubrication.

McFadden and Turnbull [114] evaluated piston secondary motion assuming that gas pressure induces the axial motion of the piston (primary motion), rather than the force resulting from the steady rotation of the crankshaft. Two different lubrication conditions were considered: first, the piston skirt was completely immersed in

oil (fully flooded); second, only two portions of the skirt were covered by the oil (partially lubricated). It was concluded that dynamics and slap are sensitive to the degree of the piston skirt being covered by lubricant.

Flexible body analysis coupled with multi-body dynamics analysis to evaluate piston dynamics and piston deformation is performed [115]. Numerical results were compared to experimental data via a novel method named battery-powered-telemetric measurement.

Tan and Ripin [116, 117] presented a nonlinear model to evaluate piston dynamics and vibration due to piston slap. To examine the effect of piston slap, high damping coefficient and stiffness of the translational hard stop were incorporated to evaluate piston secondary motion. The piston/liner clearance was considered as a nonlinear parameter. The piston ring friction was obtained by experiment then correlated with the friction force equation.

Due to high load imposed on piston, particularly in expansion stroke, piston operates at elevated temperature and experiences mechanical and thermal distortions as consequence of relatively high thermal expansion. This phenomenon affects the clearance, which complicates lubrication mechanism and skirt deformation analysis. Littlefair et al. [118, 119] introduced an approach to evaluate the contribution of piston skirt thermal and mechanical deformation and piston crown compliance on the piston/liner clearance alteration. In order to shorten the computation time, an introduced compliance matrix was manipulated in coupled with numerical solution of the Reynolds equation to accurately calculate oil film thickness at the bearing surfaces junction.

Zhu et al. [120] introduced a dynamic model to reduce piston dynamics and dveloped a solution to examine piston skirt lubrication. The piston dynamics analysis was based on four parameters: switching of stationarity, motion stability, piston kinetic energy, and friction losses. The effects of skirt profile, piston/liner clearance, and wrist-pin offset have been taken into account to evaluate piston secondary motion. The findings provide evidence that the optimized skirt profile reduces the piston lateral and rotation motions.

Later in 2016, Kobayashi improved their previous method [110] and introduced a new 3D method to examine piston slap noise, piston skirt friction and scuffing [121]. The method could not provide an index to determine the accurate estimation

of scuffing, but proved that there is the shortage of method to precisely predict the piston/liner scuffing.

4.2.2 Elasto-hydrodynamic lubrication (EHL)

Keribar et al. [122] developed an integrated model considering elasto-hydrodynamic lubrication (EHL) at skirt and liner interface to evaluate piston secondary motion. Hydrodynamic lubrication (HL) at the wrist-pin bearing was incorporated. The model has capability to estimate piston dynamics, tribological performance of the skirt, piston slap forces and wear on the skirt and liner. The effects of the piston crown and pin boss stiffness were incorporated by piston elasticity model considering conventional design.

An analytical model has been presented to study the piston dynamics considering the elastic deformation of the skirt, assuming full circumferential engulfment by oil [123]. A finite difference method was used to provide solution for Reynolds equation that governed the generated hydrodynamic pressure at skirt and liner interface. The model proved that the elastic deformation of the skirt alters the skirt profile and dramatically changes the hydrodynamic force and moment acting on the piston.

The effects of elastic and thermal deformation of the skirt as well as surface texture were studied considering two different lubrication regimes, mixed and EHL [124]. Contact analysis of the skirt and cylinder wall has been conducted. The EHL model examined thermal and elastic deformation of the skirt, generated hydrodynamic pressure and operating condition using finite element approach. The contact model only incorporates the load generated by the asperities contact and ignores the load induced by hydrodynamic pressure. The mixed lubrication evaluates the piston skirt lubrication considering the bearing surfaces as rigid surfaces that normal loads are sustained by hydrodynamic pressure and asperities contact.

Dursunkaya et al. [125] introduced an EHL skirt model to evaluate piston dynamics, skirt lubrication, and skirt elastic deformation. The model enables the evaluation of piston secondary motion for both piston configuration, conventional and articulated. Finite element analysis (FEA) was used to evaluate skirt deformation using a skirt compliance matrix to encourage the comparison of piston dynamics from a deformable piston skirt with such motion from a rigid piston skirt.

Paranjpe [126] conduct an analytical study to investigate piston dynamics and slap noise considering EHL at piston and cylinder wall. The model encourages the calculation of the normal force on the liner as a function of time, then transform to the frequency domain to obtain the behavior of harmonic content. It was found that the piston slap noise is contributed by piston top land contact with liner, skirt contact with cylinder wall and wrist-pin contact with the piston.

Kimura et al. [127] applied a multi-body dynamic simulation program to examine the piston dynamics with deformable piston skirt. The program incorporated dynamic equations of motion using one rotational degree of freedom (DoF).

Perchanok [128] conduct a simulation to evaluate how the elastic deformation of the liner and piston affects the piston/liner lubrication and piston secondary motion. The piston slap, piston tribology, and power losses were evaluated by means of asperity contact and viscous shear. The investigation also takes into account the effect of temperature and skirt deformation due to side load.

Offner et al. [129, 130] employed multi-body dynamics to study contact behavior of piston and liner under EHL. The adopted approach is based on converting the nonlinear mechanical system into subsystems with linear elastic behavior and with nonlinearities occurring only at the connections between the subsystems. The governing equations include dynamic equations to define the piston dynamics and vibration of bearing surfaces, and Reynolds equation to define hydrodynamic force and moment acting on the piston skirt. In another approach, piston secondary motion and lubrication regime were evaluated at lower computing time considering dry contact of piston and liner.

Duyar et al. [131] applied EHL analysis to evaluate the piston skirt/liner junction lubrication. It is known that the piston skirt is not completely supplied with lubricant and skirt is partially engulfed by the oil. When the skirt was fully engulfed, the Reynolds equation, Greenwood-Tripp contact model, and elasticity equations were solved within the simulation to determine the hydrodynamic pressure, piston elastic deformation, and contact pressures. The Half-Sommerfeld boundary condition was considered to take into account the dissolved bubbles within film lubrication. In order to evaluate the partial lubrication of skirt, a finite volume solution was used to solve Reynolds equation considering oil mass conservation.

Balakrishnan and Rahnejat [132] conducted an analytical analysis of piston secondary motion and piston/liner contact behavior under EHL. The model incor-

porates the skirt axial profile effect governing by the Reynolds equation. Newmark β-type for time was used as space-time solver and Newton-Raphson method for space-domain.

Sato et al. [133] studied the effect of bore distortion due to thermal expansion, cylinder head assembly load, and elastic behavior of cylinder head gasket. The variation of Young modulus and thermal expansion coefficient with respect to temperature was considered. FEA was applied to consider the effect of bore distortions on piston secondary motion under EHL condition. The obtained results were compared to experimental data but the effect of cylinder block distortion on the sensor recording accuracy has not been discussed.

Patel et al. [134] examined the effects of engine speed and inertial forces on piston dynamics. The piston misalignment becomes significant as inertial forces increase as a function of engine speed. The Newmark-β method was used as the time integration approach to evaluate the piston/liner contact behavior. As the piston secondary motion is affected by cylinder pressure, this effect on piston/liner contact was discussed.

Shah et al. [135] developed an analytical method to study the piston dynamics and piston/liner contact behavior under EHL. The oil film thickness was calculated and discretized using a finite difference scheme and 2D developed grids over the bearing surfaces. The model examined the effects of bore distortion, inertia loading, piston barrelity and ovality. The approach incorporated EHL behavior, contact algorithm, and piston dynamics.

An analytical model has been presented to evaluate the piston dynamics and tribology taking into account the effects of oil film inertia and surface roughness [136]. The findings show that oil film inertial force increases generated hydrodynamic pressure, temperature, load carrying capacity as well as piston secondary motion.

Meng and Xie studied [137] generated hydrodynamic pressure acting on skirt with quadratic profiles applying piston dynamics equation under EHL condition. The quadratic skirt profile shows better piston skirt lubrication and piston alignment through the engine strokes, and lower power losses.

Zhang et al. [138] introduced an analytical model to study the effects of system inertial variation, wrist-pin location, piston ring and skirt friction on the piston dynamics. The model is based on the variation in the system inertia comprised

piston, connecting rod and crankshaft. The model provides an estimation of oil pressure and oil squeeze action by solving the Reynolds equation.

Offner et al. [139] tried to gain insight into contact behavior of piston skirt and liner. The effect of the shape of the contacting surfaces, oil availability and rheology were evaluated under thermo-elastic-hydrodynamic condition solving Reynolds equation. The approach encourages the optimization of piston skirt design parameters such as clearance, oval and ball shape regarding piston slap induced noise, and frictional loss.

Littlefair et al. [140] studied the difference in film thickness and generated hydrodynamic pressure at skirt and liner interface between cold and thermoelastically deformed piston. The principle aim of this study is to clarify the importance of considering the true instantaneous piston skirt profile.

Ahmed et al. [141] developed a computer code to consider the effect of structural elastic deformation of piston/skirt and elastic deformation of skirt profile on the oil film thickness. The code is based on a 2D description of the lubricant film flow and a 3D deformation of solids. The governing equation is Reynolds equation that defines the hydrodynamic pressure acting on skirt, static and elastic equilibrium equations, which is used to evaluate the behavior of the bearing bodies. The coupled system of equations was solved using a finite difference method.

Littlefair et al. [142] adopted a semi-automatic methodology to predict piston skirt thermo-mechanical deflection, that takes into account skirt deformation and piston crown compliant contribution to the skirt–liner clearance. The approach is based on creation of a compliance matrix and its intricate manipulation which reduces computation time significantly. Combination of the purposed method and numerical solution of Reynolds equation encourages accurate prediction of film thickness at skirt and liner junction.

Dolatabadi et al. [143] introduced a new analytical model and numerical method to characterize piston slap noise. The model has capabilities to predict noise levels, impact characteristics and structural analysis of the engine block relying on interaction of EHL and skirt dynamics. Impact force and the squeeze film velocity were estimated with respect to oil film thickness variation and generated hydrodynamic pressure at piston and liner skirt. Piston slap force was determined to calculate the energy transferred to the engine block and then was used to estimate the structural attenuation factor to predict the induced sound.

4.2.3 Boundary and mixed lubrication

Keribar and Dursunkaya [144, 145] presented an approach to examine the lubrication of skirt/liner junction and piston secondary motion considering HL and boundary lubrication. The model has capability to evaluate the effect of skirt profile and surface texture, circumferential lubricant extension and bore distortion. The study encourage the consideration of oil starvation, which allows the axial extent of lubricant to vary circumferentially to satisfy the need for oil continuity. Finite difference scheme was adopted as one of the possible method to solve Reynolds equation incorporating surface roughness. in another investigation, the authors evaluate the effect of piston configurations, conventional (monoblock) and articulated design.

Zhu et al. [146, 147] studied the effect of surface topology, skirt profile, bulk elastic deformation and thermal distortion of piston skirt and liner under mixed lubrication. Reynolds equation incorporating the average flow factors was applied to evaluate the effect of surface texture. In addition to the forces and moments equilibrium, an initial value problem for a pair of nonlinear differential equations has been introduced to calculate piston eccentricities at skirt top and bottom. A numerical scheme was introduced to determine the piston dynamics and friction loss.

Wong et al. [148] studied piston secondary motion considering mixed lubrication at skirt and liner interface relying on investigations conducted by Zhu et al. [146, 147]. The piston lateral and rotational motions, skirt friction and impact forces were defined at each crank angle. The model evaluated partial lubrication of the skirt and besides, hydrodynamic pressure acting on the skirt contributed by hydrodynamic and asperities contact. The effects of surface roughness, surface texture, and bulk elastic and thermal deformation were incorporated by an average Reynolds equation.

Liu et al. [149] present a model considering mixed lubrication at piston skirt and liner interface to perform a comprehensive study of piston secondary motion. The effect of surface roughness was considered and piston secondary motion was defined by piston eccentricities at top and bottom of the skirt. The effect of wrist-pin offset location has been discussed. They proved that the parabolic skirt profile for piston sustains HL during up and downward strokes movement of the piston, while the linear skirt profile sustained HL only in one of the up or down strokes.

Cho et al. [150] conduct an analytical and experimental evaluation of crankshaft offset on engine tribological performance. The effect of different offset configu-

rations, connecting rod length, and crank radius were considered to maintain the original combustion chamber volume and the compression ratio. The evaluation was performed at different speed and load conditions to measure the variation of piston side force for different crankshaft offset values.

A numerical and experimental investigation has been performed to evaluate the effect of piston geometry and design parameters on piston secondary motion and tribology [151, 152]. The model takes into account the effect of surface roughness and the skirt profiles and ovality. The effects of piston liner clearance on piston impact velocity, piston skirt frictional force, and skirt dynamics have been evaluated by an experimental approach. The simulation examined the skirt elastic deformation and three different of lubrication mechanisms: hydrodynamic, mixed, and boundary lubrication regimes.

Nowadays in modern engines applying off-centered crankshafts is adopted as alternative way to reduce piston ring assembly friction rather than using wrist-pin offset. Ragot and Rebbert [153] evaluate the effect of crank offset as an alternative tool to reduce piston ring assembly friction. Two contact modes were addressed. The first one is relied on the Hertz theory of impact, which represents the structural stiffness of piston skirt and cylinder liner, and the second is based on lubrication theory to study the behavior of the hydrodynamic oil film at the skirt/liner junction. A multi-body simulation has been used to analyze a wide range of different engine working conditions and different crank offset values.

McClure and Tian [154] introduced a detailed model of piston and bore hot shape geometries. The model takes into account the piston deformation due to combustion pressure, axial inertia, and interaction with the cylinder bore. Hydrodynamic pressure at the skirt/liner junction is neglected to reduce computation time. It was noticed that the piston skirt, cylinder bore static, and dynamic deformations dramatically affect the skirt profile and must be considered to gain an estimation of piston secondary motion.

Malagi et al. [155] studied piston dynamics, including primary and secondary motion considering mixed lubrication at piston and liner junction solving 2D Reynolds equation.

Meng and Xie [156] presented a numerical model devoted to account the effect of connecting rod inertial force on the piston skirt tribology. It was assumed that connecting rod inertia is negligible and thus is ignored in the analysis. The model

incorporates connecting rod inertia, since at high speed, the connecting rod has a significant influence on piston skirt lubrication and dynamics.

Piston skirt lubrication has been studied considering the effects of surface texture and bearing surfaces deformation [157]. The model enables the better design of piston skirt in terms of reducing frictional losses.

Ning et al. [158, 159] examined the role of thermal and the elastic deformation of piston skirt and liner due to combustion chamber pressure and piston inertia on lubrication mechanism. The effect of oil temperature and shear thinning rate on oil viscosity was investigated, and detailed evaluation of piston secondary motion and tribological performance under mixed lubrication have been reported . The sensitivity of the skirt/liner lubrication to monograde and multi-grade lubricants was analyzed.

Offner [160] introduced a numerical approach to incorporate the overall flexible body system, lubricant properties. The detailed properties of the contact mechanisms at bearing surfaces interface was addressed. The study comprised the discussion on the effects of different types of mixed lubricated contacts.

4.3 Model and procedure

As aforementioned piston secondary motion can be defined by means of eccentricities at top and bottom of the skirt as shown by Fig.4.1(b). Forces and moments equilibrium about wrist-pin axis can be written as following, where the forces and moments acting on piston are gas force F_g, ring pack friction force and moment, F_{fr} and M_{fr}, piston inertial forces and moment F_{ap}, F_{zp} and M_{ip}, wrist-pin inertial forces F_{awp} and F_{zwp}, piston skirt friction force F_{fs}, connecting rod force F_{cr}, hydrodynamic force and moment due to oil pressure at piston skirt and liner interface F_h and M_h:

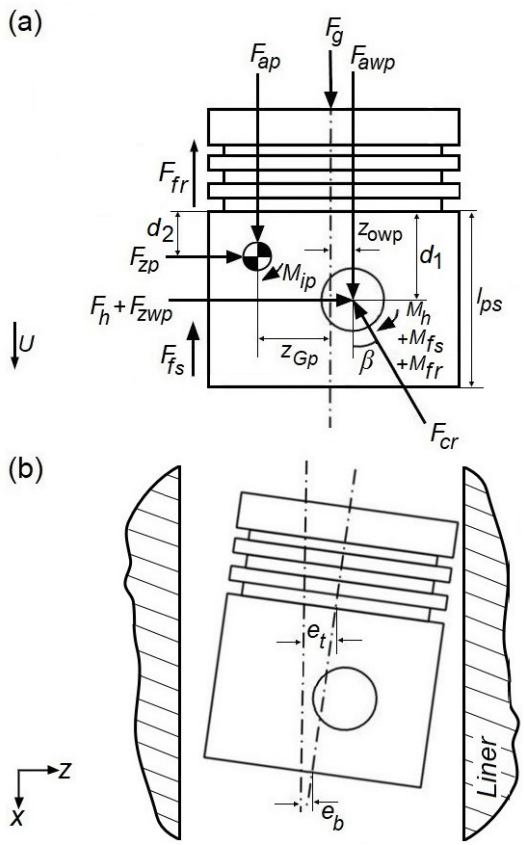

Fig. 4.1 (a) Piston free body diagram, (b) Eccentricities at top and bottom of the piston skirt.

$$\downarrow x \qquad F_g + F_{ap} + F_{awp} - F_{fs} - F_{fr} - F_{cr}\cos\beta = 0 \tag{4.1}$$

where $F_{fr} = \sum_{i=1}^{3} F_{fr_i}$ is the summation of friction force contributed by piston ring pack (two compression rings and one oil control ring);

$$\underset{\rightarrow}{z} \qquad F_h + F_{zwp} + F_{zp} - F_{cr}\sin\beta = 0 \tag{4.2}$$

$$\begin{aligned} \circlearrowleft \qquad & M_h + M_{fs} + M_{fr} + M_{ip} - \\ & + F_{ap}(z_{Gp} + z_{owp}) - F_g z_{owp} + \\ & + F_{zp}(d_1 - d_2) = 0 \end{aligned} \tag{4.3}$$

.

By writing F_{cr} from both Eqs. (4.1) and (4.2) and by re-equating the two expressions, the force equilibrium is obtained:

$$F_h - F_s = -(F_{zwp} + F_{zp}) \tag{4.4}$$

where

$$F_s = (F_g + F_{ap} + F_{awp} - F_{fs} - F_{fr}) \tan\beta. \tag{4.5}$$

Equation (4.3) can be rearranged as:

$$M_h - M_s = -(M_{ip} + F_{zp}(d_1 - d_2)) \tag{4.6}$$

where:

$$M_s = -M_{fs} - M_{fr} + F_{ap}(z_{Gp} + z_{owp}) + F_g z_{owp} \tag{4.7}$$

Connecting rod angle, piston and wrist-pin inertial forces in axial direction parallel to liner axis (at constant rotational speed, ω) can be defined as:

$$\beta = \arctan\left[\frac{r\sin\theta - z_{owp}}{\sqrt{l^2 - (r\sin\theta - z_{owp})^2}}\right] \tag{4.8}$$

$$F_{ap} = -m_p\ddot{x} \tag{4.9}$$

$$F_{awp} = -m_{wp}\ddot{x} \tag{4.10}$$

where $\ddot{x}$ (m/s^2) is piston acceleration:

$$\begin{aligned}\ddot{x} = \omega^2 r\Bigg[\cos\theta - \frac{\sin\theta\,(\Lambda\sin\theta - \delta)}{\sqrt{1-(\Lambda\sin\theta-\delta)^2}} + \\ + \frac{\Lambda\cos^2\theta}{\sqrt{1-(\Lambda\sin\theta-\delta)^2}} + \\ + \frac{\Lambda\cos^2\theta\,(\Lambda\sin\theta-\delta)^2}{\sqrt{\left(1-(\Lambda\sin\theta-\delta)^2\right)^3}}\Bigg]\end{aligned} \tag{4.11}$$

where Λ is ratio between the crank radius r (m) and the connecting rod length l (m), which is so-called elongation ratio and δ is adimensional offset $\delta = z_o/l$ which z_o is wrist-pin offset (m).

The transversal piston and wrist pin inertial forces and moment can be determined as:

$$F_{zp} = -m_p(\ddot{e}_t + \frac{d_2}{l_{ps}}(\ddot{e}_b - \ddot{e}_t)) \tag{4.12}$$

$$F_{zwp} = -m_{wp}(\ddot{e}_t + \frac{d_1}{l_{ps}}(\ddot{e}_b - \ddot{e}_t)) \tag{4.13}$$

$$M_{ip} = -j_p\frac{\ddot{e}_t - \ddot{e}_b}{l_{ps}} \tag{4.14}$$

4.3.1 Piston dynamics and tribology

Hydrodynamic and friction forces acting on piston skirt, F_h and F_{fs} respectively, and their resultant moments, M_h and M_{fs} about wrist-pin axis can be estimated using:

$$F_h = \int_0^{l_{ps}}\int_0^{2\pi} p(x,\alpha)R\cos\alpha d\alpha dx \tag{4.15}$$

$$F_{fs} = -\int_0^{l_{ps}}\int_0^{2\pi}(\frac{h}{2}\frac{dp}{dx} + \eta\frac{U}{h})Rd\alpha dx \tag{4.16}$$

$$M_h = \int_0^{l_{ps}}\int_0^{2\pi} p(x,\alpha)(d_1 - x)R\cos\alpha d\alpha dx \tag{4.17}$$

$$M_{fs} = -\int_0^{l_{ps}}\int_0^{2\pi}(\frac{h}{2}\frac{dp}{dx} + \eta\frac{U}{h})R^2\cos\alpha d\alpha dx \tag{4.18}$$

Substitution of all equations corresponds to calculate the forces and moments acting on the piston (Fig. 4.1) in Eqs. (4.4) and (4.6), results in a system of equations that governing piston secondary motion:

$$\begin{bmatrix} m_p(1-\frac{d_2}{l_{ps}}) + m_{wp}(1-\frac{d_1}{l_{ps}}) & m_p\frac{d_2}{l_{ps}} + m_{wp}\frac{d_1}{l_{ps}} \\ \frac{j_p}{l_{ps}} + m_p(d_1-d_2)(1-\frac{d_2}{l_{ps}}) & -\frac{j_p}{l_{ps}} + m_p(d_1-d_2)\frac{d_2}{l_{ps}} \end{bmatrix} \begin{bmatrix} \ddot{e}_t \\ \ddot{e}_b \end{bmatrix} = \begin{bmatrix} F_h - F_s \\ M_h - M_s \end{bmatrix} \tag{4.19}$$

4.3.2 Hydrodynamic force and moment analysis

The hydrodynamic pressure acting over the piston skirt can be determined using 2D Reynolds equation [161] due to variation of oil film thickness axially and circumferentially:

$$\frac{\partial}{\partial x}(h^3\frac{\partial p}{\partial x})+\frac{\partial}{R^2\partial\alpha}(h^3\frac{\partial p}{\partial\alpha})=-6\eta U\frac{\partial h}{\partial x}+12\eta\omega\frac{\partial h}{\partial\theta} \tag{4.20}$$

where x is the coordinate parallel to cylinder axis, α the piston circumferential coordinate (Fig. 4.2) and R the piston radius (m). Developed Finite difference mesh over the piston skirt is shown by Fig. 4.3.

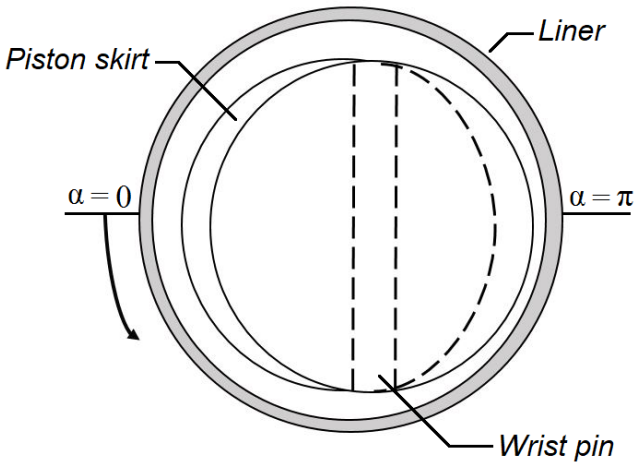

Fig. 4.2 Piston skirt and liner determination of circumferential coordinate α.

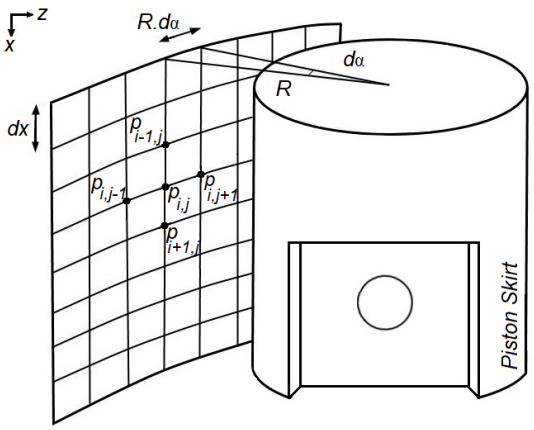

Fig. 4.3 Developed finite difference method over the piston skirt

Oil film thickness at piston/skirt interface can be expressed as:

$$h(x,\alpha) = c + [e_t + (e_b - e_t \frac{x}{l_{ps}})] \cos\alpha \tag{4.21}$$

where c is the piston skirt and liner clearance (m), l_{ps} the skirt length (m), e_t and e_b the eccentricities at top and bottom of the skirt (m) respectively.

The following quantities have been applied to form dimensionless Reynolds equation, oil film expression, pressure, forces and moments [94]:

$$\begin{gathered} \bar{d_1} = \frac{d_1}{R}; \quad \bar{l}_{ps} = \frac{l_{ps}}{R}; \quad \bar{x} = \frac{x}{R}; \quad \bar{h} = \frac{h}{c}; \quad \theta = \omega t; \\ \bar{U} = \frac{U}{r\omega}; \quad E_t = \frac{e_t}{c}; \quad E_b = \frac{e_b}{c}; \quad \bar{d_2} = \frac{d_2}{c}; \quad \bar{R} = \frac{R}{R}; \\ \dot{E}_t = \frac{\dot{e}_t}{c\omega}; \quad \dot{E}_t = \frac{\dot{e}_t}{c\omega}; \quad \bar{p} = \frac{c^2}{6r\omega\eta R} p; \\ \bar{F} = \frac{c^2}{6r\omega\eta R^3} F; \quad \bar{M} = \frac{c^2}{6r\omega\eta R^4} M \end{gathered} \tag{4.22}$$

Dimensionless form of Eqs. (4.20) and (4.21), have been rewritten as:

$$\frac{\partial}{\partial\bar{x}}(\bar{h^3}\frac{\partial\bar{p}}{\partial\bar{x}}) + \frac{\partial}{\partial\alpha}(\bar{h^3}\frac{\partial\bar{p}}{\partial\alpha}) = -\bar{U}\frac{\partial\bar{h}}{\partial\bar{x}} + K\frac{\partial\bar{h}}{\partial\theta} \tag{4.23}$$

where $K = \dfrac{2R}{r}$

$$\bar{h} = 1 + E_t\cos\alpha + \frac{\bar{x}}{\bar{l}_{ps}}(E_b - E_t)\cos\alpha. \tag{4.24}$$

Substituting Eq. (4.24) in Eq. (4.23) and perform differentiation at right side gives the dimensionless hydrodynamic pressure expression:

$$\begin{aligned} \bar{p} = -\frac{\bar{U}}{\bar{l}_{ps}}(E_b - E_t)\cos\alpha + K\dot{E}_t\cos\alpha + \\ + K\frac{\bar{x}}{\bar{l}_{ps}}(\dot{E}_b - \dot{E}_t)\cos\alpha \end{aligned} \tag{4.25}$$

Dimensionless form of Eqs. (4.15) and (4.17) are:

$$\bar{F}_h = \int_0^{\bar{l}_{ps}}\int_0^{2\pi} \bar{p}(x,\alpha)\cos\alpha d\alpha d\bar{x} \tag{4.26}$$

$$\bar{M}_h = \int_0^{\bar{l}_{ps}} \int_0^{2\pi} \bar{p}(x,\alpha)(\bar{d}_1 - \bar{x}) \cos\alpha d\alpha d\bar{x} \tag{4.27}$$

Substitution of Eq. (4.25) in Eqs. (4.26) and (4.27), and performing the integrations yields:

$$\bar{F}_h = \pi K \bar{l}_{ps} \dot{E}_t - \pi \bar{U}(E_b - E_t) + \frac{\pi K}{2} \bar{l}_{ps}(\dot{E}_b - \dot{E}_t) \tag{4.28}$$

$$\begin{aligned} \bar{M}_h = & \frac{\pi K \bar{l}_{ps}(6\bar{d}_1 - 3\bar{l}_{ps})}{6} \dot{E}_t + \\ & - \frac{\pi \bar{U}(6\bar{d}_1 - 3\bar{l}_{ps})}{6}(E_b - E_t) + \\ & - \frac{\pi K \bar{l}_{ps}(2\bar{l}_{ps} - 3\bar{d}_1)}{6}(\dot{E}_b - \dot{E}_t) \end{aligned} \tag{4.29}$$

Substitution of Eqs. (4.28) and (4.29) in dimensionless form of Eqs. (4.4) and (4.6), results in a system of first order differential equation as:

$$\begin{cases} \bar{F}_h - \bar{F}_s = -\bar{F}_{zwp} - \bar{F}_{zp} \\ \bar{M}_h - \bar{M}_s = -\bar{M}_{ip} - \bar{F}_{zp}(\bar{d}_1 - \bar{d}_2) \end{cases} \tag{4.30}$$

Finite difference scheme can be applied to solve 2D Reynolds equation and determine the pressure distribution at piston and liner junction:

$$\begin{aligned} & \frac{h^3_{i+\frac{1}{2},j} \dfrac{p_{i+1,j} - p_{i,j}}{\Delta x} - h^3_{i-\frac{1}{2},j} \dfrac{p_{i,j} - p_{i-1,j}}{\Delta x}}{\Delta x} + \\ & + \frac{1}{R^2} \frac{h^3_{i,j+\frac{1}{2}} \dfrac{p_{i,j+1} - p_{i,j}}{\Delta\alpha} - h^3_{i,j-\frac{1}{2}} \dfrac{p_{i,j} - p_{i,j-1}}{\Delta\alpha}}{\Delta\alpha} = \\ & -6\eta U \frac{h_{i+\frac{1}{2},j} - h_{i-\frac{1}{2},j}}{\Delta x} + 12\eta\omega \frac{h^{\theta+\Delta\theta}_{i,j} - h^{\theta}_{i,j}}{\Delta\theta} \end{aligned} \tag{4.31}$$

4.3.3 Numerical method and solution procedure

To consider the effect of friction force and moment F_{fs} and M_{fs}, respectively, acting on the piston skirt, the model starts at the mid phase of the expansion stroke, where the oil film thickness is expected to change slightly. By applying the finite difference method Eq. (5.13) with arbitrary values of e_t and e_b, hydrodynamic pressure at each

node can be defined. Consequently, F_{fs} and M_{fs} are calculated. Then, the oil film thickness at each node is updated for the next crank angle using Eq. (4.32), knowing the oil film thickness at current crank angle ($\theta + \Delta\theta$) and oil film thickness at previous angle (θ), the effect of squeeze action can be considered, and consequently calculate instantaneous pressure profile, F_{fs} and M_{fs}.

$$\begin{aligned} h_{i,j}^{\theta+\Delta\theta} = \frac{\Delta\theta}{12\eta\omega}\Bigg[& \frac{h_{i+\frac{1}{2},j}^{3}\dfrac{p_{i+1,j}-p_{i,j}}{\Delta x} - h_{i-\frac{1}{2},j}^{3}\dfrac{p_{i,j}-p_{i-1,j}}{\Delta x}}{\Delta x} + \\ & + \frac{1}{R^2}\frac{h_{i,j+\frac{1}{2}}^{3}\dfrac{p_{i,j+1}-p_{i,j}}{\Delta\alpha} - h_{i,j-\frac{1}{2}}^{3}\dfrac{p_{i,j}-p_{i,j-1}}{\Delta\alpha}}{\Delta\alpha} + \\ & - 6\eta U\frac{h_{i+\frac{1}{2},j}-h_{i-\frac{1}{2},j}}{\Delta x}\Bigg] + h_{i,j}^{\theta} \end{aligned} \tag{4.32}$$

After gain the first estimation of F_{fs} and M_{fs}, for whole engine cycle, and neglecting lateral inertial forces and moment (in z direction), and substituting in Eq. (4.30), piston transversal speeds ($\dot{e}_t$ and $\dot{e}_b$) and eccentricities at top and bottom of skirt (e_t and e_b) can be calculated using:

$$\begin{bmatrix} F_h(\dot{e}_t,\dot{e}_b,e_t,e_b) \\ M_h(\dot{e}_t,\dot{e}_b,e_t,e_b) \end{bmatrix} = \begin{bmatrix} F_s \\ M_s \end{bmatrix} \tag{4.33}$$

where F_s and M_s are the summation of reciprocating and inertial forces and moments. This system of first order differential equations Eq. (4.33) containing ($\dot{e}_t$, $\dot{e}_b$, e_t, e_b), must be solved at each time step (crank angle) applying numerical methods and iterative approaches in which piston starting condition ($\dot{e}_t$, $\dot{e}_b$, e_t, e_b) at the beginning of a time step are known. Using Newton-Raphson method to enjoy its fast convergence, the transversal piston speeds are obtained by:

$$\begin{bmatrix} \dot{e}_t \\ \dot{e}_b \end{bmatrix}^{\theta+\Delta\theta} = \begin{bmatrix} \dot{e}_t \\ \dot{e}_b \end{bmatrix}^{\theta} - \begin{bmatrix} \dfrac{\partial F_h}{\partial \dot{e}_t} & \dfrac{\partial F_h}{\partial \dot{e}_b} \\ \dfrac{\partial M_h}{\partial \dot{e}_t} & \dfrac{\partial M_h}{\partial \dot{e}_b} \end{bmatrix} \begin{bmatrix} F_h - F_s \\ M_h - M_s \end{bmatrix} \tag{4.34}$$

then eccentricities at the top and bottom of skirt (e_t, e_b) are given by:

$$e_t{}^{t+\Delta t} = e_t{}^{t} + \Delta t\dot{e}_t \tag{4.35}$$

$$e_b{}^{t+\Delta t} = e_b{}^{t} + \Delta t \dot{e}_b \tag{4.36}$$

where $\Delta t = \dfrac{\Delta\theta}{\omega}$ (s).

After the first estimation of piston lateral displacements (e_t and e_b), speeds ($\dot{e}_t$ and $\dot{e}_b$), and accelerations ($\ddot{e}_t$ and $\ddot{e}_b$), piston dynamic and secondary motion are recomputed with the added lateral inertial forces and moments. Finally, after defining the eccentricities at the top and bottom of skirt, the friction force can be calculated using finite difference method at each crank angle [162].

4.4 Results and discussion

The effect of ring pack tribology and lubrication has been taken into account by means of total friction force and its moment about wrist-pin axis. Three different lubrication scenarios were considered to evaluate piston ring pack tribological performance: fully flooded, oil separation and starvation and cavity (oil rupture and reformation) which are explained in Chapter 3. Piston skirt geometry and other relevant data are summarized by Table 4.1.

Table 4.1 Relevant engine parameters.

c	0.03 mm	m_{wp}	257 g
d_1	26 mm	R	41.87 mm
d_2	18.3 mm	Z_{Gp}	0.1 mm
l_{ps}	47.38 mm	Z_{owp}	0.5 mm
j_p	6.46E-04 kg/m^2	η	11.734E-03 Pa·s
m_p	540 g		

Oil film thickness extended at skirt and liner interface has been shown by Fig. 4.4 at the engine speed of 2000 rpm under fired condition. Figure 4.5 illustrated hydrodynamic pressure profile acting over the skirt in downward and upward strokes.

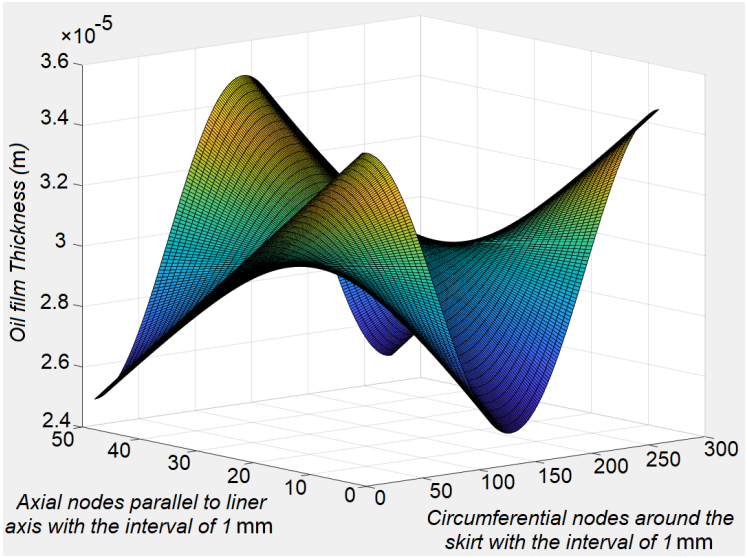

Fig. 4.4 Oil film profile at skirt and liner interface.

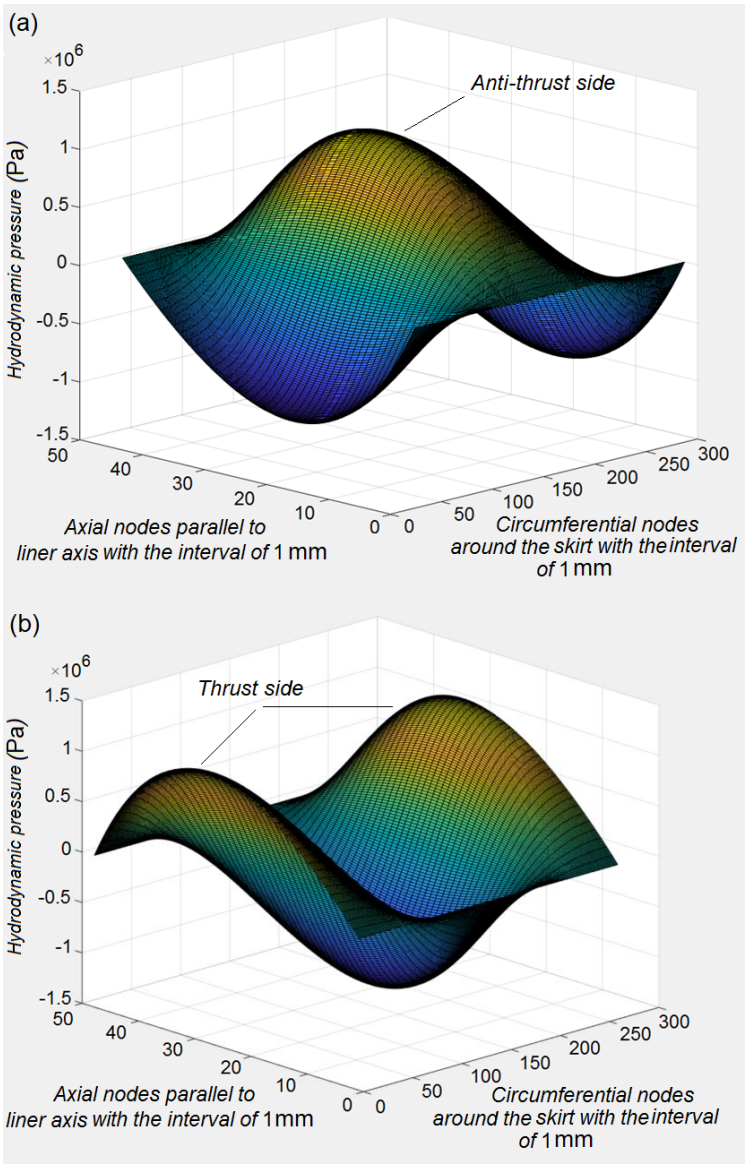

Fig. 4.5 Hydrodynamic pressure profile at skirt and liner junction; (a) downward stroke, (b) upward stroke.

Instantaneous eccentricities at top and bottom of skirt under fired condition at different engine angular velocity are shown by Fig.4.6. It has been observed that at higher crank speed or piston sliding speed (piston primary motion), lower piston misalignment is obtained as the lubricant load carrying capacity (LTC) increases due to higher shear rate and consequently lager hydrodynamic pressure at skirt and liner interface, that has capability to stand against the imposed loads acting on the piston as shown by Fig. 4.1. Instantaneous friction force and power loss at piston skirt

and liner interface are illustrated by Fig. 4.7. It is obvious that higher engine speed encourages larger friction force and power loss at skirt and liner interface. Regarding to viscous stress arising from lubricant flow rate, as the sliding speed increases and considering that the lubricant is treated as Newtonian fluid, shear rate within the oil film raises and consequently results in higher friction force and power loss.

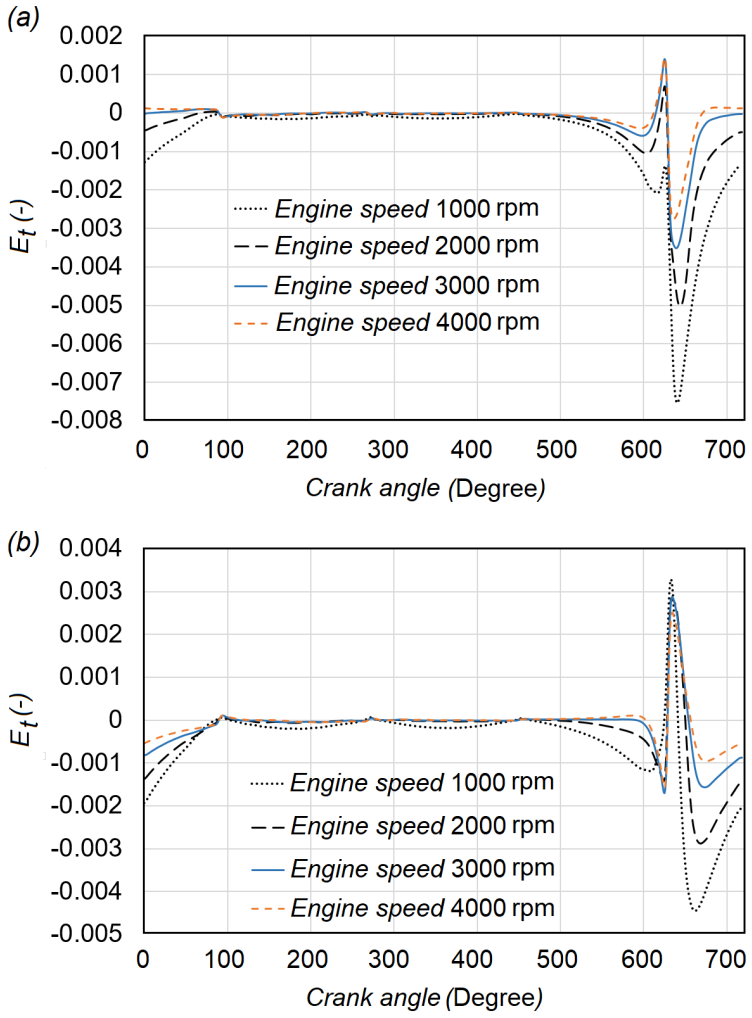

Fig. 4.6 (a) Eccentricities at the top, (b) eccentricities at the bottom of piston skirt at different engine speed.

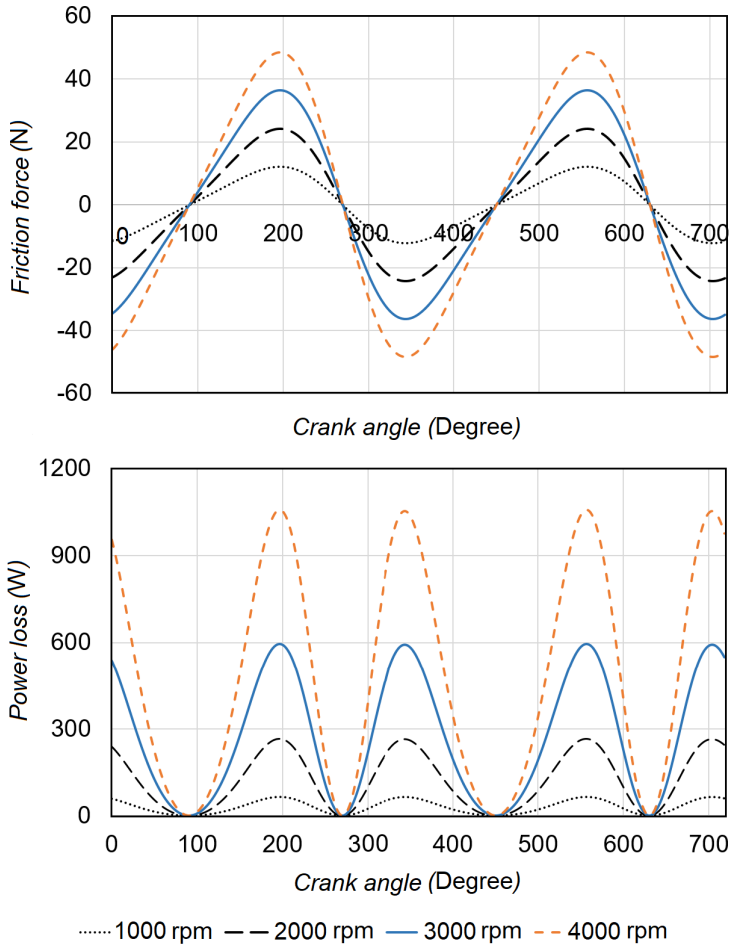

Fig. 4.7 Friction force and power loss contributed by piston skirt at different engine speed.

Eccentricities at top and bottom of piston skirt under fired condition at engine speed of 2000 rpm is shown by Fig.4.8 and considered as baseline to study the effect of influential factors such as, wrist-pin offset location, piston/liner clearance and lubricant viscosity. It is worth to mention that the wrist-pin offset is located toward the thrust side (Fig.4.1).

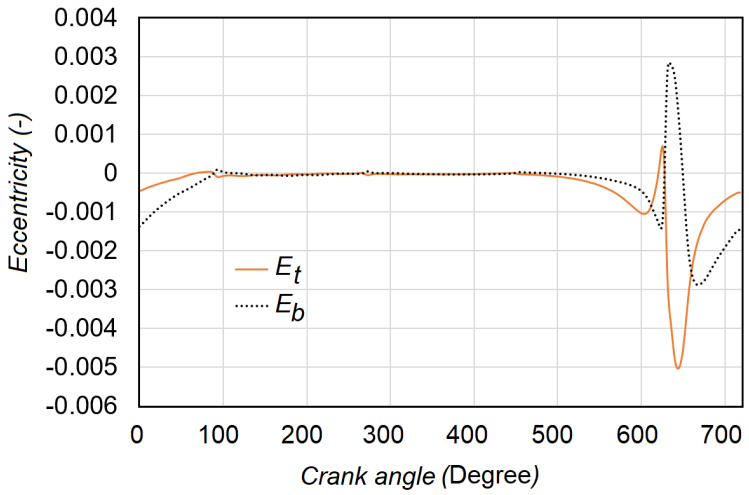

Fig. 4.8 Eccentricities at the top and bottom of piston skirt at the engine speed of 2000 rpm.

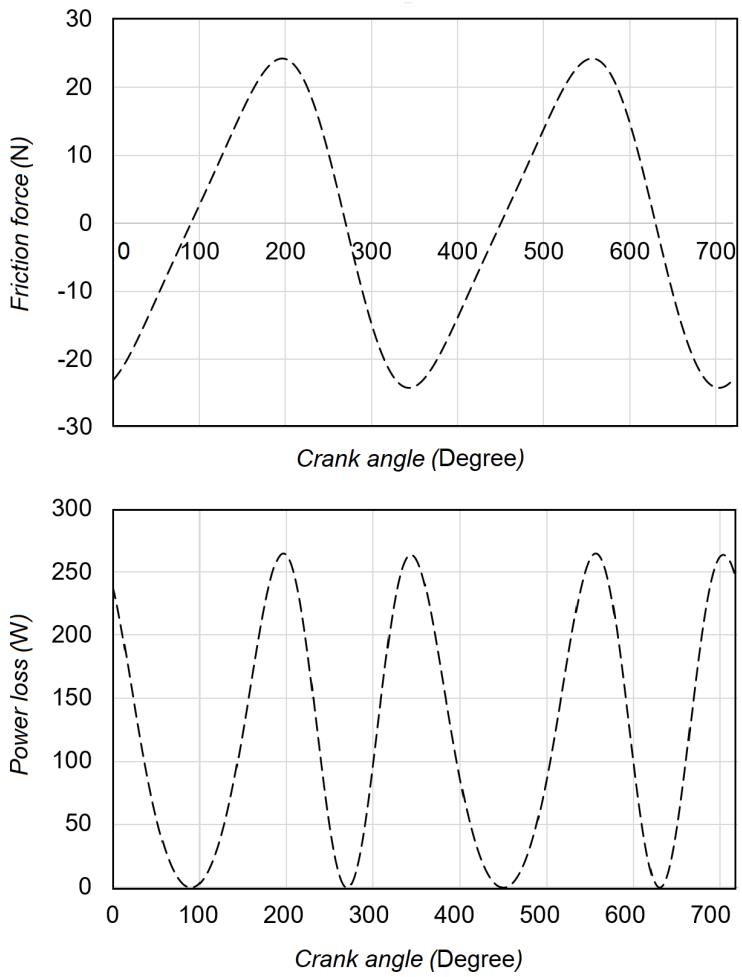

Fig. 4.9 Friction force and power loss at the engine speed 2000 rpm

4.4.1 Effect of wrist-pin offset location

Locating wrist-pin offset toward thrust side results in increasing the piston eccentricities at top and bottom of skirt fairly in most of crank angles, in contrary to locate the pin offset toward the anti-thrust side as shown by Fig.4.10. Piston misalignment in expansion stroke is more significant due to the formation of higher wedge action on the anti-thrust side and tilts piston towards the opposite side and promotes further piston tilt. In addition, piston eccentricities increase in upward strokes when wrist-pin offset locates toward the thrust side in comparison to position pin offset on anti-thrust side. This is due to the summation of couples contributed by gas force and piston mass inertial force in same direction with hydrodynamic pressure, and in

addition due to wedge action those tends to rotate the piston toward the thrust side in upward stroke. Friction force and power loss considering the different positions of wrist-pin are shown by Fig. 4.11. The higher misalignment of the skirt results in the higher wedge action and consequently the higher lubricant load carrying capacity and viscous shear stress. As the viscous shear stress increases within the lubricant layers results in higher friction force. Piston tends to tilt in the way that builds up hydrodynamic wedge action; therefore piston tilts toward thrust side in upward and rotates toward anti-thrust side in downward stroke [94]. Average power loss associated with piston skirt in both cases are 121.68 W and 123.42 W that shows around 1.43% increment in power loss as wrist-pin offset moves from anti-thrust side to thrust side.

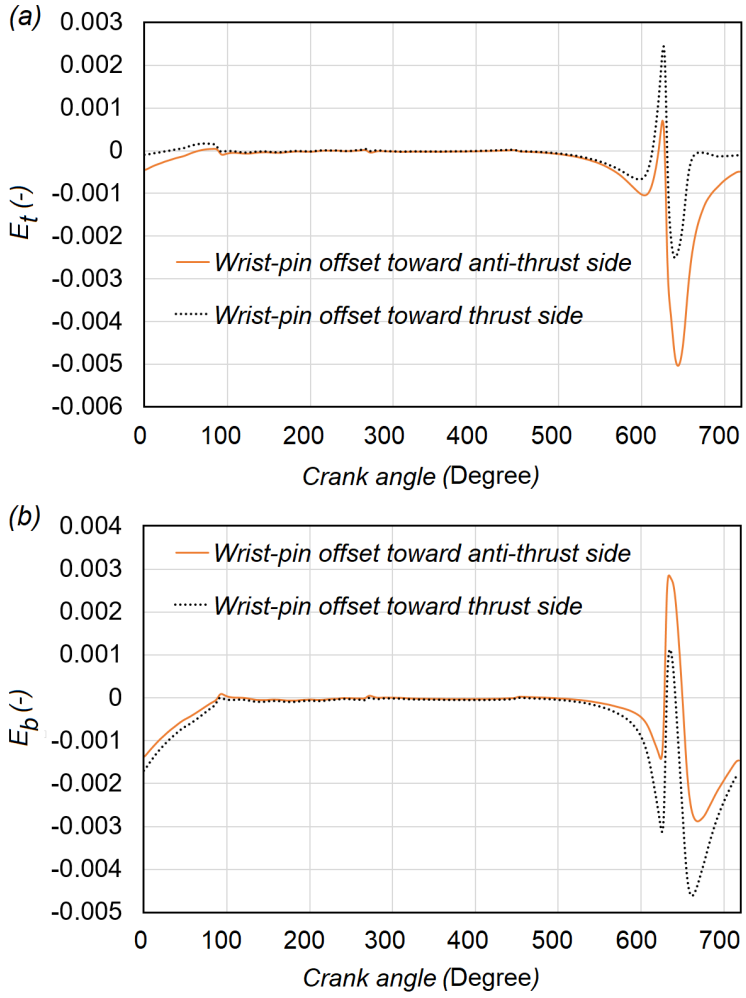

Fig. 4.10 Effect of wrist-pin offset location.

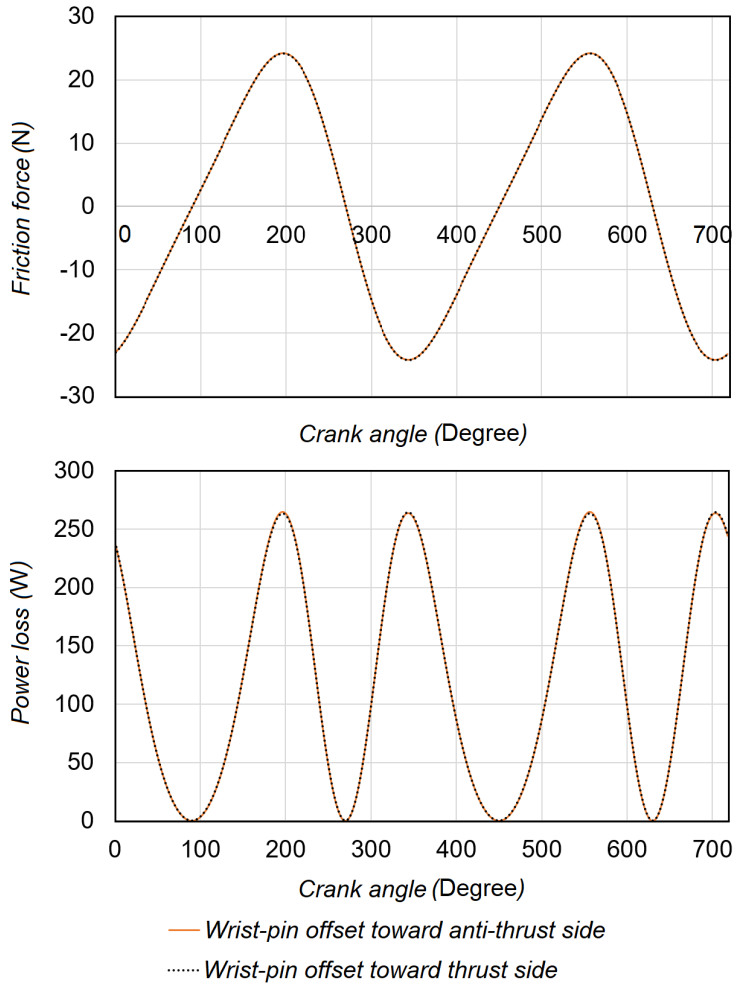

Fig. 4.11 Effect of wrist-pin offset location on friction force and power loss.

4.4.2 Effect of skirt/liner clearance

Piston eccentricity reduces as piston/liner clearance is reduced. The larger piston/liner clearance results in more piston eccentricity in comparison to close clearance as shown by Fig. 4.12. This is due to secondary motion of piston as it is effectively dampened due to a thinner layer of oil film at bearing surfaces interface. In contrary, larger clearance is associated with larger piston eccentricity, mainly due to the lack of oil film damping at skirt/liner junction. Clearance increment results in lower friction force which is due to larger gap between the bearing surfaces and it is associated with lower shear stress between oil layer and consequently lower hydrodynamic pressure.

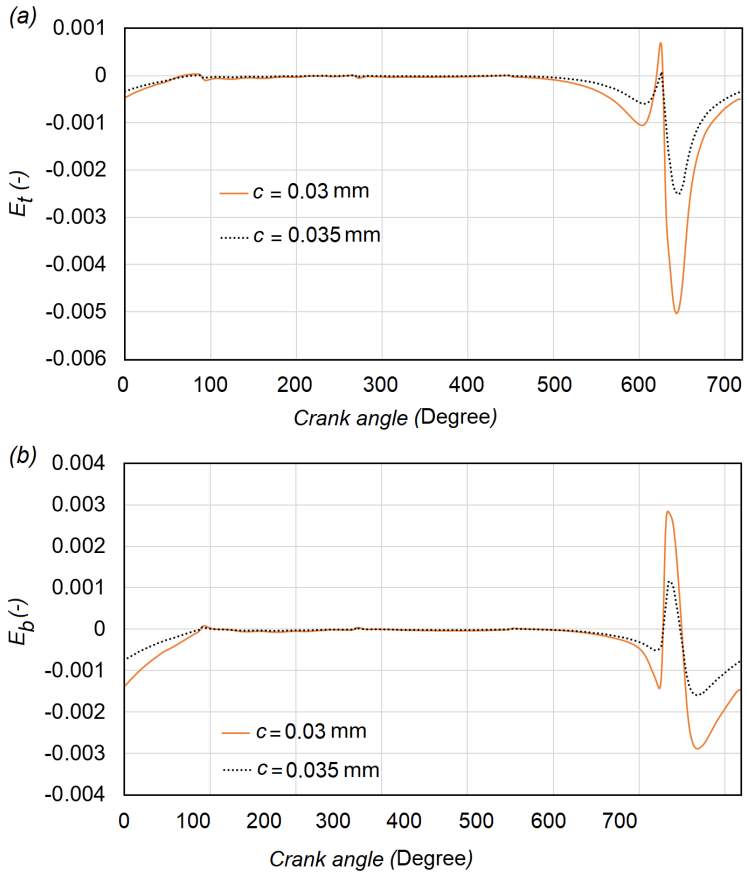

Fig. 4.12 Effect of piston/liner clearance.

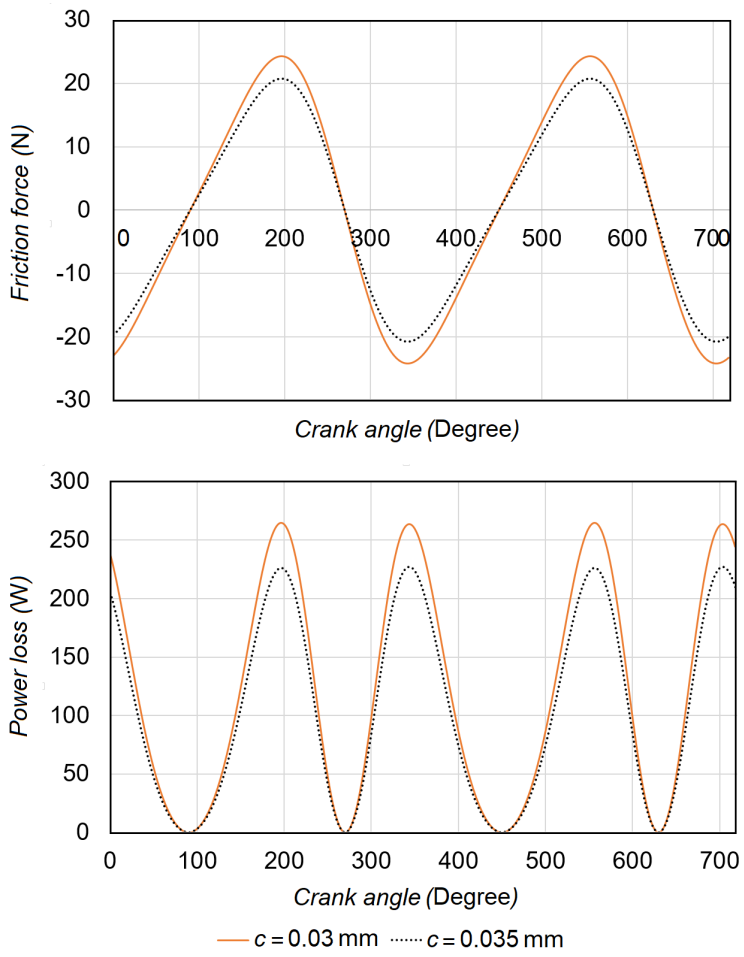

Fig. 4.13 Effect of piston/liner clearance.

4.4.3 Effect of lubricant viscosity

Figure 4.14 demonstrates the attained eccentricities at top and bottom of skirt considering lubricant viscosity at different magnitudes of temperature, 30, 60 and 90 °C. As the engine oil viscosity reduces, the lubricant load carrying capacity reduces and thereby higher piston misalignment at top and bottom is obtained. The lubricant viscosity affects load-carrying capacity and formation of supporting hydrodynamic pressure at bearing surfaces junction. These effects play remarkable role during expansion stroke where the loads and moments contributed by gas pressure, piston and pin inertial forces and ring pack friction force, reach their peak value. Due to reduction in oil load carrying capacity as lubricant viscosity reduces at higher temperature, generated hydrodynamic pressure at skirt and liner cannot sustain the

imposed loads and moments (Fig. 4.1) and consequently piston undergoes larger misalignments at top and bottom. The higher viscosity substantially results in increment of shear stress within the oil film and it can be the main reason of larger hydrodynamic friction loss at lower temperature as the higher viscosity is expected (Fig. 4.15). Despite piston skirt enjoys higher misalignment as lubricant viscosity reduces and higher friction force is expected due to significant role of wedge action (piston inclination), but friction force reduces as generated hydrodynamic pressure is affected by oil viscosity. Calculated friction force for three different magnitudes of viscosity at the engine speed of 2000 rpm is shown by Fig. 4.14.

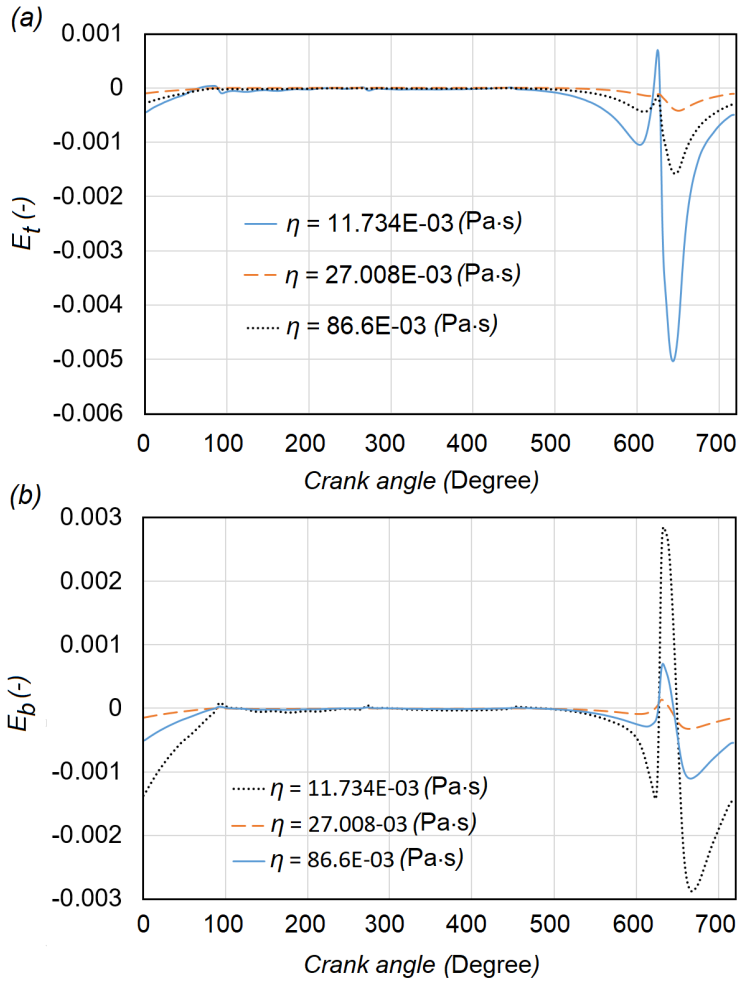

Fig. 4.14 Effect of lubricant viscosity.

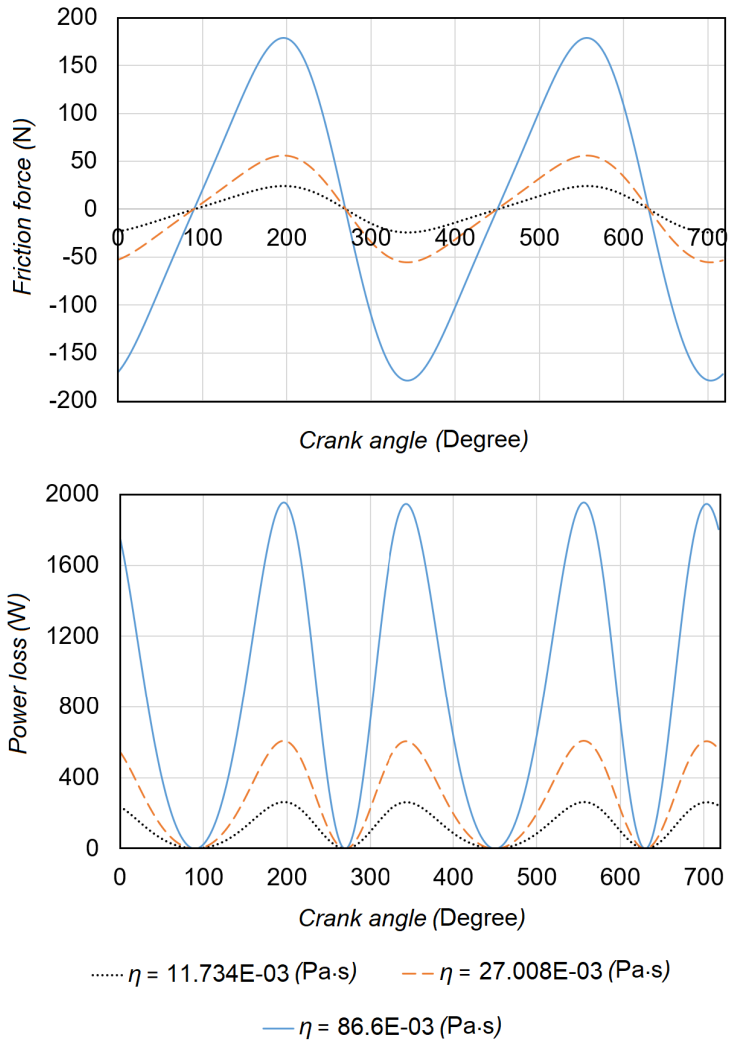

Fig. 4.15 Effect of lubricant viscosity on friction force and power loss.

4.5 Summary

Piston secondary motion and skirt lubrication model has been introduce to evaluate skirt tribological performance considering the effect of piston ring pack lubrication by means of friction force and its moment imposed by rings to the piston. The effects of engine angular velocity, wrist-pin location, skirt/liner clearance and lubricant viscosity and temperature on piston dynamics and power loss were examined. Piston skirt lubrication analysis required higher numerical efforts in comparison to piston ring pack model. Newton-Raphason approach was used to solve the nonlinear

piston motion equations to calculate eccentricities at the top and bottom of the skirt. Generated hydrodynamic pressure at skirt and liner interface was calculated applying finite difference method.

Chapter 5

Connecting Rod Big-End and Main Journal Bearing Lubrication and Tribology

5.1 Introduction

The primary purpose of hydrodynamic bearings are to support a rotating shaft and to guaranty the hydrodynamic lubrication of bearing surfaces. Journal bearings are one of the most common types of hydrodynamic bearing. They can be found in various subsystems of reciprocating engines and powertrains. Engine main bearings and connecting rod big-end bearing are the two forms of journal bearings. Journal bearings are usually design to operate under hydrodynamic lubrication. This is under influence of load and relative rotating speed of bearings component that creates hydrodynamic wedge and consequently hydrodynamic pressure within the film to stand against the applied load.

The formed hydrodynamic pressure at the journal and bearing junction, typically distributed over half of the journal and bush interface, but also this hydrodynamic pressure distribution can be limited to small fraction of the bearing area under severe conditions.

The magnitude of the hydrodynamic pressure at journal and bush interface is influenced by the film thickness in which the amount of available oil is a function

of initial clearance and instantaneous eccentricity between the centers of lubricated pairs.

Analytical and numerical approaches are the two possible ways to evaluate and estimate hydrodynamic pressure distribution and tribological performance of journal bearings.

5.2 State of the art

The huge efforts have been devoted to predict and evaluate the dynamically loaded journal tribological performance.

In 1965 Booker presented an analytical, graphical and numerical approach to simplify the solution for general problems associated with dynamically loaded bearings, so called Mobility method [163]. The method does not based on the particular solution for Reynolds equation, to guarantee this feature six different cases considering full and partially have been addressed. Later the author [164] reversed the method and provide more numerical details to be applicable for reciprocating engines.

The Mobility method is frequently applied to evaluate dynamically loaded journal bearings. Curve fitting of journal bearing is a part of the method which is affected by solution accuracy and the required details and time. A set of analytical curve fits was introduced including two components of mobility vectors, location and magnitude of maximum film pressure, as well as the starting and finishing angles of the pressure curve. From accuracy and solution detail aspect, the approach is comparable with finite-element analysis but with a computation time comparable to that required for the short bearing approximation [165].

Dynamic behavior of an elastic connecting rod bearing was evaluated and the performance of two different bearings of a petrol and a diesel engine were compared [166, 167]. Instantaneous elastic deformations and pressure distribution were calculated for different values of the load.

Hirani et al. [168] based on the Mobility method [163], proposed a close form pressure distribution over dynamically loaded journal bearings, applying combination of short and long bearing approximations. Determination of start and end points of positive pressure at journal and bush interface can be defined through simple

analytical equations, besides applying Mobility method become more easier and comfort. The model encourages the estimation of instantaneous maximum pressure and its angular location.

Paranjpe [169] incorporated the non-Newtonian effect in a general way to detailed analysis of dynamically loaded finite journal bearings. Oil viscosity was expressed as function of shear rate and the effects of shear thinning and viscoelastic were taken into account.

Later in 2006, Livanos and Kyrtatos [42] applied the method introduced by [168] and determine the instantaneous hydrodynamic pressure acting on the journal to calculate friction force and power loss using fluid shear stress (τ).

An analytical solution of the Reynolds equation for isothermal finite length journal bearings was purposed using regular perturbation method [170]. The model relied on the modification of the Ocvirk number as an expansible parameter [171].

Recently an approach to solve Reynolds equation to evaluate the lubrication of plain journal bearing with finite length has been applied to determine the impedance forces of the fluid film in closed form analytical expression [172]. The model evaluates design parameters such as the eccentricity ratio, the location of the minimum fluid film thickness, the location of the maximum pressure, the stiffness and squeeze action coefficients.

Constantinescu's theory was employed to develop a full extended Reynolds equation to evaluate tribological performance of finite length bearings considering laminar and turbulent regimes [173]. The effects of both convective and temporal inertia have been examined without consideration of the normal thin film assumption. The nonlinear contribution of convective inertia terms to damping characteristics of radial bearings was evaluated.

5.3 Connecting rod big-end and main bearing loading

Engine main journal and connecting rod big-end bearings of reciprocating engines are dynamically loaded hydrodynamic journal bearings. To calculate frictional power

loss it has prime importance to define the magnitude and direction of forces with respect to the crank angle.

5.3.1 Connecting rod big-end loads

At each time instant or crank angle, the applied load acting on a big-end bearing can be regarded as contribution of combustion chamber gas force, and inertial imbalances due to reciprocating and rotating masses. There are three simplification taking into account to have a quick estimation of connecting rod big-end tribological performance. Firstly, the imposed load acting upon the big-end, that means the analysis is applicable for a single cylinder and can be considered as an approximation to a multi-cylinder engine. Secondly, the elements are treated as rigid bodies and there is no elastic deformation associated with them. For the last, the effect of engine fluctuations caused by firing order and inertial imbalances can be confined to few harmonics.

The forces acting on connecting rod big-end due to gas force, F_{gas}, and induced by rotational and reciprocating inertial forces, F_{rot} and F_{rec}, respectively can be calculated through following equations:

$$F_{gas} = p_{gas}\frac{\pi D^2}{4} \tag{5.1}$$

$$F_{rec} = -(m_{pis} + m_{pin} + m_{cr,a})a_{pis} \approx -(m_{pis} + m_{pin} + 0.3m_{cr})a_{pis} \tag{5.2}$$

where a_{pis} is piston acceleration as:

$$\begin{aligned} a_{pis} = \omega^2 r\Bigg(\cos(\theta) - \frac{\sin(\theta)\left(\Lambda\sin(\theta) - \delta\right)}{\sqrt{1-\left(\Lambda\sin(\theta)-\delta\right)^2}} + \\ + \frac{\Lambda\cos^2(\theta)}{\sqrt{1-\left(\Lambda\sin(\theta)-\delta\right)^2}} + \frac{\Lambda\cos^2(\theta)\left(\Lambda\sin(\theta)-\delta\right)^2}{\sqrt{\left(1-\left(\Lambda\sin(\theta)-\delta\right)^2\right)^3}}\Bigg) \end{aligned} \tag{5.3}$$

$$F_{rot} = m_{cr,r}\omega_{cr}^2 r \approx 0.7 m_{cr}\omega_{cr}^2 r \tag{5.4}$$

regarding to Fig. 5.1, connecting rod big-end rotating speed, ω_{cr}, is defined as follows:

$$\sin(\beta) = \frac{r\sin(\theta) - z_o}{l} = \Lambda\sin(\theta) - \delta \tag{5.5}$$

where $\Lambda = \dfrac{r}{l}$ and $\delta = \dfrac{z_o}{l}$ and:

$$\cos(\beta) = \sqrt{1 - \left(\frac{r\sin(\theta) - z_o}{l}\right)^2} = \sqrt{1 - (\Lambda\sin(\theta) - \delta)^2} \tag{5.6}$$

$$\omega_{cr} = \frac{d\beta}{dt} = \frac{\omega\Lambda\cos(\theta)}{\cos\beta} = \frac{\omega\Lambda\cos\theta}{\sqrt{1 - (\Lambda\sin\theta - \delta)^2}} \tag{5.7}$$

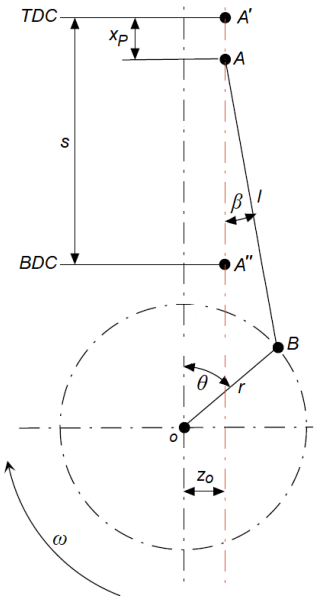

Fig. 5.1 Schematic representation of crank mechanism with offset layout.

Thus, the net load acting on the bearing is:

$$F = F_{gas} + F_{rec} - F_{rot}\cos\theta \tag{5.8}$$

5.3.2 Main bearing loads

Engine main bearing loads are slightly complicated to calculate whereas the big-end bearing loading as it is relatively simple. It is due to the loads consist of the force partly from the reaction of the big-end bearing loading and partly from the out-of-balance forces of the crankshaft (crank webs + crank pin) [174]. This is an indeterminate problem because both the crankshaft and crankcase have finite stiffness and the interactions of big-end bearings loading and crankshaft out-of-balance forces make the calculation complex. Thus for a multi-cylinder engine a simplified determinate system is used in which the crankshaft and crankcase are treated as rigid bodies and big-end pin jointed at the axial mid-position of each main bearing. Under such determined system it is assumed that the half of reaction forces from the big-end bearing and the crank webs + crank pin are carried by the adjacent main bearings.

For the calculation of the main bearing loading the big-end bearing and the crankshaft out-of-balance forces are resolved into two components that is acting along and perpendicular to the cylinder axis. Figures 5.2 and 5.3 shows the load evaluation process for the forces along the x axis for a multi-cylinder and single cylinder engine, and a similar method can be used for loads along the y axis.

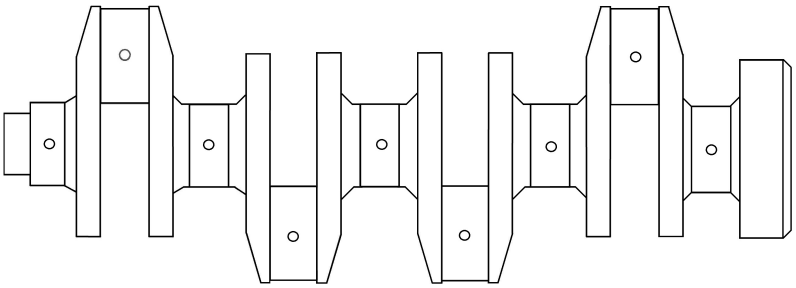

Fig. 5.2 Schematic crankshaft.

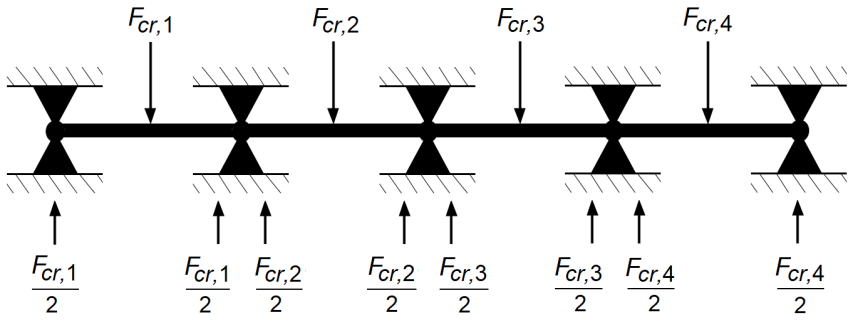

Fig. 5.3 Main bearing loading evaluation.

5.4 Model and procedure

5.4.1 Reynolds equation for bearing analysis

Generated hydrodynamic pressure at main bearings and crankshaft journals interface as well as connecting rod big-end bearings can be governed by 2D Reynolds equation as expressed by Eq. (5.9). Therefore general formulation has been described that can be applied for both cases and required manipulation of the equations are explained for main bearing and connecting rod big-end bearing in detail.

$$\frac{\partial}{R_j^2 \partial \alpha}(h^3 \frac{\partial p}{\partial \alpha}) + \frac{\partial}{\partial x}(h^3 \frac{\partial p}{\partial x}) = 6\eta U \frac{\partial h}{R_j \partial \alpha} + 12\eta \frac{\partial h}{\partial t} \tag{5.9}$$

where x is the coordinate parallel to journal axis, α the journal circumferential coordinate, R_j the journal radius (m), U the speed of entraining motion in rotation direction of the journal (m/s).

Speed of entraining motion can be calculated using Eq. (5.10) for big-end bearing and, applying Eq. (5.11) for main journal bearing.

$$U = \frac{1}{2}(\omega_{cr} + \omega j)R_j = \frac{1}{2}\left(\frac{\omega \Lambda \cos\theta}{\sqrt{1-(\Lambda \sin\theta - \delta)^2}} + \omega\right) R_j \tag{5.10}$$

$$U = \frac{1}{2}\omega R_j \tag{5.11}$$

In this study the shaft is treated as rigid body, and the radial and tangential bearing displacement have been neglected, therefore classical film thickness expression has been used [175]. Therefore, oil film thickness at connecting rod big-end and crank pin interface can be expressed as:

$$h(x,\alpha) = c(1+\varepsilon\cos\alpha) \tag{5.12}$$

where c is the clearance and ε the ratio of eccentricity between bearing bodies axes to clearance ($\varepsilon = \frac{e}{c}$).

Finite difference scheme can be applied to solve 2D Reynolds equation and determine the pressure distribution at journal and bearing interface. Finite difference mesh can be defined over the journal as shown by Fig. 5.4.

$$\begin{aligned} &\frac{h^3_{i+\frac{1}{2},j}\dfrac{p_{i+1,j}-p_{i,j}}{\Delta x} - h^3_{i-\frac{1}{2},j}\dfrac{p_{i,j}-p_{i-1,j}}{\Delta x}}{\Delta x} + \\ &+\frac{1}{R_j^2}\left(\frac{h^3_{i,j+\frac{1}{2}}\dfrac{p_{i,j+1}-p_{i,j}}{\Delta\alpha} - h^3_{i,j-\frac{1}{2}}\dfrac{p_{i,j}-p_{i,j-1}}{\Delta\alpha}}{\Delta\alpha}\right) = \\ &6\eta U\frac{h_{i+\frac{1}{2},j}-h_{i-\frac{1}{2},j}}{\Delta x} + 12\eta\omega\frac{h^{\theta+\Delta\theta}_{i,j}-h^{\theta}_{i,j}}{\Delta\theta} \end{aligned} \tag{5.13}$$

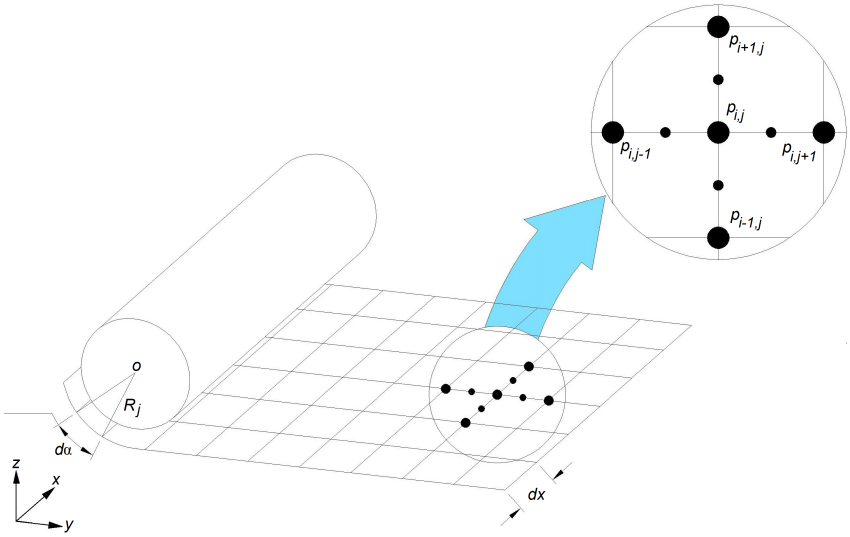

Fig. 5.4 Finite difference mesh developed over the journal.

Re-equating Eq. (5.13) yields the hydrodynamic pressure at each node $p(i,j)$ with respect to adjacent nodes can be defined via:

$$p(i,j) = (\frac{a_2}{a_1})p_{i+1,j} + (\frac{a_3}{a_1})p_{i-1,j} + (\frac{a_4}{a_1})p_{i,j+1} + \\ +(\frac{a_5}{a_1})p_{i,j-1} - (\frac{6\eta U}{a_1})a_6 - (\frac{12\eta\omega}{a_1})a_7 \tag{5.14}$$

where

$$a_1 = \frac{\left(\frac{h_{i,j+1}+h_{i,j}}{2}\right)^3}{\left(R_j\Delta\alpha\right)^2} + \frac{\left(\frac{h_{i,j}+h_{i,j-1}}{2}\right)^3}{\left(R_j\Delta\alpha\right)^2} + \frac{\left(\frac{h_{i+1,j}+h_{i,j}}{2}\right)^3}{\left(\Delta x\right)^2} + \frac{\left(\frac{h_{i,j}+h_{i-1,j}}{2}\right)^3}{\left(\Delta x\right)^2}$$

$$a_2 = \frac{\left(\frac{h_{i+1,j}+h_{i,j}}{2}\right)^3}{(\Delta x)^2} \qquad a_3 = \frac{\left(\frac{h_{i,j}+h_{i-1,j}}{2}\right)^3}{(\Delta x)^2} \qquad a_4 = \frac{\left(\frac{h_{i,j+1}+h_{i,j}}{2}\right)^3}{(R_j\Delta\alpha)^2}$$

$$a_5 = \frac{\left(\frac{h_{i,j}+h_{i,j-1}}{2}\right)^3}{(R_j\Delta\alpha)^2} \qquad a_6 = \frac{h_{i,j+1}+h_{i,j-1}}{2R_j\Delta\alpha} \qquad a_7 = \frac{h_{i,j}^{\theta+\Delta\theta}+h_{i,j}^{\theta}}{2R_j\Delta\alpha}$$

Boundary conditions that must be applied during computation are saturation pressure (crankcase pressure) at each edge of journal and $\frac{dp}{d\alpha} = 0$ at each both side of line of centers (Fig. 5.5) as follows:

$$\begin{aligned} p &= p_{atm} & x &= \pm\frac{L_x}{2} \\ \frac{dp}{d\alpha} &= 0 & \alpha &= 0, \pi \end{aligned} \tag{5.15}$$

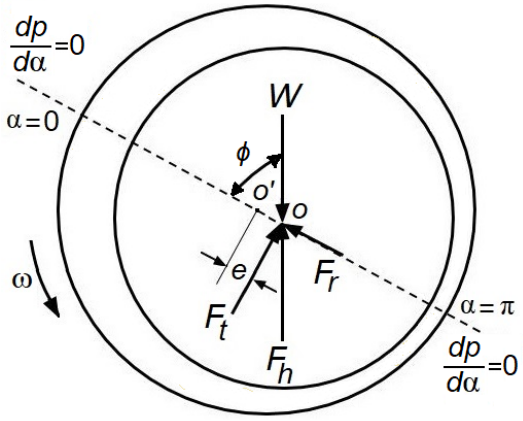

Fig. 5.5 Schematic representation of journal and bearing.

5.4.2 Numerical solution

To apply finite difference schema to calculate hydrodynamic pressure at bearing surfaces interface, it is necessary to define the instantaneous eccentricity between journal and bearing axes to update the oil film thickness at each time instant (crank angle).

The following dimensionless quantities have been applied to form an appropriate scale to non-dimensionalize Reynolds equation and oil film thickness expression:

$$\begin{gathered} \bar{x} = \frac{x}{L_x}; \quad \bar{h} = \frac{h}{c}; \quad \theta = \omega t; \quad \bar{U} = \frac{U}{R_j\omega}; \quad \bar{R} = \frac{R_j}{R_j}; \\ \bar{L} = \frac{Lx}{R_j} \quad \bar{p} = \frac{c^2}{6\eta\omega R_j^2}p \quad \bar{F} = \frac{c^2}{6\eta\omega R_j^3 L_x}F; \end{gathered} \tag{5.16}$$

where L_x is the journal length (m).

Applying dimensionless parameters to Eqs. (5.9) and (5.12), the dimensionless form of Reynolds equation and oil film thickness expression are obtained:

$$\frac{\partial}{\partial\alpha}(\bar{h}^3\frac{\partial\bar{p}}{\partial\alpha})+(\frac{R}{L_x})^2\frac{\partial}{\partial\bar{x}}(\bar{h}^3\frac{\partial\bar{p}}{\partial\bar{x}})=\bar{U}\frac{\partial\bar{h}}{\partial\alpha}+2\frac{\partial\bar{h}}{\partial\theta} \tag{5.17}$$

$$\bar{h}(x,\alpha)=(1+E\cos\alpha) \tag{5.18}$$

where $E=\dfrac{e}{c}$.

Eq. (5.17) can be written as follow and knowing that the terms on the left side are pressure terms:

$$\bar{p}=\frac{\bar{U}}{(1+(\frac{R}{L_x})^2)}\frac{\partial\bar{h}}{\partial\alpha}+\frac{2}{(1+(\frac{R}{L_x})^2)}\frac{\partial\bar{h}}{\partial\theta}. \tag{5.19}$$

Substituting Eq. (5.18) in Eq. (5.19) and performing the derivatives, the expression of hydrodynamic pressure can be defined:

$$\bar{p}=\frac{\bar{U}}{K}(-E\sin\alpha)+\frac{2}{K}\dot{E}\cos\alpha \tag{5.20}$$

where $K=(1+(\dfrac{R}{L_x})^2)$ and $\dot{E}=\dfrac{\dot{e}}{c\omega}$ which is the relative liner speed of the journal and bearing.

Instantaneous force equilibrium (Fig. 5.6) is applied to define the eccentricity between two bearing surface as follows:

$$W-F_h=0 \tag{5.21}$$

where W is contributed by gas force, F_{gas}, reciprocating inertial force due to piston, pin and connecting rod mass, $F_{rec.}$, rotating inertial mass due to crank web mass, $F_{rot.}$.

According to Fig. 5.6, hydrodynamic lifting force acting on the journal, F_h, is the resultant force of radial force, F_r and tangential force, F_t. These two force can be calculated using following equations:

$$F_r=\int_0^{\pi}\int_{-\frac{L_x}{2}}^{\frac{L_x}{2}}p(x,\alpha)R\cos\alpha dxd\alpha \tag{5.22}$$

$$F_t = \int_0^{\pi} \int_{-\frac{L_x}{2}}^{\frac{L_x}{2}} p(x,\alpha) R \sin\alpha dx d\alpha \tag{5.23}$$

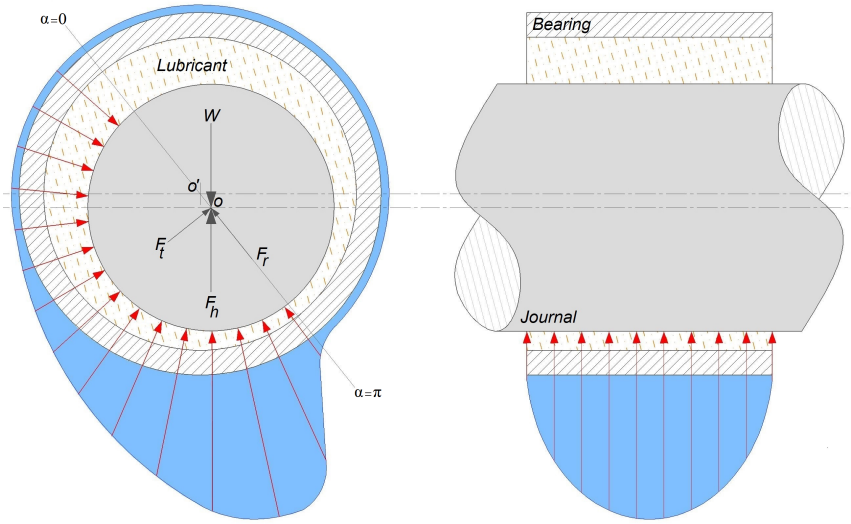

Fig. 5.6 Forces acting on journal and pressure profile at bearing surfaces interface.

Applying non-dimensionalised parameters to Eqs. (5.22) and (5.23) to obtain the dimensionless form of them as:

$$\bar{F}_r = \int_0^{\pi} \int_{-\frac{\bar{L}_x}{2}}^{\frac{\bar{L}_x}{2}} \bar{p}(\bar{x},\alpha) \cos\alpha d\bar{x} d\alpha \tag{5.24}$$

$$\bar{F}_t = \int_0^{\pi} \int_{-\frac{\bar{L}_x}{2}}^{\frac{\bar{L}_x}{2}} \bar{p}(\bar{x},\alpha) \sin\alpha d\bar{x} d\alpha \tag{5.25}$$

Solving the integrals in Eqs. (5.24) and (5.25) result in:

$$\bar{F}_r = \frac{\bar{L}_x}{K} \dot{E} \pi \tag{5.26}$$

$$\bar{F}_t = \frac{tan(\frac{\pi}{2})^2 (\frac{\bar{L}_x(8\dot{E} - 2E\bar{U}\pi)}{2} + E\bar{L}_x\bar{U}\pi) + E\bar{L}_x\bar{U}tan(\frac{\pi}{2}) - E\bar{L}_x\bar{U}tan(\frac{\pi}{3})^2}{K(tan(\frac{\pi}{2})^2 + 1)^2} + \\ - \frac{E\bar{L}_x\bar{U}\pi}{2K} \tag{5.27}$$

From Eqs. (5.26) and (5.27), hydrodynamic lifting force acting on the journal can be calculated as:

$$\bar{F}_h = \sqrt{\bar{F}_r^2 + \bar{F}_t^2} \tag{5.28}$$

In the process of computing eccentricity between journal and bearing, the first order equation derived from non-dimensional form of Eq. (5.21) containing $\dot{E}$ and E must be solved at each time step by iteration. Newton-Rophson method or "*solve*" function in MATALB can be used as solver in which initial value of E is known at the beginning of a time step. As the hydrodynamic bearing are designed to operates under hydrodynamic lubrication eccentricity between the axis of both bearing surface assumed to be in the range of $0 \leq \mathrm{e} \leq \mathrm{c} - 5\sigma$ that σ is the combined surface roughness of bearing surfaces to guarantee the hydrodynamic lubrication at journal and connecting rod big-end junction. After defining instantaneous eccentricity, hydrodynamic pressure acting over the journal can be calculated using finite difference method, and consequently power loss due to viscous shear stress and squeeze action [176] as follows:

$$\begin{aligned} P_f(\theta) = &\int_0^{\pi} \int_{-\frac{L_x}{2}}^{\frac{L_x}{2}} \left(\frac{\eta}{h(x,\alpha)} \right) U^2 R_j dx d\alpha + \\ &+ \int_0^{\pi} \int_{-\frac{L_x}{2}}^{\frac{L_x}{2}} \left(\frac{h^3(x,\alpha)}{12\eta} \right) \mid \nabla p \mid^2 R_j dx d\alpha \end{aligned} \tag{5.29}$$

On the other hand, knowing axes eccentricity and considering power loss contributed by pressure gradient and due to rotation of the journal and the bearing, journal bearing power loss [177] can be also calculated via:

$$P_f(\theta) = \frac{\eta R_j^3 L_x}{c} J_1^{00} (\omega_j - \omega_b)^2 + \left(\frac{\omega_j + \omega_b}{2} \right) eW \sin(\phi) \tag{5.30}$$

where J_1^{00} is a journal bearing integral for π film extant [178] and ϕ (Fig. 5.5) is the instantaneous angle between normal load acting on the journal and the line of centers. These two quantities can be calculated applying the following equations:

$$J_1^{00} = \frac{\pi}{\sqrt{1-\varepsilon^2}} \tag{5.31}$$

$$\phi = \arctan\left(\frac{\pi\sqrt{1-\varepsilon^2}}{4\varepsilon}\right) \tag{5.32}$$

5.4.3 Mobility method

The obtain data from aforementioned model are compared against the introduced Mobility method by Booker [163, 164], the proposed model is briefly described in this section. Substituting Eq. (5.12) in Eq. (5.9) and performing the derivatives $\frac{\partial h}{\partial \alpha}$ and $\frac{\partial h}{\partial t}$ on the right side, Reynolds equation can written as:

$$\begin{aligned}\frac{\partial}{\partial\alpha}((1+\varepsilon\cos\alpha)^3\frac{\partial p}{\partial\alpha}) + R_j^2\frac{\partial}{\partial x}((1+\varepsilon\cos\alpha)^3\frac{\partial p}{\partial x}) = \\ 12\eta\frac{R_j^2}{c^3}\left(\frac{U}{2R_j}(-c\varepsilon\sin(\alpha)) + (\dot{e}\cos(\alpha) - e\dot{\phi}\sin\alpha)\right)\end{aligned} \tag{5.33}$$

Complete solution of Eq. (5.33) is complicated and associated with huge numerical effort. Satisfactory analytical solutions were introduced by Ocvirk (short bearing solution), Sommerfeld (long bearing solution) and Goenka (finite width method) explained in much detail by Booker [163].

The Sommerfeld solution assumes that the first term in Eq. (5.33) is negligible as it assumes that if the bearing is long in the axial direction then the variation of pressure in circumferential direction is much more significant than that in the axial direction, therefore the second term is dominant and the first term is discarded. The short bearing solution assumes that the first term in Eq. (5.33) is negligible as it assumes that if the bearing is short in the axial direction then the variation of pressure in this direction is much more significant than that in the circumferential direction. This method is fairly accurate for bearings of width to diameter ratios less than 0.7, operating at moderate eccentricity ratio less than 0.6. Short bearing solutions become inaccurate at high eccentricity ratios. Besides this, it is a good method because of the simplicity of the approximated Reynolds equation and its solution, Eq. (5.34).

Therefore this method was used in the present analysis.

$$R_j^2 \frac{\partial}{\partial x}((1+\varepsilon\cos\alpha)^3 \frac{\partial p}{\partial x}) = 12\eta(\frac{R_j}{c})^2 \left(\dot{\varepsilon}\cos(\alpha) - \varepsilon(\bar{\omega}+\dot{\phi})\sin\alpha \right) \tag{5.34}$$

Two times integration of Eq. (5.34) yields the hydrodynamic expression at journal and bearing interface:

$$p(\alpha) = 12\eta \frac{1}{c^2} \frac{\left(\dot{\varepsilon}\cos(\alpha) + \varepsilon(\bar{\omega}+\dot{\phi})\sin\alpha\right)}{(1+\varepsilon\cos\alpha)^3} \frac{x^2}{2} + C_1 x + C_2 \tag{5.35}$$

where C_1 and C_2 are the integration constants that can be determined using the following boundary conditions:

$$p = 0 \qquad x = \pm\frac{L_x}{2} \tag{5.36}$$

Applying boundary condition and considering steady-state condition in which $\dot{\varepsilon}$ and $\dot{\phi}$ are null [163], hydrodynamic pressure at journal and bearing interface can be written as:

$$p(\alpha) = 6\eta \frac{1}{c^2} \left(\frac{\varepsilon\bar{\omega}\sin\alpha}{(1+\varepsilon\cos\alpha)^3} \right) (x^2 - \frac{L_x^2}{4}) \tag{5.37}$$

For a π film bearing where $\bar{\omega} > 0$, the angle between normal load and line of centers ϕ can be defined using Eq. (5.32).

Substituting Eq. (5.37) in Eqs. (5.22) and (5.23) and calculate the integrals using Booker table [178] from 0 to π (cavitated) yields:

$$F_r = \frac{R\eta\bar{\omega}L_x^3}{c^3} \left(\frac{2\varepsilon}{(1+\varepsilon)^2(\varepsilon-1)^2} \right) e \tag{5.38}$$

$$F_t = \frac{-R\eta\bar{\omega}L_x^3}{c^3} \left(\frac{\pi}{(1-\varepsilon^2)^{\frac{3}{2}}} \right) e \tag{5.39}$$

Journal and bearing instantaneous misalignment is defined via force equilibrium (Eq. 5.21) and consequently journal power loss can be calculated using Eq. (5.30).

5.5 Results and discussion

The relevant data for the connecting rod big-end and engine are summarized in Table 5.1. Generated hydrodynamic pressure at connecting rod big-end and crankpin is illustrated by Fig. 5.7; positive hydrodynamic pressure has been developed at half of the journal and bearing interface as it is treated as π film bearing. The pressure at second half of the journal and bearing junction is considered equal to saturation pressure (crankcase pressure).

Table 5.1 Relevant engine, connecting rod big-end and crankpin journal data.

c	Journal and bearing clearance (mm)	0.026
D	Cylinder bore (mm)	83.80
l	Connecting rod length (mm)	153
L_x	Journal width length (mm)	19.5
r	Crank radius (mm)	49.5
R_j	Journal radius (mm)	25.45
m_{pis}	Piston mass (kg)	0.540
m_{pin}	Wrist-pin mass (kg)	0.257
m_{cr}	Connecting rod mass (kg)	0.714
z_{owp}	Wrist-pin offset (mm)	0.5
η	Lubricant dynamic viscosity (Pa·s)	11.734E-03
σ	Combined surface roughness (μm)	0.37

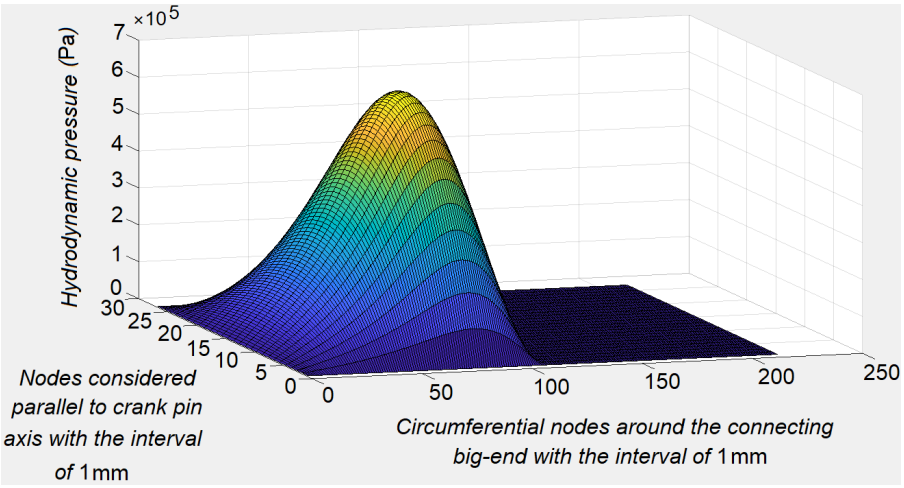

Fig. 5.7 Hydrodynamic pressure at connecting rod big-end and crankpin journal at the engine speed of 2000 rpm.

Figure 5.8 shows instantaneous normal loads acting on the crankpin which is contributed by gas pressure, reciprocating and rotating inertial forces. During the exhaust and intake strokes, inertial forces are major contributers to the normal load as the gas pressure acting on the piston mostly equals to saturation pressure. In contrary, during the compression and expansion strokes, the gas pressure acting on the piston plays significant role in comparison to reciprocating and rotating inertial forces.

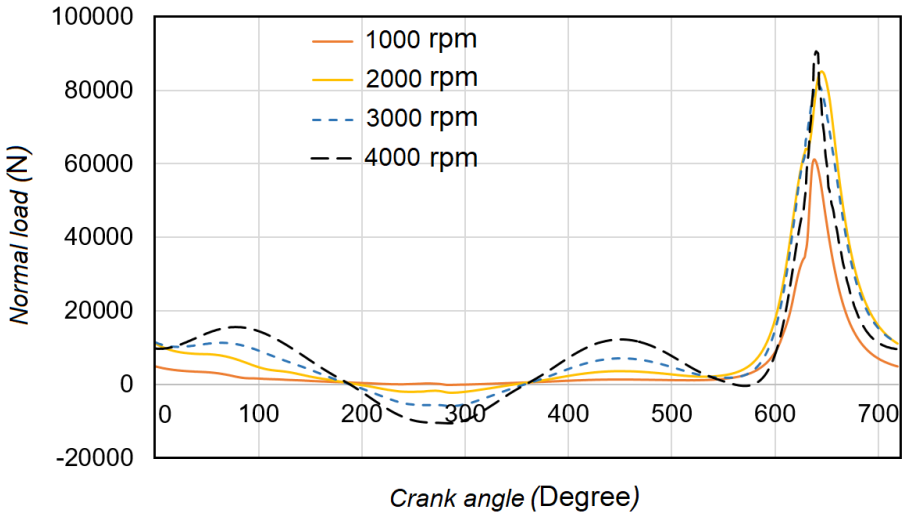

Fig. 5.8 Instantaneous normal loads contributed by the gas pressure and reciprocating masses.

Figures 5.9 and 5.10 show the power loss calculated by two methods, analytical model and Mobility approach at different engine angular speeds and operating (motored and fired) conditions, respectively.

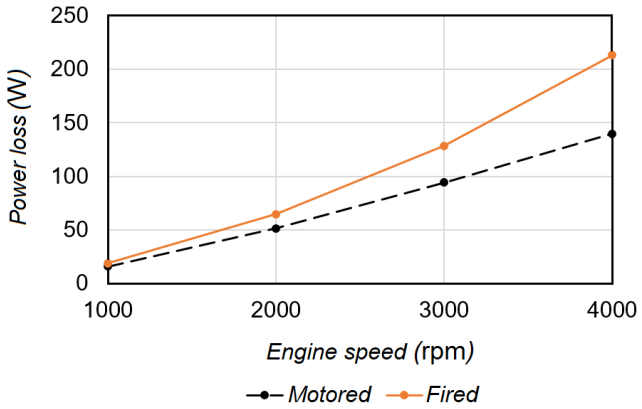

Fig. 5.9 Power loss calculated by analytical model under motored and fired conditions.

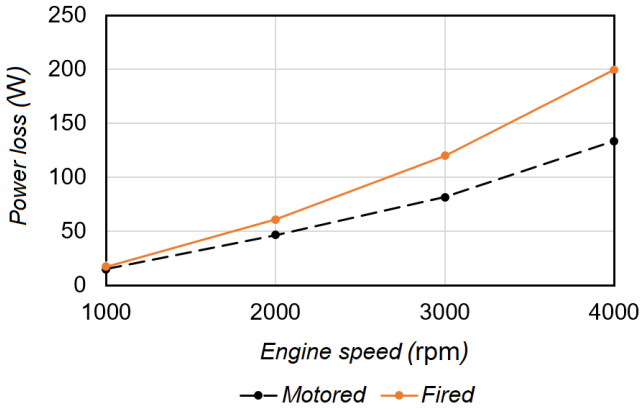

Fig. 5.10 Power loss calculated by Mobility model under motored and fired conditions.

Increment in the relative surface velocities of the connecting rod big-end and crankpin journal, increases the power loss caused by the increase in shear stress within the oil film at bearing surfaces junction. On the other hand, as hydrodynamic lubrication (HL) is considered at lubricated surfaces interface, under HL friction loss is directly proportional to engine angular speed, lubricant viscosity and inlet lubricant temperature. This effect of speed is obvious applying both approaches (analytical model and Mobility method) at inlet lubricant temperatures of 90°C (η = 11.734e^{-3} Pa·s), under both operating conditions, fired and motored as displayed by Figs. 5.11 and 5.12, respectively. The calculated power loss via Mobility method is

lower than estimated power loss by analytical model at given speed under motored and fired conditions.

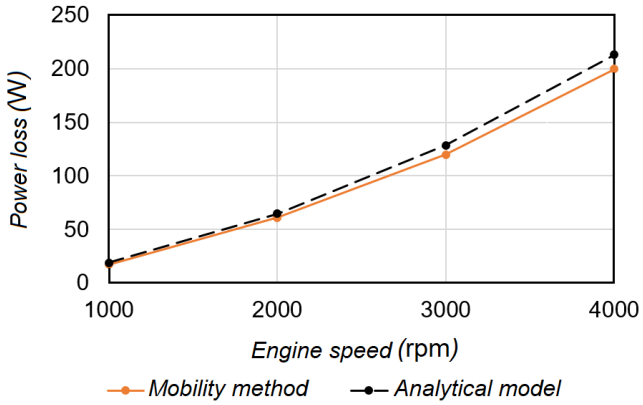

Fig. 5.11 Power loss at different engine speed under fired condition.

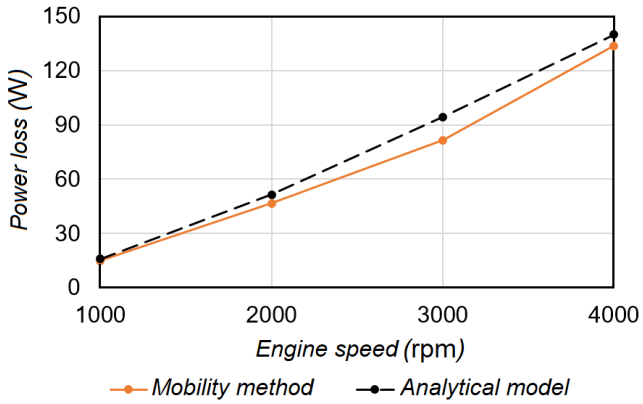

Fig. 5.12 Power loss at different engine speed under motored condition.

For a given oil (SAE 0W30), as the lubricant temperature increase, power loss reduces due to reduction of fluid viscosity and its resistance against shear stress. Figures 5.13 and 5.14 illustrate the power loss dependence on lubricant temperature under fired and motored conditions. Power loss calculated by both methods significantly reduces as oil temperature increases. One of the main disadvantages of high operating temperature is to encourage of mixed lubrication at bearing surfaces junction due to low effective oil viscosity.

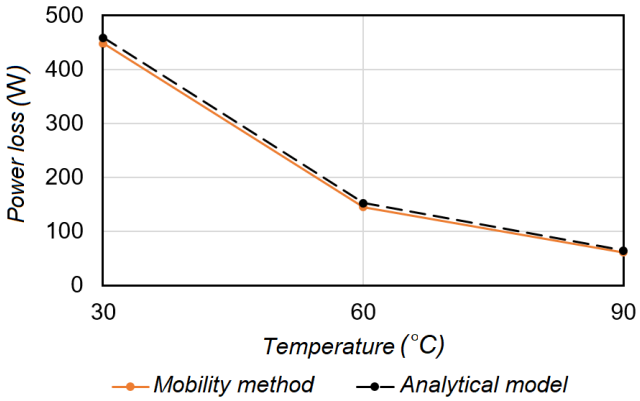

Fig. 5.13 Effect of temperature on power loss under fired condition.

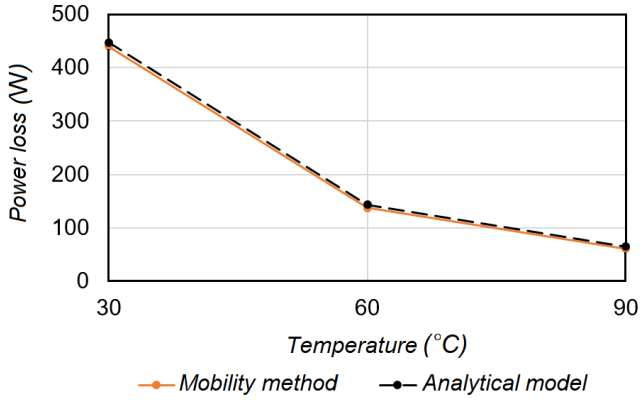

Fig. 5.14 Effect of temperature on power loss under motored condition.

The effect of different lubricant viscosity ($11.734e^{-3}$, $27.008e^{-3}$ and $86.6e^{-3}$ Pa·s) has been examined and shown by Figs. 5.15 and 5.16. It is proved that by two approaches, analytical model and Mobility method, as oil viscosity increases, its resistance against shear stress is improved and consequently higher power loss is obtained.

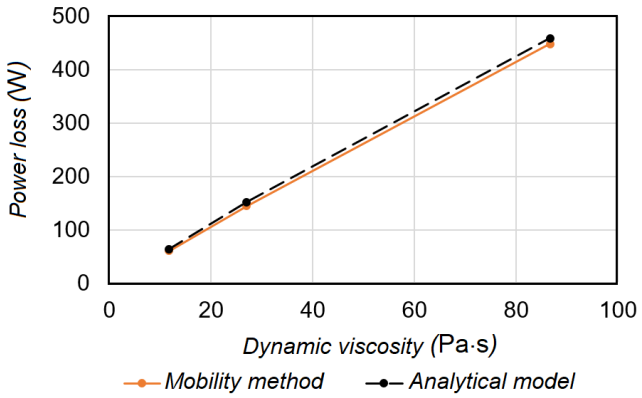

Fig. 5.15 Effect of lubricant viscosity on power loss under fired condition.

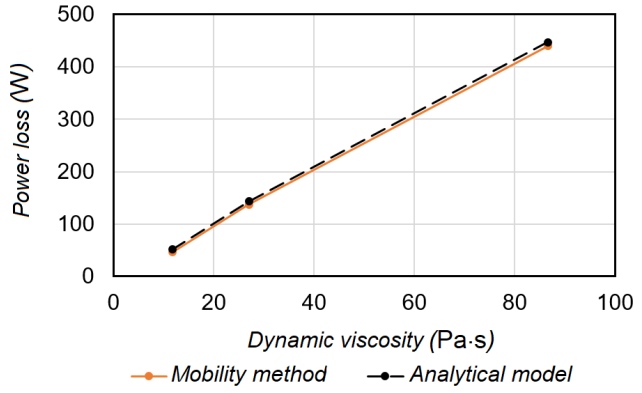

Fig. 5.16 Effect of lubricant viscosity on power loss under motored condition.

5.6 Summary

A hydrodynamic analytical model has been developed to evaluate tribological performance of journal main bearings and connecting rod big-end bearing. Instantaneous eccentricity between both journal and bearing has been calculated through force equilibrium acting on the journal using Newton–Raphson's scheme. Finite difference method was applied to calculate hydrodynamic pressure at journal and bearing interface as well as frictional power loss. Besides, well known Mobility method has been applied to be compared against the analytical model; good agreement has been observed between the two approaches. The effect of operating conditions, engine angular speed, lubricant temperature and oil viscosity are also investigated.

Chapter 6

Model Validation

6.1 Experimental procedure and model validation

Experimental measurement has been down on 2.2L cast iron 200hp engine using the strip down method. Lubricant was supplied to the lubricated parts interface by means of applying external pump. Oil and coolant temperature were stabilized using a separated external circuits. Investigated angular speed of the engine varied from 1000 (rpm) to 4000 (rpm) and oil temperature was kept constant by the value of 90°C. SAE 0W30 was used as lubricant.

The friction mean effective pressure (FMEP) measurement of the piston ring assembly (PRA) and connecting rod big-end was carried out at two steps. First, the FMEP was calculated for the crankshaft journal bearings and all the other components were dismounted. Then the FMEP has been measured for crankshaft, PRA and connecting rod big-end and at the end net FMEP was defined by subtracting the calculated crankshaft journal bearings FMEP at the first stage.

The net FMEP for PRA and connecting (4 sets) rod big-end was converted to mean power loss (W) to be compared with the obtained data from the model. Figure 6.1 shows the experimental data vs. the model and associated computational error, good agreement between them can be observed.

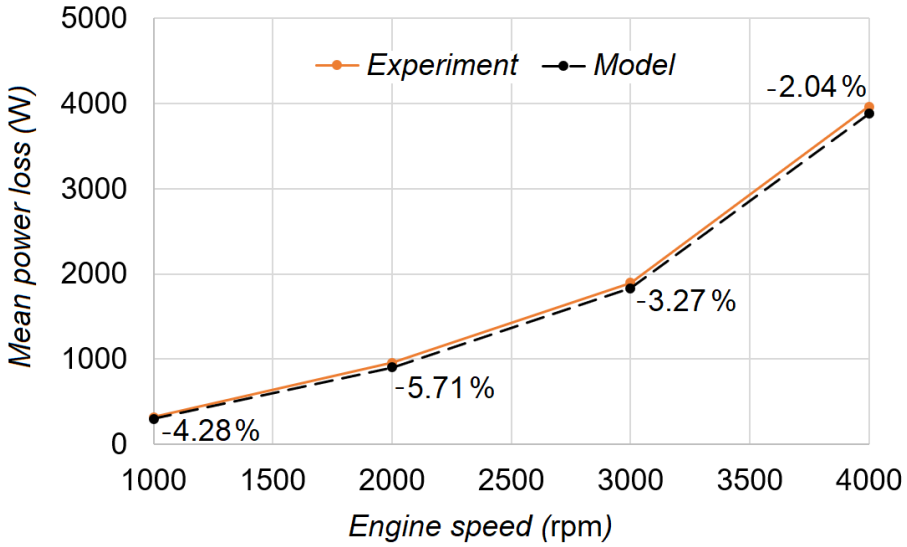

Fig. 6.1 Obtained data by model vs. experiment.

Chapter 7

Conclusions and Future Directions

7.1 Brief overview of the current work

The majority of internal combustion engines (ICEs) power loss comes from the lubricated reciprocating and rotating bearing couples. Piston ring assembly (PRA) and connecting rod big-end as well as main journal bearings have major contribution to frictional loss and engine output power. The present study makes effort to address the challenging research issue to evaluate tribological performance of PRA, connecting rod big-end and main journal bearings. This topic has been considered due to the fact that aforementioned components have a direct effect on the performance of ICEs. It is widely recognized that during the engine cycle, lubrication mechanism of the engine loaded rolling/sliding parts may experience boundary, mixed, and hydrodynamic lubrication regimes.

The main function of piston ring pack is to act as a dynamic seal preventing the gas leaking into the crankcase and vice versa. This is done in order to improve the engine thermal efficiency by reducing the blowby gases. Blowby analysis has been performed considering ring end gap as only way for gas to leakage in or out to reed piston ring pack lubrication model as boundary conditions and pressure acting on the upper and lower edges of the rings.

Hydrodynamic and boundary lubrication were considered at piston ring/liner junction that transient between these two regimes has been done with respect to calculated minimum oil film thickness at bearing surfaces interface. For each ring and regarding to operating condition (position in the ring pack and boundary pressures),

three different boundary conditions and oil film shape have been treated. For the first compression ring, Reynolds cavitation and reformation boundary conditions has been applied as the first ring works at severe condition with respect to other rings. In case of second compression ring, oil separation boundary conditions was considered as it operates under moderate circumstance in comparison to the first one. Finally, each rail of the oil control ring was treated as a single compression ring and full Sommerfeld boundary conditions have been considered as it enjoys adequate oil availability and saturation boundary pressures. Oil viscosity variation with respect to temperature was considered using Vogel model and the ring and piston were assumed to be iso-thermal bodies and thermal and mechanical distortion of them were neglected. Design of experiment (DoE) and ANOVA analysis were carried out to examine the effect of ring geometry on lubrication mechanism and power loss, and to evaluate the significance of these parameters.

Piston skirt is the lowest part of the piston, and has the task of keeping the piston from rocking excessively in the cylinder, which is typically machined with small grooves to aid oil retention and transporting lubricant to cylinder wall to encourage proper lubrication. When the piston is centered by the ring pack, unbalanced forces and moments that are perpendicular to the wrist pin axis (contains thrust and anti-thrust sides) act upon the piston. These unbalanced forces and moments result in small translations and rotations of the piston within a defined clearance. These motions are known as piston secondary motion and can be defined by means of eccentricities at the top and bottom of the skirt. In order to gain insight into the piston skirt tribological performance, the effect of piston ring pack lubrication has been considered.

An analytical model to evaluate piston secondary motion was introduced and numerical solution has been presented. Finite difference scheme was employed to govern the generated hydrodynamic pressure at skirt/liner interface and calculate friction force due to viscous stress within the oil film thickness at bearing surfaces junction.

Journal bearings are one of the most common types of hydrodynamic bearing. Engine main bearings and connecting rod big-end bearing are the two forms of journal bearings. Journal bearings are usually design to operate under hydrodynamic lubrication. This is under influence of load and relative rotating speed of bearings component that creates hydrodynamic wedge and consequently hydrodynamic pres-

sure within the oil film to stand against the applied load. The formed hydrodynamic pressure at the journal and bearing junction, typically distributed over half of the journal and bearing interface, but also this hydrodynamic pressure distribution can be limited to small fraction of the bearing area under severe conditions. The magnitude of the hydrodynamic pressure at journal and bearing junction is influenced by the oil film thickness in which the amount of available oil is a function of initial clearance and instantaneous eccentricity between the centers of lubricated pairs.

An analytical model and consequently numerical method were described to evaluate instantaneous eccentricity between journal and bearing. Besides finite difference scheme was used provide a solution for 2D Reynolds equation to calculated hydrodynamic pressure and power loss at journal and bearing interface. The results were compared against the well known short bearing Mobility method and the finite width method introduced by Booker.

7.1.1 Contributions to knowledge

Contribution to the literature can be summarized as following:

1. The effects of three different boundary conditions have been examine to gain insight the effect of this consideration on the accuracy of analytical modeling and numerical estimation of mechanical power loss and lubrication mechanism of piston ring with respect to operating condition and position of piston ring pack. The effects of ring geometry has been examined applying Doe and ANOVA analysis.

2. Detailed analysis of piston secondary motion and tribological performance has been conducted taking into account the contribution of the ring pack lubrication.

3. A simplified analytical model has been introduced and compared by Mobility method to evaluate connecting rod big end tribology.

7.1.2 Achievement of Aims

The achievements of this research objectives with respect to each chapter are summarized as following:

1. CHAPTER 3: A simplified analytical model has been developed and numerical scheme is programed using MATLAB to analyze inter ring gas pressure (blow-by) variation at each crank angle for one engine cycle. The outcome of blow-by model is served be piston ring lubrication as boundary conditions and gas pressure acting on ring. An analytical model is developed to examine the effect of different boundary condition: fully flooded, oil separation and oil starvation and cavitation with respect to ring position and operating conditions. In order to examine the effects of ring geometry on piston ring tribological performance, design of experiment (DoE) and ANOVA analysis are used.

2. CHAPTER 4: MATLAB codes have been developed to consider the effects of piston ring pack lubrication mechanism on piston secondary motion. These effects are incorporated as friction force and its moment about wrist pin axis of piston dynamics and determine the eccentricities at top and bottom of piston skirt to updated oil film thickness at each crank angle and evaluate piston skirt lubrication mechanism.

3. CHAPTER 5: An analytical model and numerical scheme have been developed to study connecting rod big-end. MATLAB code is developed to conduct the big-end tribological performance. The purposed model is compared against well known model introduced by Booker in 1965 so called Mobility method to verify the accuracy of approach. The model bring the benefit to avoid huge numerical effort associated with Mobility method with acceptable risk of error.

7.1.3 Critical assessment of approach

All the goals of this study and all the requirement of supporting company have been met, but considering some issues listed in section 7.2 could be beneficial as there are some research activities in progress to address a few of them.

7.2 Recommendations and future works

This dissertation suggests following issues to be considered for further research:

1. The effect of piston secondary motion on ring pack lubrication needs further investigations. Ring motions such as axial lifting and tilting in the groove

are affected by piston dynamics that changes the local oil film thickness. A detailed and comprehensive piston ring lubrication model is required to address this issue.

2. Piston ring/liner lubrication can be evaluated solving contact problems.In the current study, the effect of viscosity variation was taken into account using Vogel model but other possible models or approaches can be considered with accurate determination of temperature variation along the cylinder wall.

3. The effects of design parameters concerning the connecting rod, piston/liner clearance, skirt profile, wrist pin offset, lubricant rheology, and lubricant supply on lubrication mechanism and wear would be attractive domain for researchers to pay attention.

4. The accurate prediction of lubricant transport mechanisms and skirt deformation, especially 3D evaluations considering non-circular bore/piston have importance due to generated hydrodynamic pressure at skirt and liner interface along the piston and skirt deformation subjected to in cylinder pressure and temperature. In addition, to clarify the effect of piston secondary motion and to improve integration of piston ring and piston dynamics a complete three dimensional analysis can be conducted.

5. Geometry optimization of skirt profile, piston/liner clearance and wrist pin offset would result in reduction in magnitude of asperity contact pressure and help engineers and designers to improve engine efficiency.

References

[1] C. Delprete and A. Razavykia. Piston Ring-Liner Lubrication and Tribological Performance Evaluation: A Review. *J Engin. Tribol.*, 232:193–209, 2017.

[2] D. Zhu. *Elastohydrodynamic Lubrication (EHL)*. Springer, 2013.

[3] Rahnejat H. *Tribology and dynamics of engine and powertrain: fundamentals, applications and future trends*. Elsevier, 2010.

[4] C. Barus. Isothermal Isopietics and Isometrics in Relation to Viscosity. *AM. J. SCI.*, 45:87–96, 1893.

[5] C.J.A. Roelands. *Correlation Aspects of the Viscosity-Temperature-Pressure Relationships of Lubricating Oils*. PhD thesis, Delft University of technology, 1966.

[6] L. Houpert. New Results of Traction Force Calculation in Elastohydrodynamic Contacts. *J. Tribol.*, 107:241–248, 1985.

[7] S. Furuhama. A Dynamic Theory of Piston-Ring Lubrication: 1nd Report Calculation. *Bull JSME*, 2:423–428, 1959.

[8] S. Furuhama. A Dynamic Theory of Piston-Ring Lubrication: 2nd Report Experimental. *Bull JSME*, 3:291–297, 1960.

[9] S. Furuhama and S. Tadayuki. A Dynamic Theory of Piston-Ring Lubrication: 3nd Report Experimental Measurement of Oil Film Thickness. *Bull JSME*, 4:744–752, 1961.

[10] L. Ting and J. Mayer. Piston Ring Lubrication and Cylinder Bore Wear Analysis Part I- Theory. *J. Lub. Tech.*, 96:305–313, 1974.

[11] L. Ting and J. Mayer. Piston Ring Lubrication and Cylinder Bore Wear Analysis Part II- Theory Verification. *J. Lub. Tech.*, 96:258–266, 1974.

[12] B. Ruddy D. Dowson and P. Economou. The Elastohydrodynamic Lubrication of Piston Rings. *Math. Phy. Eng. Sci.*, 386:409–430, 1983.

[13] H. Chu-Jung and W. Cheng. Elastohydrodynamic Lubrication of Piston Rings. *Wear*, 150:203–215, 1991.

[14] Y.R. Jeng. Theoretical Analysis of Piston-Ring Lubrication Part I—Fully Flooded Lubrication. *Tribol. Trans.*, 35:696–706, 1992.

[15] Y.R. Jeng. Theoretical Analysis of Piston-Ring Lubrication Part II—Starved Lubrication and its Application to a Complete Ring Pack. *Tribol. Trans.*, 35:707–714, 1992.

[16] D.E. Richardson and G.L. Borman. Theoretical and Experimental Investigations of Oil
Films for Application to Piston Ring Lubrication. *SAE Technical Paper*, 922341, 1992.

[17] M. Soejima Y. Wakuri, T. Hamatake and T. Kitahara. Piston Ring Friction in Internal Combustion Engines. *Tribol. Int.*, 25:299–308, 1992.

[18] H. Schock Y. Chung and L. Brombolich. Fire Ring Wear Analysis for a Piston Engine. *SAE Technical Paper*, 930797, 1993.

[19] D.M. Thompson R.I. Taylor, M.A. Brown and J.C. Bell. The Influence of Lubricant Rheology on Friction in the Piston Ring-pack. *SAE Technical Paper*, 941981, 1994.

[20] M. Brown R. Taylor and D.M. Thompson. Validation of a Piston Ring-Pack Lubrication Model that Includes Realistic Lubricant Rheology. *Tribol. Ser.*, 30:345–354, 1995.

[21] Q. Yang and T.G. Keith Jr. An Elastohydrodynamic Cavitation Algorithm for Piston Ring Lubrication. *Tribol. Trans.*, 38:97–107, 1995.

[22] E.H. Smith M. Ma and I. Sherrington. A Three-Dimensional Analysis of Piston Ring Lubrication Part 1: Modelling. *J. Eng. Tribol.*, 209:1–14, 1995.

[23] E.H. Smith M. Ma and I. Sherrington. A Three-Dimensional Analysis of Piston Ring Lubrication Part 2: Sensitivity Analysis. *J. Eng. Tribol.*, 209:15–27, 1995.

[24] Q. Yang and T.G. Keith Jr. Two-Dimensional Piston Ring Lubrication-Part i: Rigid Ring and Liner Solution. *Tribol. Trans.*, 39:757–768, 1996.

[25] Q. Yang and T.G. Keith Jr. Two-Dimensional Piston Ring Lubrication-Part ii: Elastic Ring Consideration. *Tribol. Trans.*, 39:870–880, 1996.

[26] M. Ichinose Y. Harigaya and M. Suzuki. Effect of Temperature on the Lubrication Characteristics Between the Piston Ring and the Cylinder Liner of Internal Combustion Engine. *ASME*.

[27] I. Sherrington M. Ma and E. Smith. Implementation of an Algorithm to Model the Starved Lubrication of a Piston Ring in Distorted Bores: Prediction of Oil Flow and Onset of Gas Blow-by. *J. Eng. Tribol.*, 210:29–44, 1996.

[28] S. Brown and G. Hamilton. The Partially Lubricated Piston Ring. *J. Mech. Eng. Sci.*, 19:81–89, 1977.

[29] I. Sherrington M. Ma and E. Smith. Analysis of Lubrication and Friction for a Complete Piston-Ring Pack with an Improved Oil Availability Model: Part 1: Circumferentially Uniform Film. *J. Eng. Tribol.*, 211:1–15, 1977.

[30] I. Sherrington M. Ma and E. Smith. Analysis of Lubrication and Friction for a Complete Piston-Ring Pack with an Improved Oil Availability Model: Part 1: Circumferentially Variable Film. *J. Eng. Tribol.*, 211:17–27, 1977.

[31] D.C. Han and J.S. Lee. Analysis of the Piston Ring Lubrication with a New Boundary condition. *Tribol. Int.*, 31:753–760, 1998.

[32] B.J. Hamrock M. Esfahanian and A.A. Elsharkawy. On the Hydrodynamic Lubrication Analysis of Piston Rings. *Lub. Sci.*, 10:265–286, 1998.

[33] D. Taraza R. Stanley and N. Henein. A Simplified Piston Ring Assembly Friction Model. *ASME*, 1998.

[34] D. Taraza R. Stanley and N. Henein. A Simplified Piston Ring Assembly Friction Model. *SAE Technical Paper*, 010974, 1999.

[35] J.T. Sawicki and B. Yu. Analytical Solution of Piston Ring Lubrication Using Mass Conserving Cavitation Algorithm. *Tribol. Trans.*, 43:587–594, 2000.

[36] B. Jakobsson and L. Floberg. *The Finite Journal Bearing, Considering Vaporization*. PhD thesis.

[37] K.O. Olsson. *Cavitation in Dynamically Loaded Bearings*. PhD thesis, Cholmers Univercity of Technology, 1965.

[38] T.I. Tian. Dynamic Behaviours of Piston Rings and Their Practical Impact Part 1: Ring Flutter and Ring Collapse and Their Effects on Gas Flow and Oil Transport. *J. Eng. Tribol.*, 216:209–228, 2002.

[39] T.I. Tian. Dynamic Behaviours of Piston Rings and Their Practical Impact Part 2: Oil Transport, Friction and Wear of Ring/Liner Interface and the Effects of Piston and Ring Dynamics. *J. Eng. Tribol.*, 216:229–248, 2002.

[40] M. Priest R.J. Gamble and C.M. Taylor. Detailed Analysis of Oil Transport in the Piston Assembly of a Gasoline Engine. *Tribol. Lett.*, 14:147–156, 2003.

[41] M. Priest R.A. Mufti and R.J. Chittenden. Experimental and Theoretical Study of Instantaneous Piston Assembly Friction in a Gasoline Engine. *ASME*, pages 907–921, 2004.

[42] G. Livanos and N. P. Kyrtatos. A Model of the Friction Losses in Diesel Engines. *SAE Technical Paper*, 2006-01-0888, 2006.

[43] G. Livanos and N.P. Kyrtatos. Friction Model of a Marine Diesel Engine Piston Assembly. *Tribol. Int.*, 40:1441–1453, 2007.

[44] S. Balakrishnan P. Mishra and H. Rahnejat. Tribology of Compression Ring-to-Cylinder Contact at Reversal. *J. Eng. Tribol.*, 222:815–826, 2008.

[45] C.L. Felter. Numerical Simulation of Piston Ring Lubrication. *Tribol. Int.*, 41:914–919, 2008.

[46] P. Kumar R. Kumar and M. Gupta. Starvation Effects in Elasto-Hydrodynamically Lubricated Line Contacts. *Int. J. Adv. Tech.*, 1:73–84, 2010.

[47] R. Taylor. Squeeze Film Lubrication in Piston Rings and Reciprocating Contacts. *J. Eng. Tribol.*, 229:977–988, 2015.

[48] H. Christensen. A Theory of Mixed Lubrication. *Proc. Ins. Mech. Engineer.*, 186:421–430, 1972.

[49] S. K. Rhow and H. G. Elrod. Effects on Bearing Load-Carrying Capacity of Two-Sided Striated Roughness. *J. Lub. Tech.*, 96:554–560, 1974.

[50] D. Dowson et al. Piston Ring Lubrication-Part ii. Theoretical Analysis of a Single Ring and a Complete Ring Pack. *Fron. Res. Des.*, pages 23–52, 1979.

[51] B. L. Ruddy et al. The Influence of Thermal Distortion and Wear of Piston Ring Grooves Upon the Lubrication of Piston Rings in Diesel Engines. *Mech. Eng. Pub.*, pages 84–94, 1980.

[52] S. M. Rohde. A Mixed Friction Model for Dynamically Loaded Contacts With Application to Piston Ring Lubrication. *GM Res. Lab.*, 1980.

[53] N. Patir and H. Cheng. Application of Average Flow Model to Lubrication Between Rough Sliding Surfaces. *J. Lub. Tech.*, 101:220–229, 1979.

[54] D. G. Patterson G. K. Miltsios and T. C. Papanastasiou. Solution of the Lubrication Problem and Calculation of the Friction Force on the Piston Rings. *J. Tribol.*, 11:635–641, 1989.

[55] Z. Dursunkaya R. Keribar and M. F. Flemming. An Integrated Model of Ring Pack Performance. *J. Eng. Gas. Turb. Power.*, 113:382–389, 1991.

[56] J. Greenwood and J. Tripp. The Contact of Two Nominally Flat Rough Surfaces. *Proc. Ins. Mech. Eng.*, 185:625–633, 1970.

[57] P. C. Sui and S. Ariga. Piston Ring Pack Friction and Lubrication Analysis of an Automotive Engine Using a Mixed Lubrication Model. *SAE Technical Paper*, 31937, 1993.

[58] Y. Hu et al. Numerical Simulation of Piston Ring in Mixed Lubrication-a Nonaxisymmetrical Analysis. *J. Tribol.*, 116:470–478, 1994.

[59] s. Michail and G. Barber. The Effects of Roughness on Piston Ring Lubrication-Part ii: The Relationship Between Cylinder wall Surface Topography and Oil Film Thickness. *Tribol. trans.*, 38:173–177, 1995.

[60] s. Michail and G. Barber. The Effects of Roughness on Piston Ring Lubrication-part i: Model Development. *Tribol. trans.*, 38:19–26, 1995.

[61] C. Eiglmeier M. Knopf and G. Merker. Calculation of Unsteady Hydrodynamic Lubrication and Surface Contact at the Piston-Ring/Cylinder-Liner Interface. *SAE Technical Paper*, 981402., 1998.

[62] S. Gulwadi. A Mixed Lubrication and Oil Transport Model for Piston Rings Using a Mass-Conserving Algorithm. *J. Eng. Gas. Turb. Power.*, 120:199–208, 1998.

[63] D. Dowson M. Priest and C. Taylor. Predictive Wear Modelling of Lubricated Piston Rings in a Diesel Engine. *Wear*, 231:89–101, 1999.

[64] D. Dowson M. Priest and C. Taylor. Theoretical Modelling of Cavitation in Piston Ring Lubrication. *J. Mech. Eng. Sci.*, 214:435–447, 2000.

[65] S. D. Gulwadi. Analysis of Tribological Performance of a Piston Ring Pack. *Tribol. Trans.*, 43:151–162, 2000.

[66] Y. Z. Hu and D. Zhu. A Full Numerical Solution to the Mixed Lubrication in Point contacts. *J. Tribol.*, 122:1–9, 2000.

[67] O. Akalin and G. M. Newaz. Piston Ring-Cylinder Bore Friction Modeling in Mixed Lubrication Regime: Part i-Analytical Results. *J. Tribol.*, 123:211–218, 2001.

[68] O. Akalin and G. M. Newaz. Piston Ring-Cylinder Bore Friction Modeling in Mixed Lubrication Regime: Part ii-Correlation with Bench Test Data. *J. Tribol.*, 123:219–223, 2001.

[69] H. Xu et al. Friction Predictions for Piston Ring-Cylinder Liner Lubrication. *ASME*, pages 773–784, 2004.

[70] N. W. Bolander et al. Film Thickness and Friction Measurement of Piston Ring Cylinder Liner Contact with Corresponding Modeling Including Mixed Lubrication. *ASME*, pages 811–821, 2004.

[71] M. Teodorescu W. W. Chong and N. D. Vaughan. Cavitation Induced Starvation for Piston-Ring/Liner Tribological Conjunction. *Tribol. Int.*, 44:483–497, 2011.

[72] N. Morris et al. The Influence of Piston Ring Geometry and Topography on Friction. *J. Eng. Tribol.*, 227:141–153, 2013.

[73] N. Morris et al. Tribology of Piston Compression Ring Conjunction under Transient Thermal Mixed Regime of Lubrication. *Tribol. Int.*, 59:248–258, 2013.

[74] Y. Guo et al. A Mixed-Lubrication Model Considering Elastoplastic Contact for a Piston Ring and Application to a Ring Pack. *J. Auto. Eng.*, 229:174–188, 2015.

[75] M. K. Ahmed Ali et al. An Analytical Study of Tribological Parameters between Piston Ring and Cylinder Liner in Internal Combustion Engines. *J. Multi-body Dyn.*, 230:329–349, 2016.

[76] C. Gu et al. A Study on the Tribological Behavior of Surface Texturing on the Nonflat Piston Ring under Mixed Lubrication. *J. Eng. Tribol.*, 230:452–471, 2016.

[77] A. Zavos and P. G. Nikolakopoulos. A Tribological Study of Piston Rings Lubricated by Power Law Oils. *J. Eng. Tribol.*, 230:506–524, 2016.

[78] A. Zavos and P. G. Nikolakopoulos. Thermo-Mixed Lubrication Analysis of Coated Compression Rings with Worn Cylinder Profiles. *Indus. Lub. Tribol.*, 69:15–29, 2017.

[79] S. R. Bewsher et al. A Study into the Effects of Cylinder De-Activation on the Tribological Performance of Piston Ring-Liner Conjunction. 2017.

[80] Y. Hu et al. A New Efficient Flow Continuity Lubrication Model for the Piston Ring-Pack with Consideration of Oil Storage of the Cross-Hatched Texture. *Tribol. Int.*, 119:443–463, 2018.

[81] C. Gu et al. Analysis of the Coated and Textured Ring/Liner Conjunction Based on a Thermal Mixed Lubrication Model. *Friction*, 6:420–431, 2018.

[82] A. Zavos and P. G. Nikolakopoulos. Measurement of Friction and Noise from Piston Assembly of a Single-Cylinder Motorbike Engine at Realistic Speeds. *J Auto. Eng.*, 232:1715–1735, 2018.

[83] A. Zavos and P. G. Nikolakopoulos. Tribology of New Thin Compression Ring of Fired Engine under Controlled Conditions-a combined Experimental and Numerical Study. *Tribol. Int.*, 128:214–230, 2018.

[84] X. Meng C. Wen and W. Li. Numerical Analysis of Textured Piston Compression Ring Conjunction Using Two-Dimensional-Computational Fluid Dynamics and Reynolds methods. *J Eng. Tribol.*, 11:1467–1485, 2018.

[85] S. R. Bewsher et al. An Investigation into the Oil Transport and Starvation of Piston Ring Pack. *J. Eng. Tribol.*, 233:112–124, 2019.

[86] S. R. Bewsher et al. Boundary Friction Characterisation of a Used Cylinder Liner Subject to Fired Engine Conditions and Surface Deposition. *Tribol. Int.*, 131:424–437, 2019.

[87] Z. Zheng N. Liu and G. Li. Analysis of the Blow-by in Piston Ring Pack of the Diesel Engine. *Chem. Engineer. Trans.*, 46:1045–1050, 2015.

[88] Morris et al. The Influence of Piston Ring Geometry and Topography on Friction. *J. Eng. Tribol.*, 227:141–153, 2013.

[89] C. Delprete and A. Razavykia. Modeling of Oil Film Thickness in Piston Ring/Liner Interface. *Imt. J. Mech. Engin. Robot. research*, 6:210–214, 2017.

[90] J.F. Booker. Basic Equations for Fluid Films with Variable Properties. *J. Tribol.*, 111:475–479, 1989.

[91] C. Delprete and A. Razavykia. Statistical Study of Ring Geometry Effect on Piston Ring/Liner Tribology Using Classical Design of Experiment. *SAE Technical Paper*, 2018-01-1658, 2018.

[92] D. Dowson M. Priest, R.I. Taylor and D.C. Taylor. Boundary Conditions for Reynolds Equation with Particular Reference to Piston Ring Lubrication. *Tribol. Series*, 31:441–452, 1996.

[93] G. Knoll and H. Peeken. Hydrodynamic Lubrication of Piston Skirts. *J. Lubr. Technol.*, 104:504–508, 1982.

[94] S.M. Rohde D.F. Li and H.A. Ezzat. An Automotive Piston Lubrication Model. *ASLE trans.*, 26:151–160, 1983.

[95] S.F. Rezeka and N.A. Henein. A New Approach to Evaluate Instantaneous Friction and Its Components in Internal Combustion Engines. *SAE Technical Paper*, 932944, 1984.

[96] K. Yamamoto K. Ohta, Y. Irie and H. Ishikawa. Piston Slap Induced Noise and Vibration of Internal Combustion Engines. *SAE Technical Paper*, 870990, 1987.

[97] Z.P. Mourelatos. Trajectory of a Ringless Piston Within the Cylinder of an Internal Combustion Engine with a Crosshead Design. *SAE Technical Paper*, 880194, 1988.

[98] E. Ciulli. A Review of Internal Combustion Engine Losses Part 1: Specific Studies on the Motion of Pistons, Valves and Bearings. *J. Auto. Engineer.*, 206:223–236, 1992.

[99] S.D. Haddad and K.T. Tjan. An Analytical Study of Offset Piston and Crankshaft Designs and the Effect of Oil Film on Piston Slap Excitation in a Diesel Engine. *Mech. Mach. Theory*, 30:271–284, 1995.

[100] C.D. Radcliffe and D. Dowson. Analysis of Friction in a Modern Automotive Piston Ring Pack. *J. Eng. Tribol.*, 30:355–365, 1995.

[101] A. Yamamoto T. Nakada and T Abe. A Numerical Approach for Piston Secondary Motion Analysis and Its Application to the Piston Related Noise. *SAE Technical Paper*, 972043, 1997.

[102] N. Lalor J.C. De Luca and S.N. Gerges. Piston Slap Assessment Model. *SAE Technical Paper*, 982942, 1998.

[103] Y. Yajima K. Nakashima and K. Suzuki. Approach to Minimization of Piston Slap Force for Noise Reduction–Investigation of Piston Slap Force by Numerical Simulation. *JSAE Rev.*, 20:211–216, 1999.

[104] N. Henein D. Taraza and W. Bryzik. Friction Losses in Multi-cylinder Diesel Engines. *SAE Technical Paper*, 2000-01-0921, 2000.

[105] F. G. Haubner. Simulation of the Piston and Piston Ring Dynamic. *SAE Technical Paper*, 2001-01-3368, 2001.

[106] J. De Luca S. Gerges and N. Lalor. The Influence of Cylinder Lubrication on Piston Slap. *J. Sound Vib.*, 257:527–557, 2002.

[107] X. Du R. M. Hoffman, A. Sudjianto and J. Stout. Robust Piston Design and Optimization Using Piston Secondary Motion Analysis. *SAE Technical Paper*, 2003-01-0148, 2003.

[108] S. Jang and J. Cho. Effects of Skirt Profiles on the Piston Secondary Movements by the Lubrication behaviors. *Int. J. Automot. Tech.*, 257:23–31, 2004.

[109] J.L. Ligier and P. Ragot. Robust Piston Design and Optimization Using Piston Secondary Motion Analysis. *SAE Technical Paper*, 2005-01-1651, 2005.

[110] Y. Takahashi T. Kobayashi and D. J. Bell. How to Predict the Piston slap-Noise Using 3d Piston Motion Simulation. *SAE Technical Paper*, 2007-01-1245, 2007.

[111] P. Wang et al. Modeling and Simulation of Internal Combustion Engine Piston Slap. *J. Syst. Simul.*, 20:014, 2008.

[112] B Khelidj A. Kellaci, R. Mazouzi and A. Bounif. The Effect of Lubricant Rheology on Piston Skirt/Cylinder Contact for an Internal Combustion Engine. *Mechanics*, 81:30–36, 2010.

[113] Z. Cheng X. Zhou, G. Cai and Z. Zhang. A coupling Model for Dynamic and Tribological Behaviors of Piston System in ic Engine. *In Intelligent Systems and Applications*, pages 1–5, 2010.

[114] P. McFadden and S. Turnbull. Dynamic Analysis of Piston Secondary Motion in an Internal Combustion Engine Under Non-Lubricated and Fully Flooded Lubricated Conditions. *J. Mech. Engineer. Sci.*, 225:2575–2585, 2011.

[115] N. Ono H. Murakami, N. Nakanishi and T. Kawano. New Three-Dimensional Piston Secondary Motion Analysis Method Coupling Structure Analysis and Multi Body Dynamics Analysis. *SAE Technical Paper*, 2011-32-0559, 2011.

[116] Y.C. Tan and Z.M. Ripin. Technique of Measuring Piston Secondary Motion Using Laser Displacement Sensors. *Exp. Mech.*, 52:1447–1459, 2012.

[117] Y.C. Tan and Z.M. Ripin. Analysis of piston secondary Motion. *J. Sound. Vib.*, 332:5162–5176, 2013.

[118] B. Littlefair et al. Lubrication of a Flexible Piston Skirt Conjunction Subjected to Thermo-Elastic Deformation: A Combined Numerical and Experimental Investigation. *Tribol. Lett.*, 228:69–81, 2014.

[119] B. Littlefair et al. Lubrication of a Flexible Piston Skirt Conjunction Subjected to Thermo-Elastic Deformation: Transient Tribo-Dynamics of Thermo-Elastic Compliant High-Performance Piston Skirts. *Tribol. Lett.*, 53:51–70, 2014.

[120] Z.Y. Hao J. Zhu and K. Zheng. Analysis and Optimization Design on Piston Secondary Motion of Gasoline Engine. *Eng. Sci.*, 48:334–341, 2014.

[121] T. Kobayashi. Prediction of Piston Skirt Scuffing via 3d Piston Motion Simulation. *SAE Technical Paper*, 2016-01-1044, 2016.

[122] Z. Dursunkaya R. Keribar and V. Ganapathy. An Integrated Design Analysis Methodology to Address Piston Tribological Issues. *SAE Technical Paper*, 930793, 1993.

[123] C. Li K. Oh and P. Goenka. Elastohydrodynamic Lubrication of Piston Skirts. *J. Tribol.*, 109:356–362, 1987.

[124] P.K Goenka and P.R. Meernik. Lubrication Analysis of Piston Skirts. *SAE Technical Paper*, 920490, 1992.

[125] R. Keribar Z. Dursunkaya and V. Ganapathy. A Model of Piston Secondary Motion and Elastohydrodynamic Skirt Lubrication. *J. Vib. Acoust.*, 116:777–785, 1994.

[126] R. S. Paranjpe. Development of a Math-Based Piston Noise Model. *SAE Technical Paper*, 980564, 1998.

[127] R. S. Paranjpe. Development of a Piston Secondary Motion Analysis Program with Elastically Deformable Piston Skirt. *SAE Technical Paper*, 1999-01-3303, 1999.

[128] M. Perchanok. Modeling of Piston-Cylinder Lubrication with a Flexible Skirt and Cylinder Wall. *SAE Technical Paper*, 2000-01-2804, 2000.

[129] O. Laback G. Offner, J. Krasser and H. H. Priebsch. Simulation of Multi-Body Dynamics and Elastohydrodynamic Excitation in Engines Especially Considering Piston-Liner contact. *J. Multi-body Dynamic.*, 215:93–102, 2001.

[130] H. M. Herbst G. Offner and H. H. Priebsch. Modeling of Piston-Cylinder Lubrication with a Flexible Skirt and Cylinder Wall. *SAE Technical Paper*, 2001-01-0565, 2001.

[131] D. Bell M. Duyar and M. Perchanok. A Comprehensive Piston Skirt Lubrication Model Using a Mass Conserving EHL Algorithm. *SAE Technical Paper*, 2005-01-1640, 2005.

[132] S. Balakrishnan and H. Rahnejat. Isothermal Transient Analysis of Piston Skirt-to-Cylinder Wall Contacts under Combined Aaxial, Lateral and Tilting Motion. *Appl. Phys.*, 38:787, 2005.

[133] M. Ito K. Sato, K. Fujii and S. Koda. Application to Engine Development of Friction Analysis by Piston Secondary Motion Simulation in Consideration of Cylinder Block Bore Distortion. *SAE Technical Paper*, 2006-01-0428, 2006.

[134] Z. P. Mourelatos P. Patel and P. Shah. A Comprehensive Method for Piston Secondary Dynamics and Piston-Bore Contact. *ASME*, pages 555–556, 2006.

[135] Z. P. Mourelatos P. Shah and P. Patel. Piston Secondary Dynamics Considering Elastohydrodynamic Lubrication. *SAE Technical Paper*, 2007-01-1251, 2007.

[136] Y. Z. Hu F. M. Meng, Y. Y. Zhang and H. Wang. Thermo-Elasto-Hydrodynamic Lubrication Analysis of Piston Skirt Considering Oil Film Inertia Effect. *Tribol. Int.*, 40:1089–1099, 2007.

[137] X. Meng and Y. Xie. On the Elastic Fluid Dynamic Lubrication of Liner-Piston System with Quadratic Skirt Profiles. *Lubr. Eng.*, 33:1–4, 2008.

[138] X. Zhang Z. Zhang, Y. Xie and X. Meng. Analysis of Piston Secondary Motion Considering the Variation in the System Inertia. *J. Auto. Engineer.*, 223:549–563, 2009.

[139] N. Lorenz G. Offner and O. Knaus. Piston Clearance Optimization Using Thermo-Elasto Hydrodynamic Simulation to Reduce Piston Slap Excitation and Friction Loss. *SAE Technical Paper*, 2012-01-1530, 2012.

[140] Littlefair et al. Assessment of Thermo-Structural Effects on EHL Piston Skirt Lubrication. *ASME*, pages 973–978, 2012.

[141] M. Redha K. Ahmed, K. Benyoucef and L. Mourad. The Effect of Piston Skirt Profile on EHD Lubrication in an Internal Combustion Engine. *Adv. Mat. Res.*, 787:704–710, 2013.

[142] Littlefair et al. Lubrication of a Flexible Piston Skirt Conjunction Subjected to Thermo-Elastic Deformation: A Combined Numerical and Experimental Investigation. *J. Eng. Tribol.*, 228:69–81, 2013.

[143] N. Dolatabadi et al. A Transient Tribodynamic Approach for the Calculation of Internal Combustion Engine Piston Slap Noise. *J. Sound Vib.*, 352:192–209, 2015.

[144] R. Keribar and Z. Dursunkaya. A Comprehensive Model of Piston Skirt Lubrication. *SAE Technical Paper*, 920483, 1992.

[145] Z. Dursunkaya and R. Keribar. Simulation of Secondary Dynamics of Articulated and Conventional Piston Assemblies. *SAE Technical Paper*, 920484, 1992.

[146] T. Arai D. Zhu, H. S. Cheng and K. Hamai. A Numerical Analysis for Piston Skirts in Mixed Lubrication-Part i: Basic Modeling. *J. Tribol.*, 114:553–562, 1992.

[147] T. Arai D. Zhu, H. S. Cheng and K. Hamai. A Numerical Analysis for Piston Skirts in Mixed Lubrication-Part ii: Deformation Considerations. *J. Tribol.*, 115:125–133, 1993.

[148] V. W. Wong et al. A Numerical Model of Piston Secondary Motion and Piston Slap in Partially Flooded Elastohydrodynamic Skirt Lubrication. *SAE Technical Paper*, 940696, 1994.

[149] T. Arai D. Zhu, H. S. Cheng and K. Hamai. A Comprehensive Study of the Friction and Dynamic Motion of the Piston Assembly. *J. Engineer. Tribol.*, 212:221–226, 1998.

[150] T. S. Moon M. R. Cho, D. Y. Oh and D. C. Han. Theoretical Evaluation of the Effects of Crank Offset on the Reduction of Engine Friction. *J. Auto. Engineer.*, 217:891–898, 2003.

[151] S. Mansouri and V. Wong. Effects of Piston Design Parameters on Piston Secondary Motion and Skirt-Liner Friction. *SAE Technical Paper*, 2004-01-2911, 2004.

[152] S. Mansouri and V. Wong. Effects of Piston Design Parameters on Piston Secondary Motion and Skirt-Liner Friction. *J. Auto. Engineer.*, 219:435–449, 2005.

[153] P. Ragot and M. Rebbert. Investigations of Crank Offset and It's Influence on Piston and Piston Ring Friction Behavior Based on Simulation and Testing. *SAE Technical Paper*, 2007-01-1248, 2007.

[154] F. McClure and T. Tian. A Simplified Piston Secondary Motion Model Considering the Dynamic and Static Deformation of Piston Skirt and Cylinder Bore in Internal Combustion Engines. *SAE Technical Paper*, 2008-01-1612, 2008.

[155] S. N. Kurbet R. R. Malagi and R. Krishnakumar. A Comprehensive Model to Study the Dynamic Motion of Piston and Friction and Lubrication in ic Enignes. *SAE Technical Paper*, 2008-28-0061, 2008.

[156] X. Meng and Y. Xie. A New Numerical Analysis for Piston Skirt–Liner System Lubrication Considering the Effects of Connecting Rod Inertia. *Tribol. Int.*, 47:235–243, 2012.

[157] X. H. Meng J. LI B. Wu, L. P. Ning and Y. B. Xie. Tribological Simulation and Design of Piston Skirt-Liner System to Reduce Friction of Automotive Engines. *Tribol. Int.*, 47:235–243, 2012.

[158] X. Meng L. Ning and Y. Xie. Effects of Lubricant Shear Thinning on the Mixed Lubrication of Piston Skirt-Liner System. *J. Mechan. Engineer. Sci.*, 227:1585–1598, 2013.

[159] X. Meng L. Ning and Y. Xie. Incorporation of Deformation in a Lubrication Analysis for Automotive Piston Skirt–Liner System. *J. Engineer. Tribol.*, 227:654–670, 2013.

[160] G. Offner. Friction Power Loss Simulation of Internal Combustion Engines Considering Mixed Lubricated Radial Slider, Axial Slider and Piston to Liner Contacts. *Tribol. Trans.*, 3:503–515, 2013.

[161] C. Delprete and A. Razavykia. Piston Dynamics, Lubrication and Tribological Performance Evaluation: A Review. *J. Engin. Research*, 1468087418787610, 2018.

[162] A. Razavykia C. Delprete and P. Baldissera. Detailed Analysis of Piston Secondary Motion and Tribological Performance. *J. Engin. Research*, 1468087419833883, 2019.

[163] J.F. Booker. Dynamically Loaded Journal Bearings: Mobility Method of Solution. *J. Basic Engineer.*, 87:537–546, 1965.

[164] J.F. Booker. Dynamically-Loaded Journal Bearings: Numerical Application of the Mobility Method. *J. Lub. Tech.*, 87:537–546, 1965.

[165] P.K. Goenka. Analytical Curve Fits for Solution Parameters of Dynamically Loaded Journal Bearings. *J. Tribol.*, 106:421–427, 1984.

[166] M. Godet B. Fantino and J. Frene. Dynamic Behaviour of an Elastic Connecting–Rod Bearing–Theoretical Study. *SAE Technical Paper*, 830307, 1983.

[167] P.K. Goenka. Comparison of Dynamic Behavior of Elastic Connecting-Rod Bearing in Both Petrol and Diesel Engines. *J. Tribol.*, 102:87–91, 1985.

[168] H. Hirani. Dynamically Loaded Finite Length Journal Bearings: Analytical Method of Solution. *J. Tribol.*, 121:844–852, 1999.

[169] R.S. Paranjpe. Analysis of Non-Newtonian Effects in Dynamically Loaded Finite Journal Bearings Including Mass Conserving Cavitation. *J. Tribol.*, 114:736–744, 1992.

[170] G.B. Dubois and F.W. Ocvirk. Analytical Derivation and Experimental Evaluation of Short-Bearing Approximation for Full Journal Bearing. *NACA Report*, 1157, 1953.

[171] D.O. Barilá G.G. Vignolo and L.M. Quinzani. Approximate Analytical Solution to Reynolds Equation for Finite Length Journal bearings. *Tribol. Int.*, 44:1089–1099, 2011.

[172] A. Chasalevris and D. Sfyris. Evaluation of the Finite Journal Bearing Characteristics, Using the Exact Analytical Solution of the Reynolds Equation. *Tribol. Inter.*, 57:216–234, 2013.

[173] T. Dimond J. Cao S. Dousti, P. Allaire. An Extended Reynold Equation Applicable to High Reduced Reynolds Number Operation of Journal Bearings. *Tribol. Int.*, 102:182–197, 2016.

[174] R. Seung-Hyuk C. Myung-Rae, O. Dae-Yoon and H. Dong-Chul. Load Characteristics of Engine Main Bearing: Comparison Between Theory and Experiment. *KSME Inter.*, 1:1095–1101, 2002.

[175] M. Godet B. Fantino and J. Frêne. Dynamic Behaviour of an Elastic Connecting–Rod Bearing–Theoretical Study. *SAE Technical Paper*, 830307, 1983.

[176] J.F. Booker. Basic Equations for Fluid Films with Variable Properties. *J. Tribol.*, 111:475–479, 1989.

[177] F.A. Martin. Friction in Internal Combustion Engine Bearings. *Instn. Mech. Engrs.*, C67/85:1–17, 1985.

[178] J.F. Booker. A Table of the Journal-Bearing Integral. *J. Basic Engineer.*, 87:533–535, 1965.

Appendix A

Influential factors and corresponding data, applied to DoE

Calculated average minimum oil film thickness and average power loss for 34 combination of influential parameters considered in design of experiment (DoE) are tabulated by Table A.1.

Table A.1 Influential factors and corresponding data

Factors (Inputs)						Responses (Outputs)	
No	*A*	*B*	*C*	*D*	E	$Ave.h_{min}(\mu m)$	$Ave.powerloss(W)$
1	1	3	6	0.2	Absence	4.35	32.71
2	1.8	3	6	0.2	Absence	6.21	41.02
3	1	15	6	0.2	Absence	4.21	13.99
4	1.8	15	6	0.2	Absence	8.24	18.23
5	1	3	18	0.2	Absence	2.64	38.4
6	1.8	3	18	0.2	Absence	4.49	47.23
7	1	15	18	0.2	Absence	1.99	17.56
8	1.8	15	18	0.2	Absence	4.41	24.55
9	1	3	6	1	Absence	4.33	29.21
10	1.8	3	6	1	Absence	6.98	43.56
11	1	15	6	1	Absence	4.2	13.95
12	1.8	15	6	1	Absence	8.24	18.17
13	1	3	18	1	Absence	2.64	38.28
14	1.8	3	18	1	Absence	4.49	47.09
15	1	15	18	1	Absence	1.99	17.5
16	1.8	15	18	1	Absence	4.41	24.48
17	1	3	6	0.2	presence	3.48	37.26
18	1.8	3	6	0.2	presence	6.03	40.46
19	1	15	6	0.2	presence	4.41	16.32
20	1.8	15	6	0.2	presence	8.07	21.26
21	1	3	18	0.2	presence	2.28	45.87
22	1.8	3	18	0.2	presence	3.97	56.04
23	1	15	18	0.2	presence	2.41	23.55
24	1.8	15	18	0.2	presence	4.68	30.13
25	1	3	6	1	presence	3.48	37.15
26	1.8	3	6	1	presence	6.03	40.33
27	1	15	6	1	presence	4.41	16.27
28	1.8	15	6	1	presence	8.07	21.2
29	1	3	18	1	presence	2.28	45.74
30	1.8	3	18	1	presence	3.98	55.87
31	1	15	18	1	presence	2.41	23.48
32	1.8	15	18	1	presence	4.68	30.03
33	1.4	9	12	0.6	Absence	4.5	24.89
34	1.4	9	12	0.6	presence	4.4	29.37

Appendix B

Booker table of integrals for cavitated journal bearings

Hydrodynamic force components

According to Fig. 5.6, hydrodynamic force components acting on the journal, F_h, is the resultant force of radial force, F_r and tangential force, F_t can be calculated using following equations:

$$F_r = \int_0^{\pi} \int_{-\frac{L_x}{2}}^{\frac{L_x}{2}} p(x,\alpha) R \cos\alpha dx d\alpha \tag{B.1}$$

$$F_t = \int_0^{\pi} \int_{-\frac{L_x}{2}}^{\frac{L_x}{2}} p(x,\alpha) R \sin\alpha dx d\alpha \tag{B.2}$$

where

$$p(\alpha) = 6\eta \frac{1}{c^2} \left(\frac{\varepsilon \bar{\omega} \sin\alpha}{(1+\varepsilon\cos\alpha)^3} \right) (x^2 - \frac{L_x^2}{4}) \tag{B.3}$$

Substituting (B.3) in (B.1) gives:

$$F_r = \frac{R\eta\bar{\omega}L_x^3}{c^3} e \int_0^{\pi} \left(\frac{\sin(\alpha)\cos(\alpha)}{(1+\varepsilon\cos(\alpha))^3} \right) d\alpha \tag{B.4}$$

Regarding the solution presented by Booker [163], Equation (B.4) can be written as:

$$F_r = \frac{R\eta\bar{\omega}L_x^3}{c^3} e\Big(I_3^{11}(\pi) - I_3^{11}(0)\Big) \tag{B.5}$$

where

$$I_3^{11}(\alpha) = \frac{1}{\varepsilon}\Big(-I_3^{10}(\alpha) + I_2^{10}(\alpha)\Big) \tag{B.6}$$

and

$$I_3^{10}(\alpha) = \frac{1}{2\varepsilon(1+\varepsilon\cos(\alpha))^2} \tag{B.7}$$

$$I_2^{10}(\alpha) = \frac{1}{\varepsilon(1+\varepsilon\cos(\alpha))} \tag{B.8}$$

Substituting (B.3) in (B.2) gives:

$$F_t = \frac{R\eta\bar{\omega}L_x^3}{c^3} e \int_0^{\pi} \left(\frac{\sin^2(\alpha)}{(1+\varepsilon\cos(\alpha))^3}\right) d\alpha \tag{B.9}$$

Applying Booker table of integrals [163] yields:

$$F_t = \frac{-R\eta\bar{\omega}L_x^3}{c^3} e\Big(I_3^{20}(\pi) - I_3^{20}(0)\Big) \tag{B.10}$$

where

$$I_3^{20}(\alpha) = \frac{1}{\varepsilon^2}\Big(-(1-\varepsilon^2)I_3^{00}(\alpha) + 2I_2^{00}(\alpha) - I_1^{00}(\alpha)\Big) \tag{B.11}$$

and

$$I_3^{00}(\alpha) = \frac{1}{2(1-\varepsilon^2)}\left(\frac{-\varepsilon\sin(\alpha)}{(1+\varepsilon\cos(\alpha))^2} + 6I_2^{00} - I_1^{00}\right) \tag{B.12}$$

$$I_3^{00}(\alpha) = \frac{1}{(1-\varepsilon^2)}\left(\frac{-\varepsilon\sin(\alpha)}{(1+\varepsilon\cos(\alpha))} + I_1^{00}\right) \tag{B.13}$$

$$I_1^{00}(\alpha) = \frac{1}{\sqrt{(1-\varepsilon^2)}} \cos^{-1}\left(\frac{\varepsilon + \cos(\alpha)}{1 + \varepsilon\cos(\alpha)}\right) \tag{B.14}$$